MIOCENE ROTATION AND QUATERNARY UPLIFT OF CARMEN ISLAND, BAJA CALIFORNIA SUR, MEXICO

by Jamie Patrick Macy

A Thesis

Submitted in Partial Fulfillment

Of the Requirements for the Degree of

Master of Science

In Geology

Northern Arizona University

August, 2005

Approved:

_____

Paul J Umhoefer, Ph.D., Chair

_____

Michael H Ort, Ph.D.

_____

Lee Amoroso, Ph.D.

ABSTRACT

MIOCENE ROTATION AND QUATERNARY UPLIFT OF CARMEN ISLAND, BAJA CALIFORNIA SUR, MEXICO

JAMIE PATRICK MACY

The Gulf of California is a young oblique-divergent plate boundary. The plate margin is characterized by rift segments and accommodation zones that contain strike-slip and normal faulting. The Baja California peninsula strikes 330^{o} and many elongate islands in the Gulf of California also follow a NW-SE trend, parallel to the rift trend. Carmen Island, however, has a NNE-SSW, anomalous trend.

Carmen Island, located east of the town of Loreto, Baja California Sur, was studied for possible vertical-axis rotation and uplift. Paleomagnetic samples were collected from sites around Carmen Island and compared to locally collected samples on the Baja California peninsula. Uplifted marine terraces were surveyed and shells were collected as dating material.

Paleomagnetic samples from Carmen Island showed variable results. Miocene rocks from Carmen Island were found to have varying amounts of rotation ranging from ~2^{o} – 135^{o}. Pliocene rock samples collected from Carmen Island showed little to no rotation when compared to rocks from the Baja California peninsula.

Uplifted Quaternary marine terraces were surveyed at Bahia Marquer on Carmen Island to determine uplift rates. Three sets of uplifted marine terraces were surveyed at 18 m, 25 m, and 55 m above sea level at Bahia Marquer. Shells and corals were collected from two marine terraces at Bahia Marquer and one terrace at Punta El Bajo, on the Baja

California peninsula. Amino acid racemization was used to date and correlate shells collected from Bahia Marquer and Punta El Bajo. U-Th ages of corals were also used to calibrate the amino acid racemization analysis. An uplift rates of ~0.15 m/ka was found for the western side of Carmen Island. These rates suggest that the island is uplifting much faster than the adjacent Baja California peninsula.

Carmen Island has been tectonically active since Miocene time and continues today. Paleomagnetic and uplifted marine terrace data confirm this idea.

ACKNOWLEDGMENTS

There are several individuals who are directly responsible for helping me finish my thesis. I would foremost like to thank my advisor, Paul Umhoefer, who has stuck with me through the years and guided my research and writing. I would also like to thank my committee members Michael Ort and Lee Amoroso, for their insight and expertise when editing my work. A special thank you goes out to Darrel Kaufman who, although couldn't be a part of my final committee, was an original committee member and a tremendous help in my marine terrace work. And my thesis would never have been started without the tutelage and mentoring of Larry Mayer, my deepest thanks.

While working in the field I was lucky enough to have an old friend as a field assistant and a great deal of gratitude is owed to Eric Meltzer. My parents have supported and encouraged me even when it looked like nothing was happening. Thanks mom and dad for hanging tough and always being there for me. I may never have completed my thesis had it not been for the inspiration and motivation of the closest person in the world to me, Renata Dolecka. She has helped in every aspect of life and was an important part in finishing my work, thank you.

This research was partly funded by an NSF Grant awarded to Paul Umnoefer.

TABLE OF CONTENTS

LIST OF TABLES

LIST OF FIGURES

CHAPTER 1

INTRODUCTION

The better understood rift systems of the world, such as the Gulf of Suez, the East African Rift and the Rio Grande Rift, are orthogonal in extension direction relative to the rift axis and have been extensively studied in recent years. Oblique rifts, however, are poorly understood and much current research is focused on establishing tectonic models for oblique rift systems. The oblique rift system in the Gulf of California is ideal to study because it is young and both margins are preserved (Figure 1.1). The Gulf of California has experienced two distinct stages of tectonic evolution (Hausback, 1984; Stock and Hodges, 1989; Lonsdale, 1989). The first stage is a period from ~12 Ma to ~8 - 6 Ma, during which the Gulf of California was primarily an orthogonal rift system with typical rift characteristics. At ~8 to 6 Ma, the Gulf of California changed to an oblique rift system. The change of tectonics at ~8 to 6 Ma marks the onset of en-echelon strike-slip faults through the middle of the Gulf of California that evolved into the present plate boundary. This study aims to contribute to the understanding of the evolution of the Loreto area and the formation of transform faults in the southern Gulf of California. In addition, this study will attempt to understand the geologic processes associated with transform fault systems including the pattern of uplift of the continental margin.

Significance of Problem

Continental rifts are an expression of extended terrains. Continental rifts (Figure 1.2) are characterized as asymmetrical in cross-section with respect to the long axis and

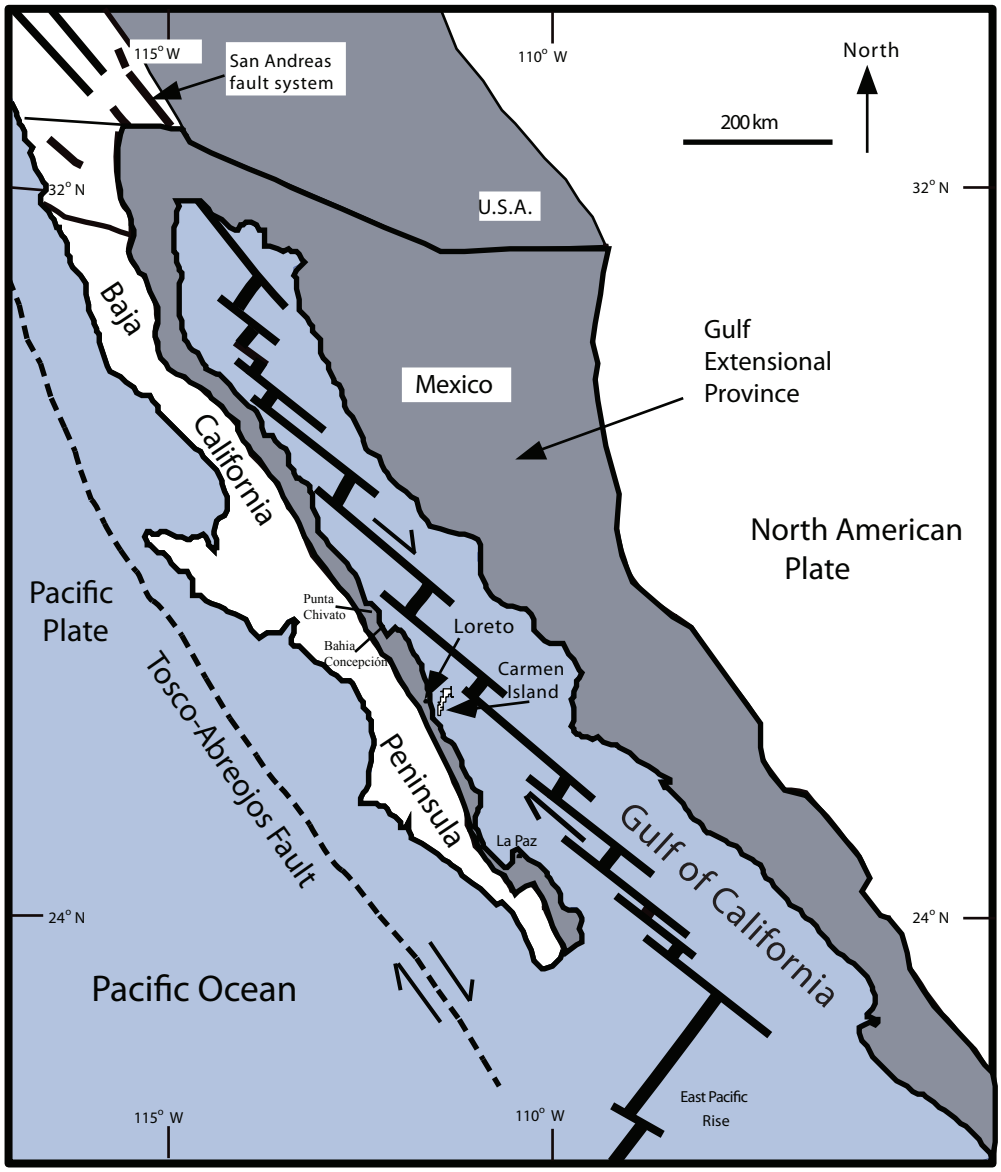

Figure 1.1: Location map of the Gulf of California with tectonic features and the Gulf extensional province highlighted in dark gray (from Umhoefer and Stone, 1996).

have dimensions on the order of a few tens of kilometers wide and many hundred to a few thousand kilometers long (Bosworth, 1985; Rosendahl, 1987; Colleta et al., 1988). A series of normal faults and half grabens with alternating asymmetry typically segment the rift along its axis, and a major normal fault dominates one side of each rift segment (Figure 1.2). The border faults commonly alternate in dip direction along the rift axis. Many secondary synthetic and antithetic faults form within the hanging wall of the major border normal faults (Figure 1.2) (Bosworth, 1985).

Continental rift segments are bordered by transfer zones and accommodation zones that separate individual segments (Faulds and Varga, 1998). Transfer zones are relatively narrow zones of strike-slip and oblique-slip faulting that accommodate the strain between extended domains or segments. Transfer zones trend parallel to the extension direction. Accommodation zones are similar, but they are wider than transfer zones and include overlapping smaller normal faults that terminate and separate domains of oppositely dipping normal faults. Accommodation zones trend parallel, perpendicular, and oblique to the extension direction (Faulds and Varga, 1998).

Axen (1985) first noted rift segments separated by accommodation zones in the Gulf Extensional Province (Figures 1.1 and 1.3). Umhoefer et al. (2002) described the 85 km long Loreto segment, Baja California Sur, as one of these rift segments; it is dominated by a series of discontinuous down-to-the-east monoclines and normal faults (Figure 1.4).

The strike-slip faults associated with transfer zones joining rift segments are related to Carmen Island in Baja California Sur. Strike-slip faults are projected from present transform faults and are interpreted to border Carmen Island to the north and

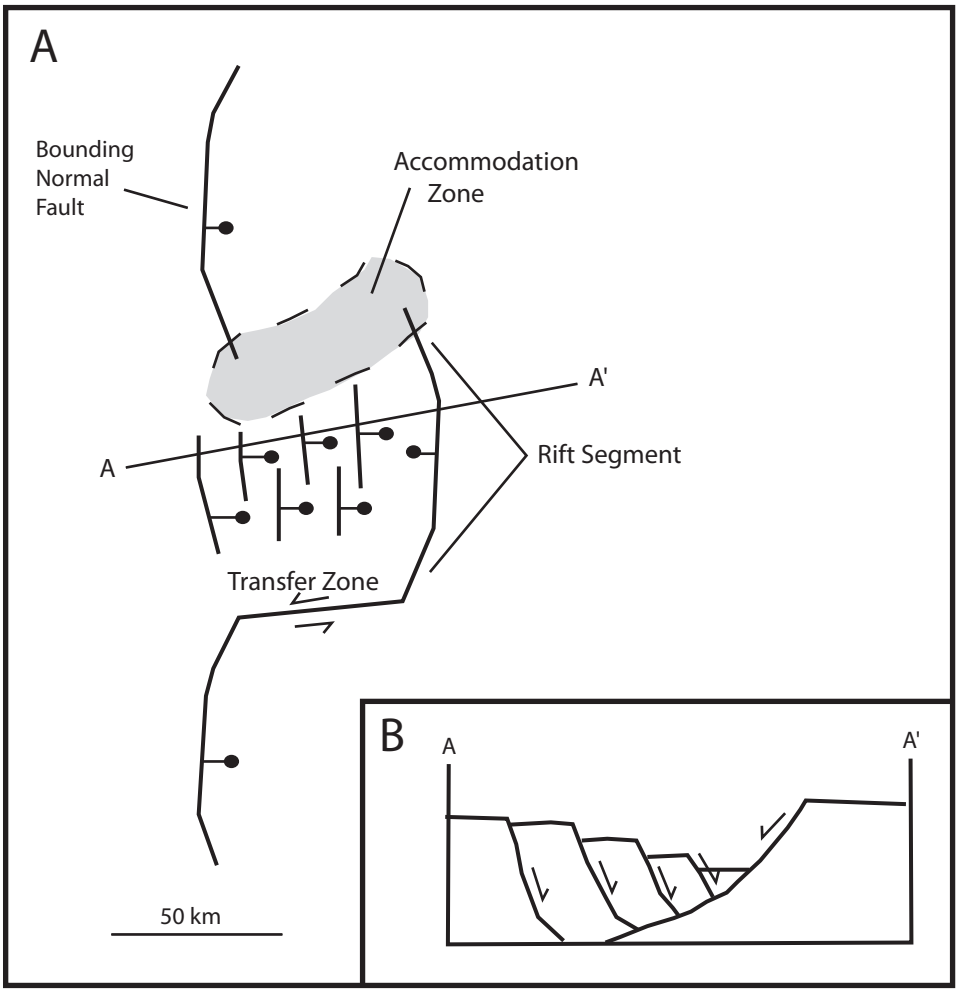

Figure 1.2: General rift geometry in a continental rift. A: Map view of rift segment, accommodation zone, and transfer zone. B: Cross section view of typical half-graben geometry observed in rift segments (after Rosendahl, 1987).

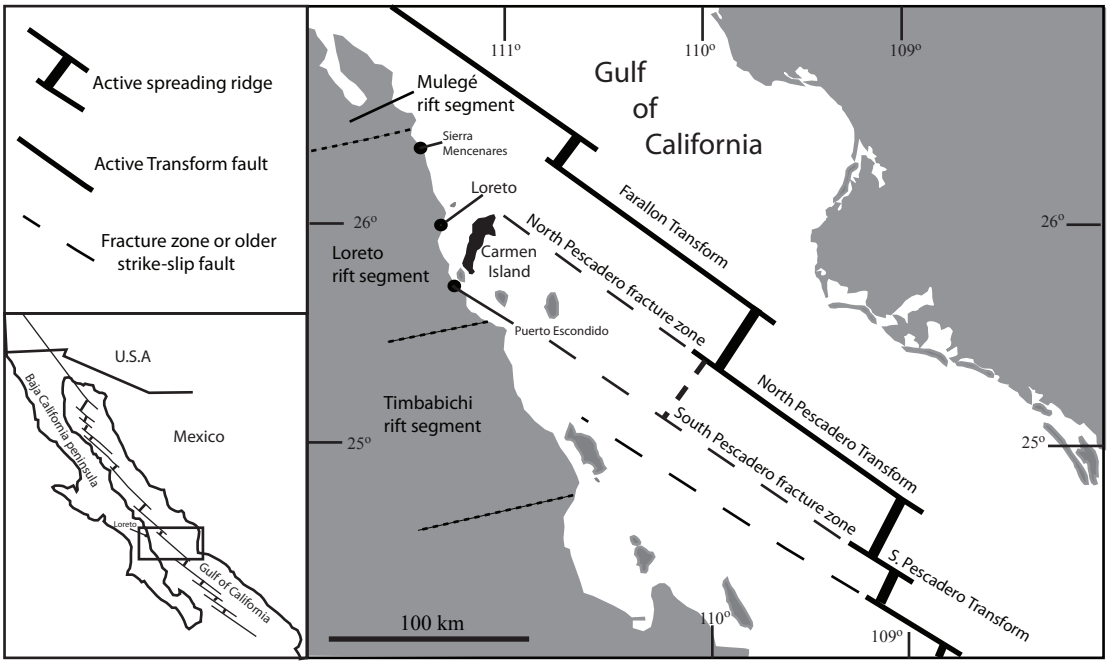

Figure 1.3: Map showing Gulf of California and area of study, Carmen Island. The proposed Mulegé, Loreto, and Timbabichi rift segments are designated by dashed lines. The Alt and Pescadero transform faults are projected with dashed lines to the Alt and Pescadero fracture zones (after Dorsey et al., 2001; Umhoefer et al., 2002).

south. The uplift of Carmen Island is related to normal faulting and horst and graben geology. Carmen Island is tectonically active and has peaked the interest of some researchers.

Umhoefer et al. (2001, 2002) proposed the idea that Carmen Island has rotated over the last ~6 Ma. The Baja California peninsula trends NNW-SSE and many elongate islands located along the peninsula in the Gulf of California follow the same trend (Figure 3.1). Other islands in the Gulf of California exhibit a N-S trend, which is perpendicular to the approximate E-W extension direction related to NW Pliocene to Quaternary dextral shear (Umhoefer and Stone, 1996; Umhoefer et al., 2001). Carmen Island is one island that does not follow either the NNW-SSE or N-S trends, but it is oriented NNE-SSW. Observations of rock bedding on Carmen Island and bedding on the Baja California peninsula near Loreto, suggest 40^{o} of clockwise difference. Carmen Island's anomalous trend may be due to vertical-axis rotation and warrants further study.

The development of the Loreto segment is fundamentally important to the evolution of the Gulf of California. The Loreto segment has experienced much tectonic movement associated with transtension in the Gulf of California (Umhoefer et al., 2002). Most importantly, features of the Loreto segment have recorded tectonic activity since Pliocene time related to development of the oblique margin of the Gulf of California. This stratigraphic and structural record helps constrain the timing and development of the margin. There is good evidence that faulting onshore in the Loreto segment slowed and largely moved offshore to the east at ~2 Ma. Quaternary movement along offshore faults of the Loreto segment is related to Carmen Island and is important to understand because it reflects the current changing plate margin.

Area of Study

The study area is the western margin of the Gulf of California near Loreto, Baja California Sur. The Loreto segment extends from the Sierra Mencenares to Puerto Escondido (Figures 1.3 and 1.4). The Loreto segment is bordered by major normal faults on its western side. The northern boundary is marked by the end of a monocline that extends 8 km north of the northern end of the Loreto fault (Figure 1.4). The southern boundary of the Loreto segment is the southern termination of the Escondido fault (Figure 1.4).

This study focuses on Carmen Island which is located about 5-10 km east of Loreto, and also includes areas around Punta El Bajo, southwest of Loreto, and Puerto Escondido. Carmen Island is 31 km long and 12 km wide at its widest point. The island is dominated by a mountain ridge with its highest peak at 479 meters. Cliffs of Pliocene strata and uplifted marine terraces flank the mountainous terrain on the north, southeast, southwest, and the southern tip. Part of this study will focus on Bahia Marquer, where Pliocene marine terraces are exposed on the southeastern side of Carmen Island.

Based on limited bathymetry and mapping, Carmen Island is interpreted to be bordered by fracture zones to the northeast and southwest and normal faults to the east and west (Figure 1.4). The Loreto fault, located just north of the city of Loreto, is a normal fault with dextral motion (Dorsey and Umhoefer, 2000) possibly kinematically linked to strike-slip and normal faulting in the Gulf of California near Carmen Island (Umhoefer et al., 2002). Before 2 Ma, the Loreto fault may have been linked to NW-striking dextral faults and N-NNW striking normal faults offshore. Two of the dextral

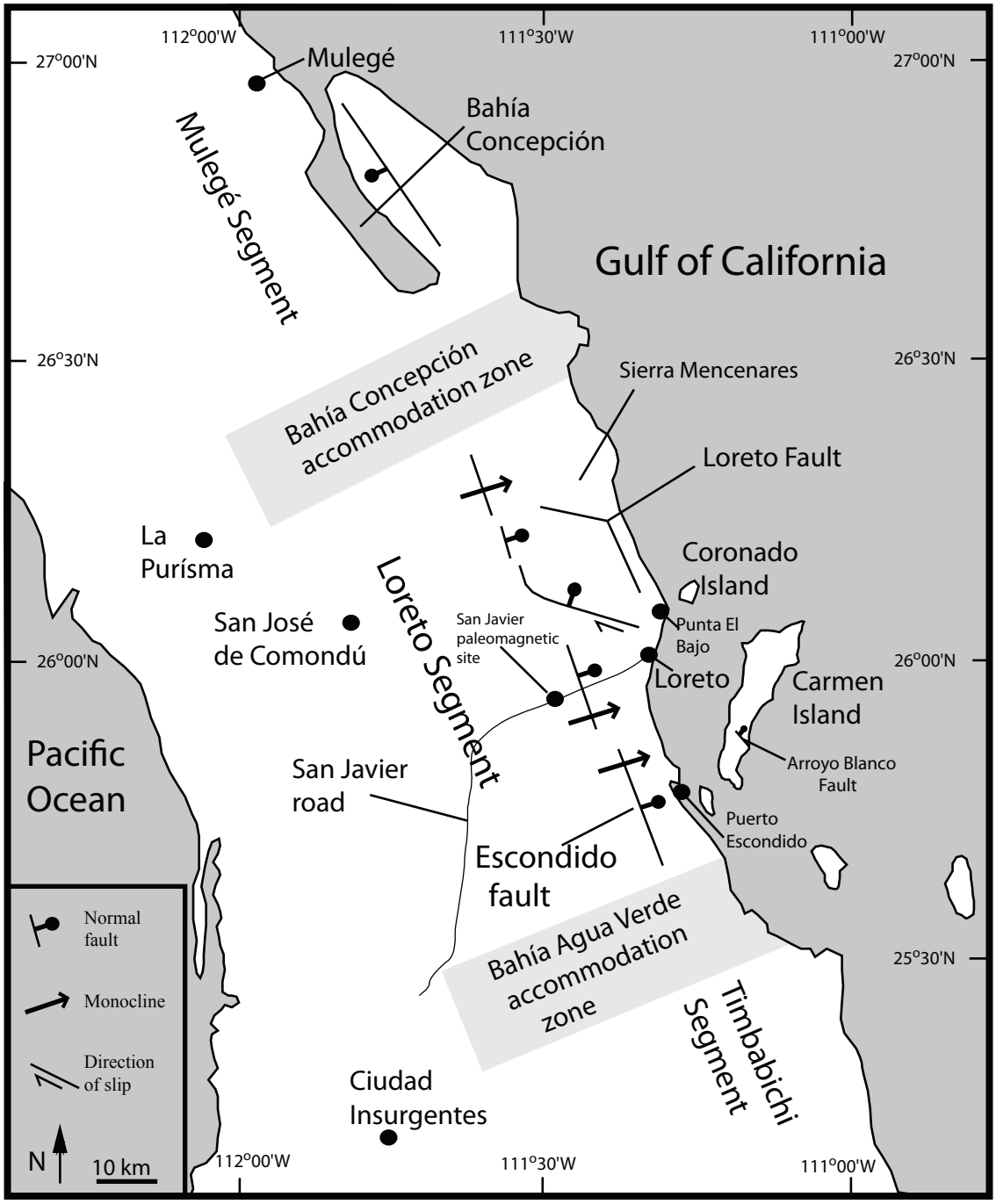

Figure 1.4: Regional map of central Baja California showing the location of rift segments and accommodation zones (modified from Umhoefer et al., 2001).

strike-slip faults that may be associated with the Loreto fault are the early North and South Pescadero transform faults (Figure 1.3). The North and South Pescadero faults are currently fracture zones that project from active transform faults (Figure 1.3). If these strike-slip faults extend to the northwest these structures may control movement and rotation for Carmen Island (Figure 1.3). Therefore, we can treat Carmen Island as a block, bounded by strike-slip faulting to the northeast and southwest and normal faulting to the west and east (Umhoefer et al., 2002).

Objectives and Methods of this study

This study involves work on Carmen Island and the Baja California peninsula.

Objective 1: Determine the amount of rotation of Carmen Island

A tectonic framework was developed for Carmen Island by using existing geologic maps and interpretations of the Loreto segment. The tectonic setting of the Loreto segment is one where Carmen Island is hypothesized to be bounded by strike-slip and normal faulting and can be treated like a block undergoing vertical-axis rotation (Umhoefer et al., 2002). Paleomagnetism is a fundamental tool for exploring vertical-axis rotations (Butler, 1992). Expected magnetic declination can be compared with observed tilt-corrected declinations and the result is an observed rotation. Oriented paleomagnetic samples were collected from Carmen Island and the adjacent mainland. Paleomagnetic samples from Carmen Island were compared with rocks from the peninsula near San Javier road and Puerto Escondido. Magnetic properties from the paleomagnetic samples on Carmen Island and the Baja California peninsula were also compared to expected magnetism at the time the rocks were formed.

Objective 2: Determine the amount and timing of Quaternary uplift at Bahia Marquer, Carmen Island

Marine terraces record tectonic uplift by preserving a paleo-record of approximate high stands of sea level (Ortlieb, 1980; Mayer and Vincent, 1999; Burbank and Anderson, 2001; Keller and Pinter, 2002). Marine terraces cut into Pliocene strata and are found in the Loreto region at Punta El Bajo and on Carmen Island. The Loreto basin was uplifted in latest Pliocene and early Pleistocene time (McLean, 1988) and marine terraces near Loreto at Punta El Bajo record this uplift movement (Mayer and Vincent, 1999).

Uplifted marine terraces were surveyed along the southeast coast of Carmen Island at Bahia Marquer. Shells were collected along uplifted marine terraces for dating by amino acid racemization and a geochronology for the terraces was established. Two U-Th series ages of corals were used to calibrate the amino acid dating. Uplift rates were then calculated based on the geochronology of the terraces (Ortlieb, 1991; Wehmiller and Miller, 2000). Marine terraces at Punta El Bajo exhibit uplift rates on the order of 0.08 m/ka (Mayer and Vincent, 1999). Marine terraces at Bahia Marquer are compared to El Bajo for correlative purposes. Uplift rates on Carmen Island and in the Loreto region are important for understanding the geometry and timing of a segment of a rift.

Objective 3: Develop a tectonic model for Carmen Island

The results of the first two objectives of this study will yield a general tectonic understanding of the Carmen Island study area. Paleomagnetic results and marine terrace work illustrate that Carmen Island is tectonically active and has been active at least since

~6 Ma, and possibly since 12 Ma. Paleomagnetic results are compared with proposed models by Umhoefer et al. (2002) and this study presents a new tectonic model for the timing of the rotation of Carmen Island. Tectonic block rotations on Carmen Island are very complex and warrant further study. For the purpose of this study, Carmen Island is divided into two paleomagnetic domains and the tectonic model established for Carmen Island reflects varying amounts of movement of each paleomagnetic domain. Marine terrace data support tectonic uplift related to horst and graben normal faulting in the Gulf of California. Marine terrace data also support tectonic activity along the Loreto rift segment. Carmen Island has been tectonically active since mid-Miocene time and this study will support evidence for rotation and uplift of the island.

CHAPTER 2

TECTONIC AND GEOLOGIC SETTING

Evolution of the Gulf of California

The Gulf of California is a young oblique-divergent plate boundary where the Pacific plate is moving in a northwesterly vector relative to the North American plate (Figure 1.1) (Moore and Buffington, 1968; Karig and Jensky, 1972; Stock and Hodges, 1989; Lonsdale, 1989). The plate margin is characterized by rift segments and accommodation zones that contain both strike-slip and normal faulting (Axen, 1995).

There have been a number of proposed models for the evolution of the Gulf of California and all models point to either a two- or three-stage evolution from about 12 Ma to the present. Before the development of the Gulf of California, from about 25 to 12 Ma, western Mexico was a convergent plate margin where the Farallon and related microplates were subducted under the North American plate (Hausback, 1984; Stock and Hodges, 1989; Sawlan, 1991). Then, from about 12 to 8 - 6 Ma, the Gulf of California exhibited orthogonal rifting and was evolving into an oblique rift. From ~8 to 6 Ma to the present, the present oblique-divergent plate boundary formed (Stock and Hodges, 1989; Lonsdale, 1989). The present stage of oblique rifting started about 6 to 3 Ma when seafloor spreading began in the southern Gulf of California, largely transferring Baja California to the Pacific plate, although the interior of the Baja California peninsula remains a separate microplate (Dixon et al., 2000).

Pre-12 Ma Subduction and arc-related volcanism

A long narrow volcanic arc was produced by the eastward subduction of the Farallon plate beneath the North American plate during Mesozoic to mid-Cenozoic time. Oligocene to Miocene volcanic rocks related to the subduction of the Farallon plate are observed today along the eastern Baja California peninsula and east of the Gulf of California in the Sierra Madre Occidental (Figure 2.1) (Sawlan, 1991). The Sierra Madre Occidental volcanic field is composed of ~36-27 Ma rhyolite ash-flow tuffs that generally show a trend to increased alkalinity and are younger to the west (Figure 2.1) (Wark et al., 1990). By ~27 Ma, volcanic activity in the Sierra Madre ceased with the exception of a volcanic pulse in the southern portion around ~23-21 Ma (Figure 2.1) (Ferrari et al., 1999). The end of volcanic activity in the Sierra Madre is important because it coincides with the initial interaction of the North American and Pacific plates in southern California and the slowing of Farallon plate subduction (Atwater, 1970; Nicholson et al., 1994; Atwater and Stock, 1998).

Arc-related rocks found along the eastern Baja California peninsula are classified as the Comondú Formation and range in age from ~25-12 Ma (Heim, 1922; Hausback, 1984) and more recently modified to the Comondú Group by McFall (1968) and Umhoefer et al. (2001). The Comondú Group rocks are part of the volcanic arc and the forearc basin that formed west of the volcanic. The group is composed of minor lava flows, tuff breccia, volcanic breccia, volcaniclastic conglomerate, and fluvial and eolian sandstone (Figure 2.1) (Hausback, 1984; Sawlan, 1991; Umhoefer et al., 2001).

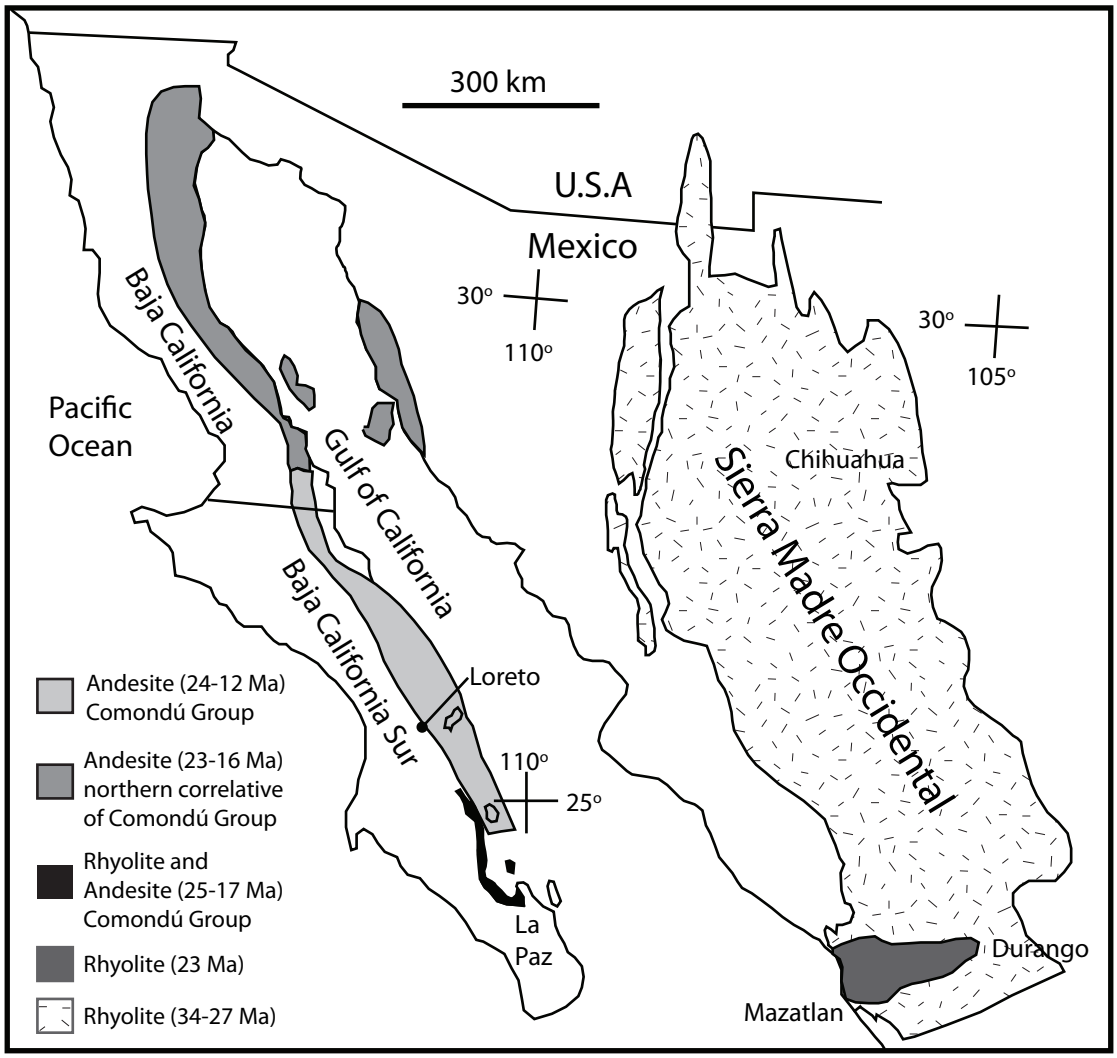

Figure 2.1: Map of northwest Mexico and Baja California peninsula showing Oligocene and Miocene volcanic rock belts (after Sawlan, 1991; Umhoefer et al., 2001; Drake et al., 2005).

At ~15 Ma, the migration of the East Pacific Rise to the subduction zone caused the north end of the Farallon plate to break apart into a series of "microplates" (Lonsdale, 1991). These microplates were either captured by the Pacific plate or subducted beneath the North American plate (Stock and Lee, 1994). Arc-related volcanism slowed as Farallon microplates were subducted beneath the North American plate. The rate of subduction of these microplates slowed and the ability of melt to ascend decreased, therefore slowing arc volcanism. Volcanism outlasted subduction by 1 to 2 m.y. as the mantle of the overriding plate continued to melt (Sawlan and Smith, 1984). Volcanism finally ceased in northern Baja California by ~17 to14 Ma and in southern Baja California volcanism continued until ~12 Ma (Hausback, 1984; Umhoefer et al., 2001). The cessation of volcanism can be closely traced to the southern migration of the Rivera triple junction because there was a general cessation of volcanism from north to south (Hausback, 1984; Sawlan and Smith, 1984; Lonsdale, 1991; Stock and Lee, 1994).

12 to 8/6 Ma Orthogonal Rifting

The southern movement of the Rivera triple junction and the coinciding activity of the Pacific plate around ~12 Ma mark a tectonic change at the continental margin of western North America. The migration of the Rivera triple junction produced the right-lateral, strike-slip Tosco-Abreojos fault zone west of Baja California (Figures 1.1 and 2.2). The relative Pacific-North American plate motion direction shows a distinct change in direction at ~8 Ma (Figure 2.2) (Atwater and Stock, 1998). There is discrepancy between a change in plate motion between 8 Ma and 6 Ma. Atwater and Stock (1998) place the change at ~8 Ma, whereas other researchers place the change

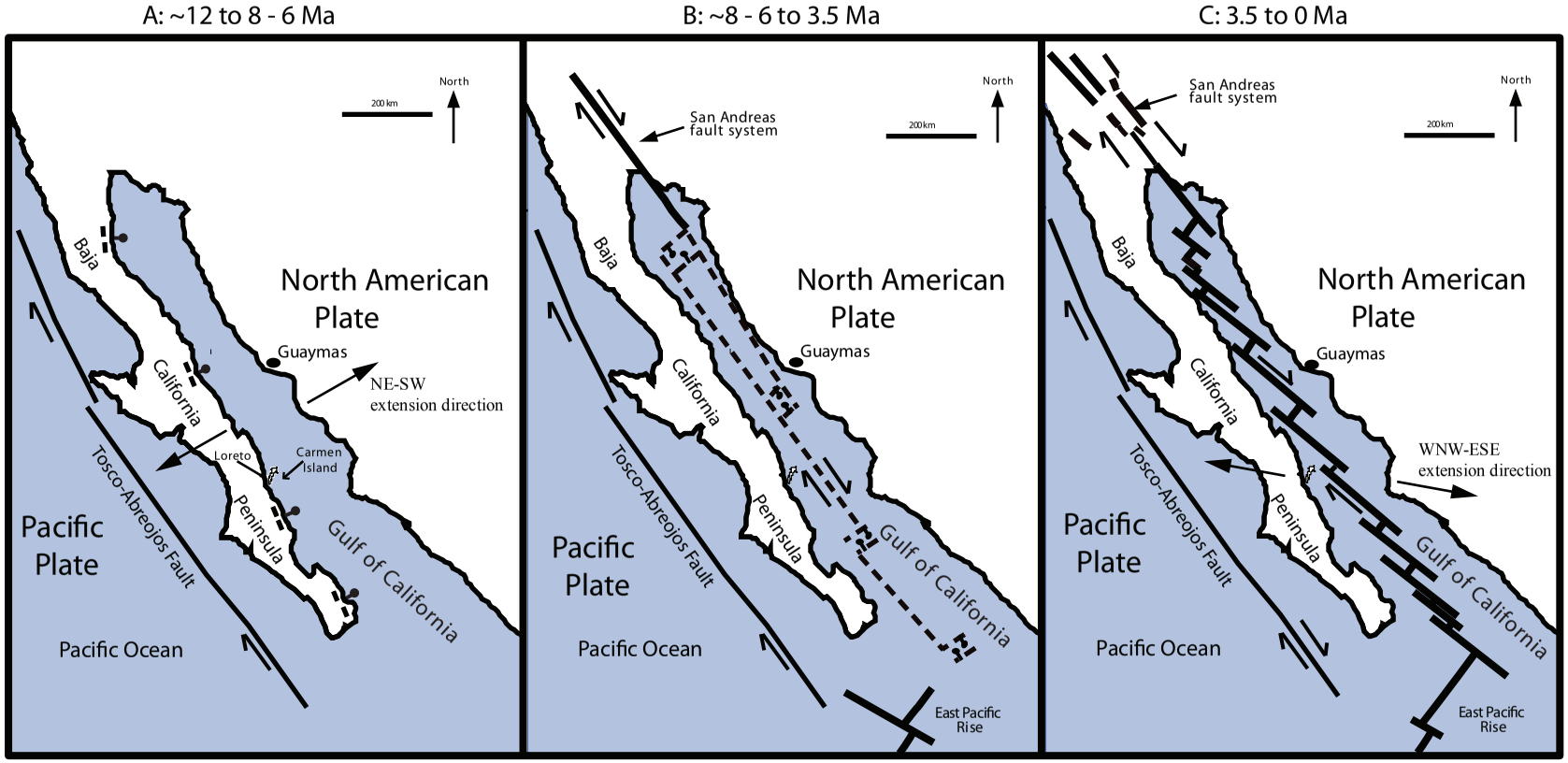

Figure 2.2: Tectonic evolution of the Gulf of California from ~12 Ma to present. A: Oblique rifting of North American plate and the Pacific Plate. B: East Pacific rise migrates into Gulf and faulting begins in proto-Gulf. C: Spreading ridges and strike-slip faulting dominate the present tectonic phase of the Gulf of California. Large black arrows indicate extension direction (after Lonsdale, 1989).

closer to ~6 Ma, coinciding with the propagation of the East Pacific Rise into the mouth of the Gulf of California (Lonsdale, 1989; DeMets, 1995). Prior to ~8 Ma, the relative direction of the Pacific-North American plate motion, ~286^{o}, was oblique to motion on the Tosco-Abreojos fault zone, which strikes ~310^{o} (DeMets, 1995; Atwater and Stock, 1998). The difference between the plate motion and Tosco-Abreojos fault was taken up in the present Gulf of California, which became a typical extensional rift system (Figure 2.2) (Stock and Hodges, 1989). Transtensional strain along the plate boundary was partitioned in two areas; the Tosco-Abreojos fault accommodated dextral strike-slip motion and north-northeast to west-southwest extension was accommodated by normal faults forming in the new Gulf of California (Figure 2.2) (Stock and Hodges, 1989; Oskin et al., 2001). These normal faults were located ~200 km east of the plate boundary and formed a series of grabens and half-grabens along the axis of the extinguished volcanic arc (Hausback, 1984; Stock and Hodges, 1989; Umhoefer et al., 2002; Fletcher et al., 2000). After 8 Ma, the relative Pacific-North American plate motion changed to more northerly.

6 Ma to Present Oblique Rifting

The modern system of transform faults and rift basins in the Gulf of California formed from 8 to 6 Ma to the present (Figure 2.2) (Lonsdale, 1989; Umhoefer et al., 2002). At ~8 Ma, the Pacific-North America plate motion in the southern Gulf of California shifted to ~305^{o}, more northwesterly (Atwater and Stock, 1998) Movement along the Tosco-Abreojos fault between ~6 and 3.5 Ma continued and a poorly understood transitional period transpired in the Gulf where strike-slip faulting was

occurring (Lonsdale, 1989). The propagation of the East Pacific Rise into the Gulf of California at 6 Ma marks the onset of strike-slip faulting in the Gulf of California (Figure 2.2) (Lonsdale, 1989). At this time, the Baja California peninsula became a separate "microplate" detached from the North American and Pacific plates (Lonsdale, 1989; Stock and Hodges, 1989), a situation that continues to today (Dixon et al., 2000).

The present tectonic phase began 3 to 6 Ma when spreading centers began to form in the Gulf of California, transferring Baja California to the Pacific plate (Dixon et al., 2000). Motion on the Tosco-Abreojos fault had been transferred into the Gulf of California as seen in the initial development of transform-spreading ridge systems (Figure 2.2). These spreading centers did not fully develop until ~3 Ma and the transform faults in the Gulf of California then linked to the San Andreas fault system to the north forming the "big bend" in the San Andreas transform fault in California. Dixon et al. (2000) used GPS data to show that acceleration of the Gulf Rise spreading rates since 3 Ma implies either recent or ongoing transfer of Baja California to the Pacific plate. Dixon et al. (2000) also suggested the possibility that some or all of the Baja California peninsula south of the Agua Blanca fault has not yet been fully transferred to the Pacific plate. The Baja California peninsula has experienced ~300 km of displacement northwestward since the initial onset of oblique rifting at ~6 Ma (Curray and Moore, 1984; Lonsdale, 1989; Oskin et al., 2001).

Loreto Rift Segment

A large rift system generally consists of several smaller rift segments on the order of 50 – 150 km long and are linked by transfer or accommodation zones

(Rosendahl, 1987; Axen, 1995). Rift segments begin as a series of unconnected normal faults that grow to form a continuous zone of extension (Figure 1.2) (Van der Pluijm and Marshak, 1997). Accommodation zones transfer strain from one normal fault system to the next and the geometry of an accommodation zone can be quite variable (Faulds and Varga, 1998).

Central Baja California Sur is an area marked by rift segments and accommodation zones (Figure 1.4). Axen (1995) recognized three particular rift segments in central Baja California; the Mulegé segment, the Loreto segment, and Timbabichi segment. Important to this study is the ~85 km long Loreto rift segment (Figure 2.3). The Loreto segment is bordered to the north by the Bahía Concepción accommodation zone and to the south by the Bahía Agua Verde accommodation zone (Figure 1.4). Normal faulting in the Loreto segment is dominated by down-to-the-east faults (Figure 1.4) (Umhoefer et al., 2002). The western boundary of the Loreto segment is a series of discontinuous structures with approximately 1-2 km of down-to-the-east offset. From north to south these structures are the northern monocline, the Loreto fault, the Nopolo structure, and the Escondido fault (Figure 2.3). The northern monocline is a continuation of the Loreto fault to the north and it continues the en echelon pattern of the Loreto fault (Figure 2.3) (Umhoefer et al., 2002). The northern monocline and Escondido fault mark the northern and southern extent of the Loreto segment and are important because there are no other down-to-the-east structures for tens of kilometers (Umhoefer et al., 2002).

Both the Escondido fault and the northern Loreto fault are found near the base of a steep Gulf escarpment and both are active faults (Mayer and Vincent, 1999; Umhoefer

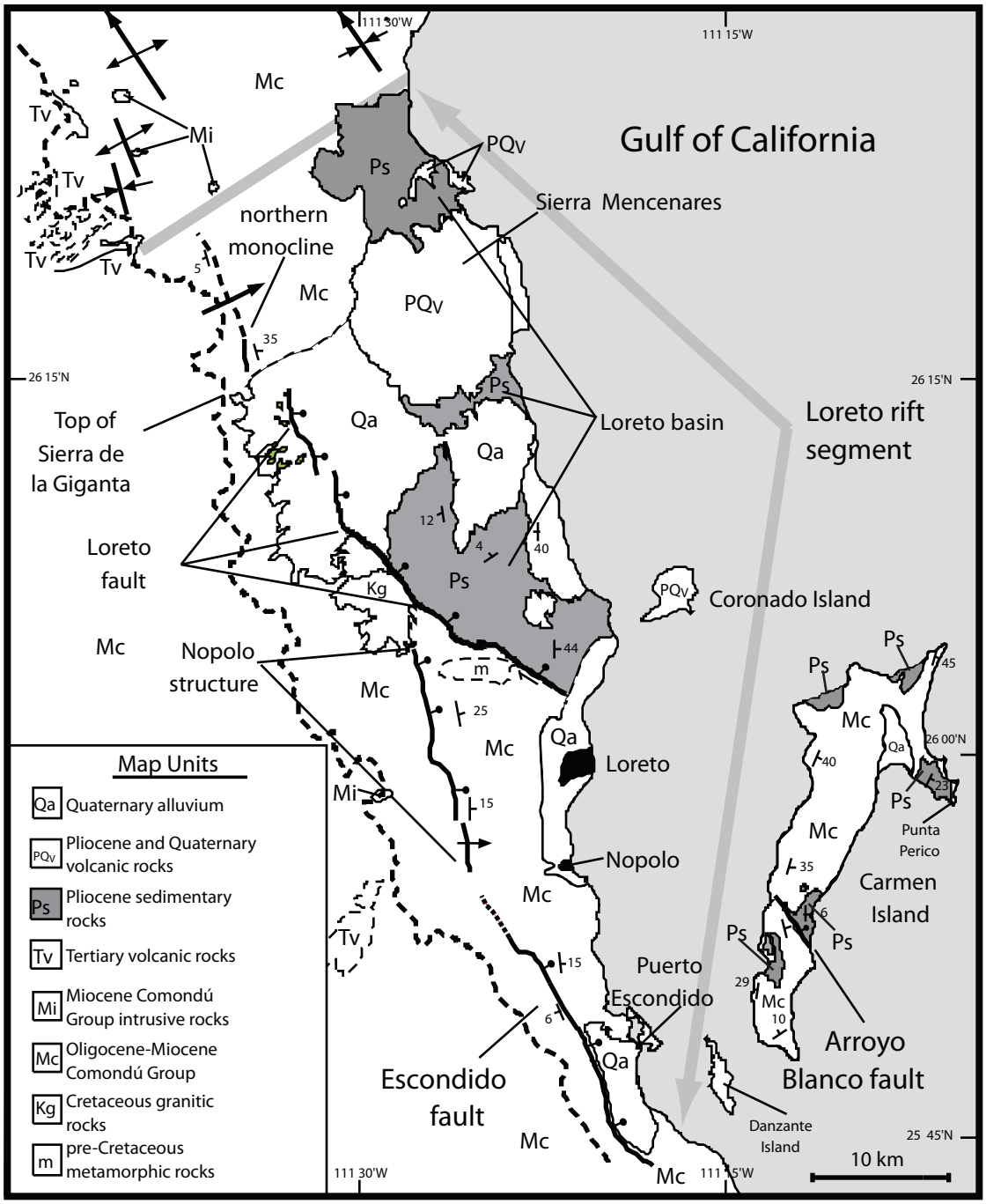

Figure 2.3: Generalized geologic map of the Loreto segment. The northern termination of the Loreto segment is the northern monocline and the southern termination is the southern portion of the Escondido fault (after Umhoefer et al., 2002).

et al., 2002). The topographic expression of the Gulf escarpment mimics the major structures that define the segment. The topographic relief is greatest near the Escondido fault and Loreto fault with a lower area behind the Nopolo structure and behind the accommodation zones (Umhoefer et al., 2002).

The Loreto rift segment is dominated by the Oligocene to Miocene Comondú Group rocks. Other units of the Loreto segment include pre-Cretaceous metamorphic rocks, Cretaceous granites, Pliocene sedimentary and volcanic rocks, and Quaternary alluvium (Figure 2.3). Rocks to the west of the segment are flat-lying to gently west-dipping volcanic and sedimentary rocks of the Comondú Group (Figure 2.3) (McLean, 1988; Umhoefer et al., 2002).

Another important structural feature in the Loreto segment is the Loreto basin. The Loreto basin is composed of Pliocene marine and non-marine sedimentary rocks associated with strike-slip and normal faulting along the Loreto fault. The basin is an oblique half-graben formed in the releasing bend of the Loreto fault (Dorsey and Umhoefer, 2000). Pliocene rocks are faulted against Cretaceous intrusive or Oligocene-Miocene volcanic and sedimentary rocks in the southwestern part of the basin, whereas the southeastern portion contains Pliocene sedimentary rocks overlying volcanic rocks of the Comondú Group.

Two volcanic centers are also found in the Loreto segment, the Sierra Mencenares and Coronado Island (Figure 2.3). Extensional tectonics during oblique rifting stages of the Gulf of California controlled the location and evolution of both volcanic centers (Bigioggero et al., 1995). The Sierra Mencenares is composed of

rhyolitic and andesitic domes and flows and Coronado Island is Quaternary basaltic andesite (Bigioggero et al., 1995).

The offshore portion of the Loreto rift segment contains a few islands including Carmen Island, 5-10 km east of Loreto; it is dominated by Miocene Comondú Group rocks (Figures 2.3 and 2.4). Pliocene marine and non-marine sedimentary rocks are found in five patches on the island, typically underlying Quaternary marine terraces (Figure 2.4). Bedding on Carmen Island strikes approximately parallel to the trend of the island. Miocene rocks on Carmen Island typically strike ~008^{o} and dip 18^{o} east (Umhoefer et al., 2002). Comondú Group bedding onshore strikes 328^{o} and dips 25^{o} to the northeast and the strike of the four main rift bounding structures is 335^{o}. A ~40^{o} clockwise difference distinguishes the mean bedding of Comondú Group rocks on Carmen Island from the mean bedding of Comondú Group onshore and the rift-bounding structures (Umhoefer et al., 2002). Gulf rift bounding structures include the right-lateral Farallon fracture zone, the Pescadero fracture zone, and the Tamayo fracture zone (Lonsdale, 1989).

Carmen Island is structurally divided into two domains by the Arroyo Blanco fault located on the southern portion of the island (Figures 2.3 and 2.4). The Arroyo Blanco fault is a northwest-striking, down-to-the-northeast dextral-normal fault and could be a discontinued segment of the Loreto fault (Vlad, 2001). Further exploration of Carmen Island will help to better understand timing of rifting of the Loreto segment. This study will use paleomagnetic data and survey data on marine terraces to constrain the timing of Carmen Island's movement and role in rifting of the Loreto rift segment.

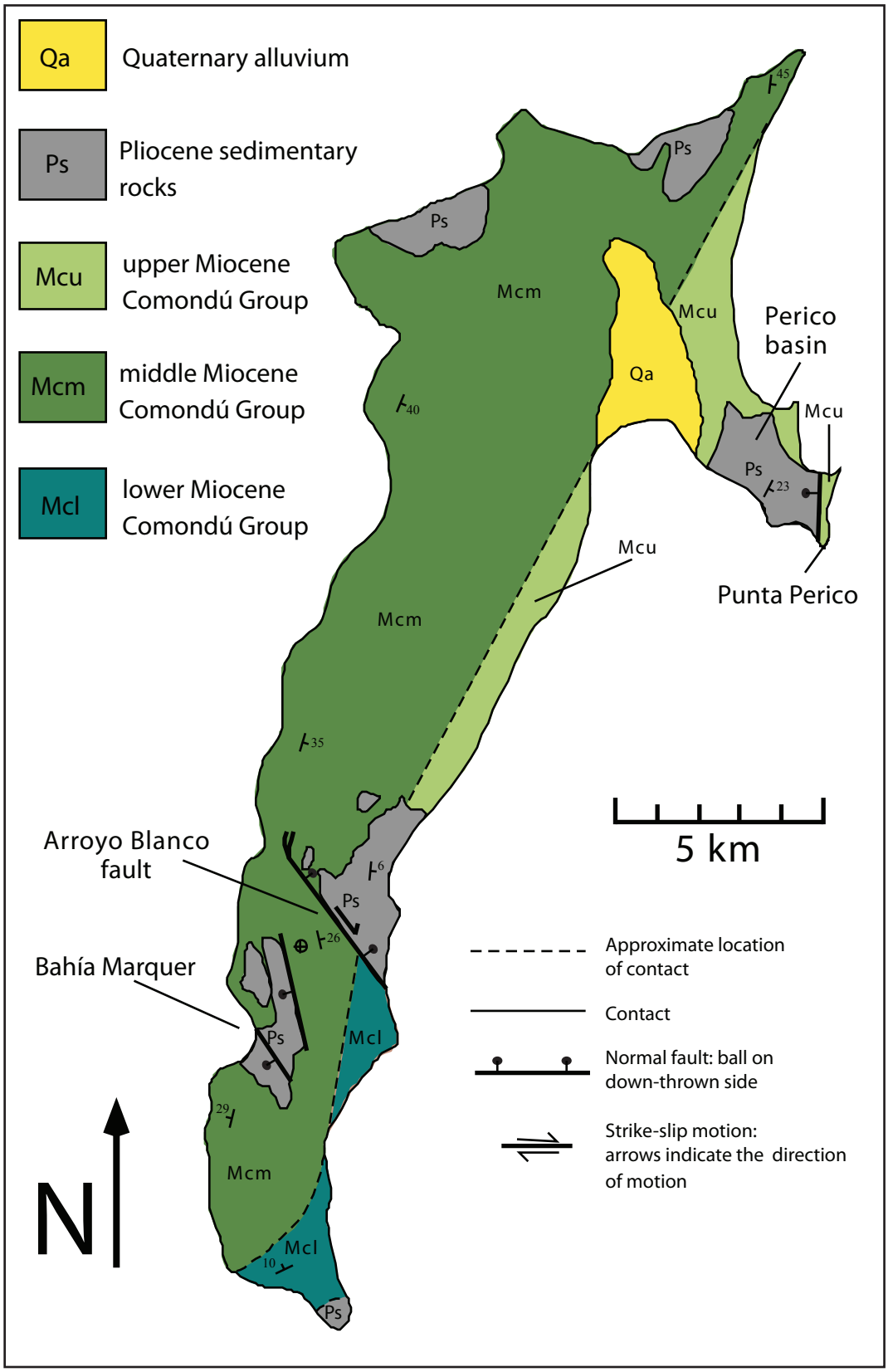

Figure 2.4: Geologic map of Camen Island (after Vlad, 2001).

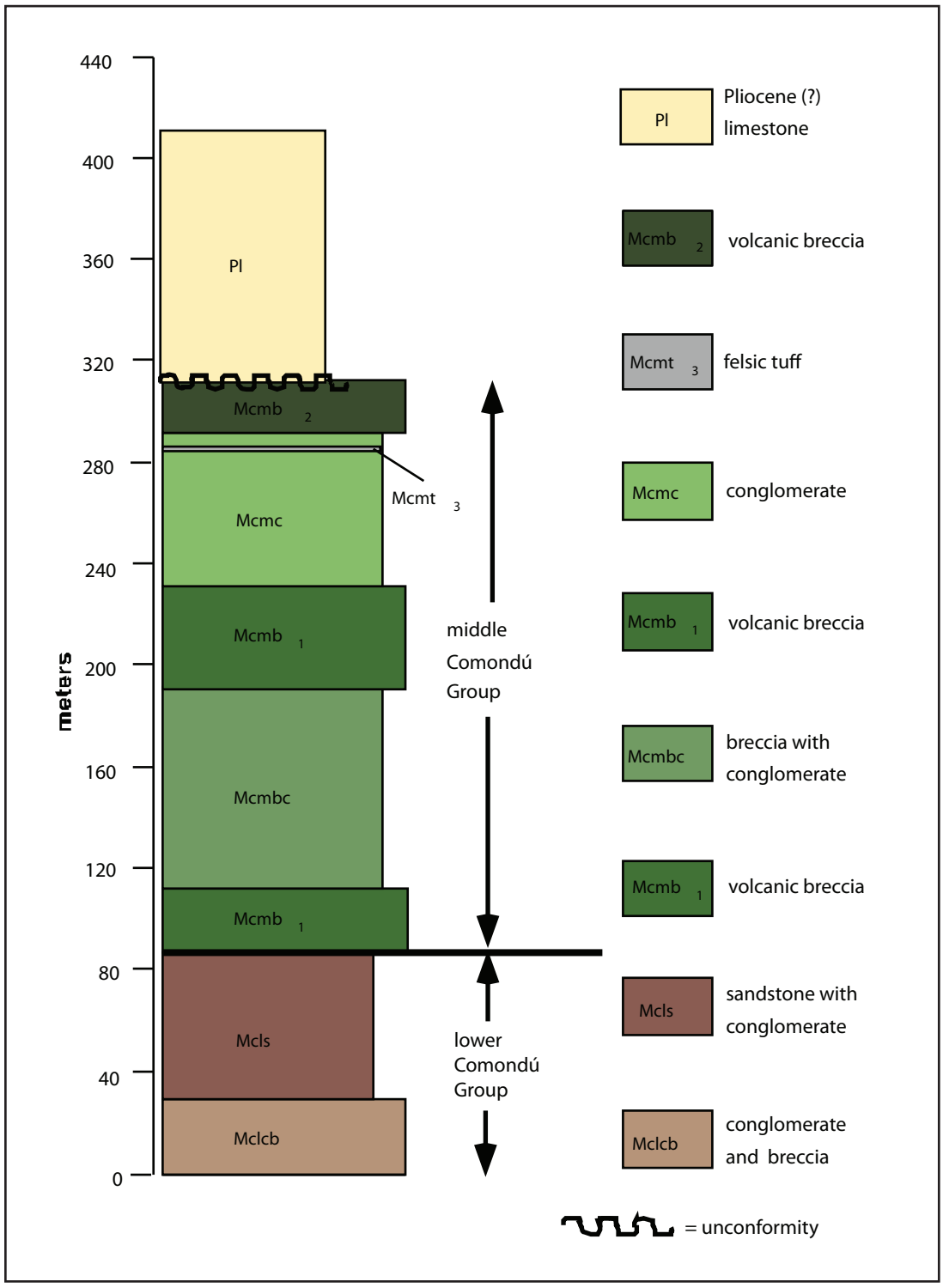

Figure 2.5: Stratigraphic column of map units on Carmen Island from the footwall of the Arroyo Blanco fault (from Vlad, 2001).

Carmen Island Geology

Carmen Island geology is dominated by Oligocene - Miocene Comondú Group (Figures 2.4 and 2.5) (Umhoefer et al., 2002). Comondú Group rocks have been described by a number of authors and include a wide range of facies. Heim (1922) first used the term Comondú Formation to describe sandstones and conglomerates near the village of Comondú. Heim also included thick breccia and lava flows of the Sierra de la Giganta in the Loreto region as part of the Comondú Formation. Beal (1948) further considered the Comondú Formation to include the entire section of Miocene sedimentary and volcanic rocks of the Sierra de la Giganta including alkalic basalts. McFall (1968) studied the area around Bahía Concepción and included all Oligocene-Miocene arc-related rocks in a single unit he deemed the Comondú Group. Then Gastil et al. (1979) limited the usage of Comondú Formation to include only the pre-Pliocene lavas in the Comondú area that overlie sandstones and conglomerates. Dement (1975) and Hausback (1984) described the Comondú Formation more closely to Heim (1922) and restricted the Comondú Formation to breccia, lava flows, tuffs and related volcaniclastic sedimentary rocks of the Sierra de la Giganta, but excluded the alkalic basalts described by Beal (1948). Usage of the term Comondú Formation has caused much confusion about exactly what to include when describing these rocks. Umhoefer et al. (2001) agreed with Dement (1975) and Hausback (1984) when looking at the stratigraphy of the Comondú Formation and argued that this formation should be revised to a group status following McFall (1968). Hence we arrive at the current nomenclature of the Comondú Group (Umhoefer et al., 2001).

The Comondú Group on Carmen Island is primarily composed of lower Miocene clastic and middle Miocene breccia and flow breccia units described by Umhoefer et al. (2001) and Vlad (2001). Carmen Island is structurally divided by the Arroyo Blanco fault and this fault constrains tilting of bedding on the island. Pliocene sedimentary outcrops are also found on Carmen Island and they are observed below uplifted marine terraces. Pliocene strata are found on the east, west, northeast, northwest, and southern tip of the island (Figure 2.4). A stratigraphic column of rocks found on Carmen Island from the footwall of the Arroyo Blanco fault is provided in Figure 2.5 and the following discussion summarizes those units from Vlad (2001).

Comondú Group conglomerate and breccia (Mclcb)

The oldest of the units found on Carmen Island is a purplish brown to grayish-purple matrix-supported conglomerate and breccia. The unit is ~30 m thick, the matrix is a lithic sandstone with gray to green andesite, sub-angular to rounded clasts. Beds of these conglomerates are defined by interbedded sandstones. Interbedded sandstones are red and are found both thinly and thickly bedded (Figure 2.5) (Vlad, 2001).

Comondú Group sandstone with conglomerate (Mcls)

Lower Comondú Group rocks consist of a 50-60 m unit of brown sandstone with conglomerate beds. The sandstone is well sorted, well bedded, and medium to coarse grained. Conglomerate lenses are moderately well sorted with clast sizes up to 20 cm (Figure 2.5) (Vlad, 2001).

Comondú Group breccia (Mcmb)

There are two different volcanic breccias found on Carmen Island. The first breccia is found throughout the sedimentary section ($Mcmb_1$) of the middle Comondú

Group and the other is found at the top of the middle Comondú Group ($Mcmb_2$, Figure 2.4). $Mcmb_1$ is a moderately to moderately well sorted breccia with a matrix dominated by angular, yellowish white andesite clasts containing hornblende, plagioclase, and pyroxene phenocrysts. Bedding within the breccia is diffuse and weathering of the breccia commonly results in tan conical shapes and a range of colors from tan, gray, to red-brown (Figure 2.5) (Vlad, 2001).

The second volcanic breccia, ($Mcmb_2$) is pinkish tan with thinly bedded sandstone. The matrix is a lithic-rich sandstone with hornblende phenocrysts. The dominant clast is andesite and clasts are subrounded and poorly sorted. Sandstone beds are coarse grained and well sorted (Figure 2.5) (Vlad, 2001).

Comondú Group breccia with conglomerate (Mcmbc)

This breccia is an 80 m thick section that grades from a basal sandstone up to a conglomerate, and then into a breccia. The sandstone is coarse grained and continues to coarsen upward into a conglomerate. The overlying breccia is reddish brown to purple with subrounded to subangular clasts. The matrix of both the conglomerate and the breccia is a lithic sandstone. This breccia unit changes facies rapidly vertically and it is breccia in some areas and conglomerate in other areas of Carmen Island (Figure 2.5) (Vlad, 2001).

Comondú Group conglomerate (Mcmc)

The upper section of the middle Comondú group is a poorly sorted, brown conglomerate with thin sandstone beds. Clasts are dominantly rounded andesite, and the matrix of the conglomerate is a coarse-grained sandstone. Thin sandstone beds are the only way to discern bedding in this unit (Figure 2.5) (Vlad, 2001).

Comondú Group Felsic Tuff (Mcmt)

A thin unit found within the upper conglomerate (Mcmc) in the footwall of the Arroyo Blanco fault is a non-welded felsic tuff. This tuff contains flattened pumice fragments and biotite crystals. A very distinctive characteristic of the tuff is the white, plagioclase lithophysae (Figure 2.5) (Vlad, 2001).

Pliocene Limestone (Pl)

Found throughout Carmen Island are Pliocene limestone outcrops that are cut by uplifted marine terraces. These limestone patches unconformably overlie Comondú Group rocks. Near the Arroyo Blanco fault, Pliocene limestone patches are juxtaposed against Comondú Group rocks. Limestone patches are observed as a white, coarse grained, sandy, limestone (Figure 2.5) (Vlad, 2001). In contrast, the northern Pliocene sedimentary patch, or Perico basin, is made of alternating units of 1) well stratified sandy pebble-cobble conglomerate with thin interbeds of bioclastic limestone and variable amounts of broken shell debris in the matrix and 2) well stratified sandy to pebbly bioclastic limestone (calcarenite and shell hash) commonly with thin sandstone and conglomerate interbeds (Dorsey et al., 2001). Stratification primarily consists of planar bedding with some low-angle cross-bedding and rare shallow channel geometries (Dorsey et al., 2001). There is a varying degree of mixing of coarse siliciclastic detritus and fragmented bioclastic carbonate, where an area could range from pure concentrations to equal mixtures of both components (Dorsey et al., 2001). Limestone patches located on more southerly Carmen Island at Bahía Marquer are a gray to tan calcarenite with abundant shell hash and debris. Conglomerates are widespread in upper sections, but

bedding is not distinct like in the Perico basin. Pleistocene shell and coral deposits commonly cover limestone patches.

Structural Aspects of Carmen Island

The dominant structural control on Carmen Island is the Arroyo Blanco fault. The Arroyo Blanco fault is probably Pliocene in age and is a dextral-normal fault that structurally divides the southern third of Carmen Island from the northern two-thirds (Figure 2.4) (Vlad, 2001). The Arroyo Blanco fault does not cut across the entire island, but it decreases in displacement and terminates in a transtensional zone of normal faults that strike north to northeast (Vlad, 2001). North of the Arroyo Blanco fault, Comondú Group is oldest to the west and beds primarily dip east (Figure 2.4). South of the Arroyo Blanco fault, however, Comondú Group is oldest to the east and beds dip west.

Other structural controls on Carmen Island can be grouped into two areas. First, along the northern part of the Carmen Island we see secondary faults that cut Miocene Comondú Group where there are no Pliocene strata (Umhoefer et al., 2002). These faults are dominantly northeast-striking, northwest-dipping normal faults and they record northwest-southeast extension (Umhoefer et al., 2002). The second group of faults on Carmen Island is located on the northeastern and southern parts of the island. Faults from this group are primarily mixed normal and dextral-normal faults with minor sinistral-normal faults (Umhoefer et al., 2002). The extension direction recorded by the second group of faults is east-west to east-northeast to west-southwest and does not vary with the age of the rocks (Umhoefer et al., 2002). The change in extension direction recorded

between the two groups of faults on Carmen Island suggests possible rotation of the island as will be discussed in chapter 5.

CHAPTER 3

ROTATION OF CARMEN ISLAND

As summarized in Chapter 2, most islands in the Gulf of California trend northwest-southeast parallel to the Gulf itself, and some islands trend north-south, perpendicular to the Pliocene-Quaternary extension direction (Figure 3.1). Carmen Island, however, trends north northeast-south southwest. Bedding in the Comondú Group on Carmen Island also strikes north-northeast to south-southwest, approximately 35^{o}-40^{o} clockwise from bedding in the Comondú Group on the adjacent mainland Baja California peninsula. Carmen Island's anomalous trend and bedding suggest vertical-axis rotation (Umhoefer et al., 2002).

Vertical-axis Block Rotation

Nur and Ron (1987) characterized a kinematic model where blocks bound by strike-slip faults would rotate. Many domains where block rotations have occurred have been identified in the western United States along the San Andreas fault system (Luyendyk et al., 1985) and the Las Vegas Valley shear zone (Sonder et al., 1994), near the Andean margin of South America (Laj et al., 1989; Roperch and Carlier, 1992), along the Marlborough fault system in New Zealand (Lamb, 1988; Roberts, 1995), and along strike-slip faults in northern Israel (Ron et al., 1984; Nur et al., 1989). Vertical-axis rotations are a fundamental component of continental deformation, particularly in environments with a component of strike-slip deformation (Ron et al., 1984; Nelson and Jones, 1987; Nur et al., 1989; Sonder et al., 1994). Traditionally, vertical-axis rotations

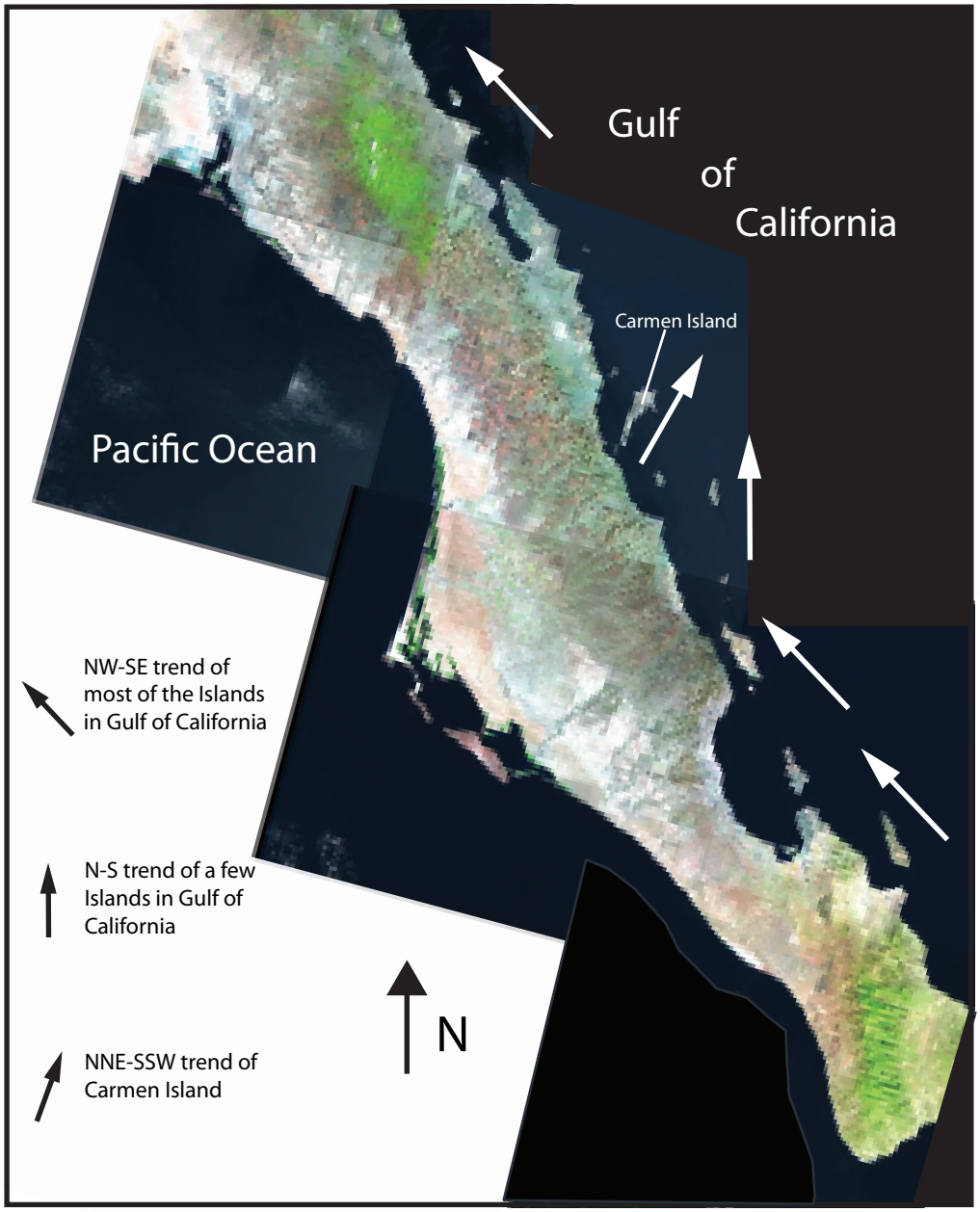

Figure 3.1: Satellite image of southern Baja California peninsula depicting orientation trends of islands in the Gulf of California. Satellite image highlights Carmen Island's anomalous trend.

have been determined by examining discrepancies between expected paleomagnetic inclinations and declinations with observed tilt-corrected inclinations and declinations (Ron et al., 1984). Vertical-axis rotations can be distributed over the scale of tens to hundreds of kilometers with proximity to the fault zone. Generally clockwise rotations occur in areas of dextral shear and counterclockwise rotations in areas of sinistral shear. Block rotation is dependent on the sense of fault slip, spacing of faults and blocks, orientation of the faults, and dimensions of the shear zone (Lewis and Stock, 1998). Predictions of rotation within block domains are often independently supported by paleomagnetic data.

On larger scales, hundreds to thousands of kilometers, block rotation predictions are consistent with the predicted viscous model for lithospheric deformation (Sonder et al., 1994). At smaller scales (10–100 km), however, the kinematics of block rotations are much more controversial (Sonder et al., 1994). Several models attempt to explain the degree and distribution of small block rotations. The two dominant models of small block rotations include block tectonics and ball bearing tectonics.

The block tectonic model proposes a more uniform block rotation, where displacement across a shear zone is accommodated by two bounding faults (Figure 3.2B). Blocks that experience rotation can be on the order of tens of kilometers wide and the amount of paleomagnetic rotation is the same throughout the rotated block (McKenzie and Jackson, 1983, 1986; Ron et al., 1984, 1986). When these blocks remain rigid, the model predicts a quantitative relationship between fault spacing, movement of slip, and block rotation (Figure 3.2B) (van der Pluijm and Marshak, 1997).

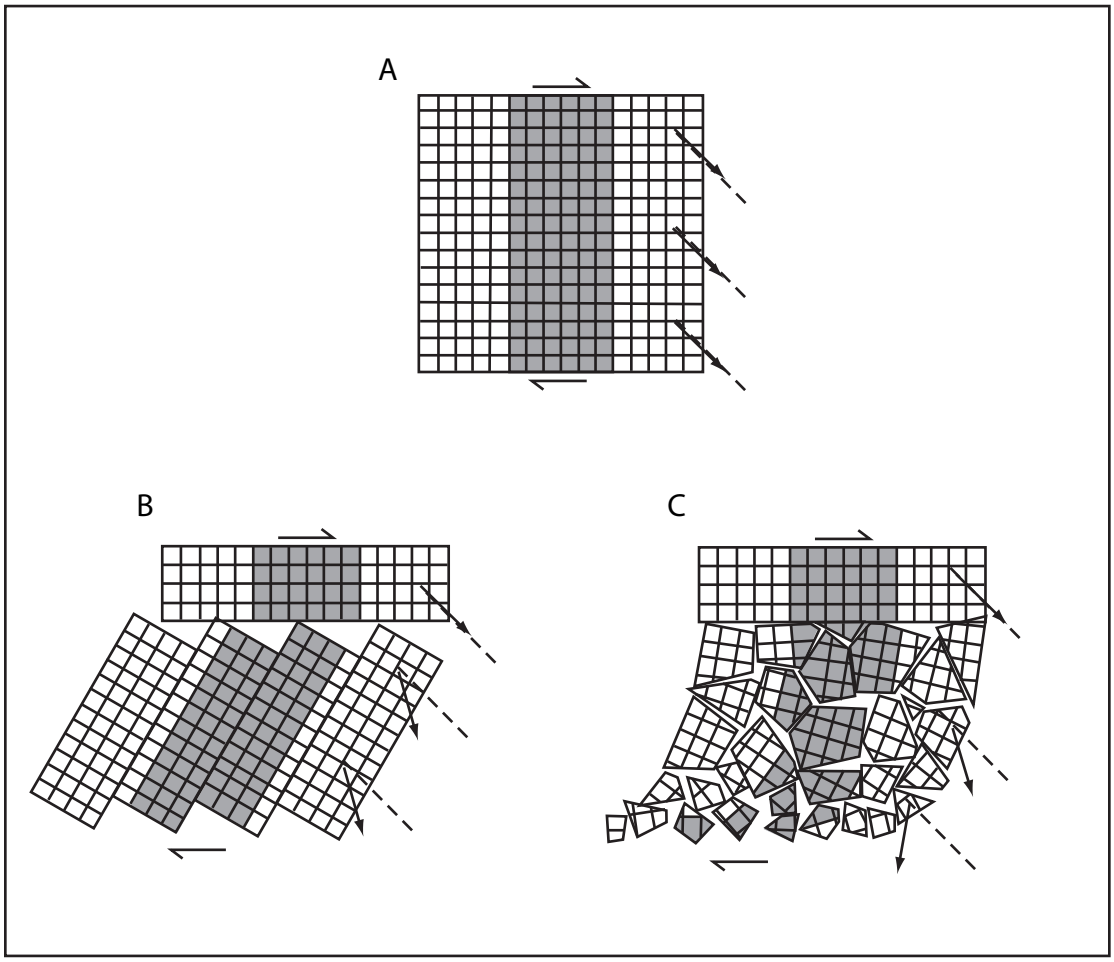

Figure 3.2: Diagram of deformation in right-lateral strike-slip setting. Relative rotations are designated by solid arrows relative to a reference dashed line. A) Undeformed crustal block. B) Block (domino) model, rotation is same for each block. C) Zone is broken into many smaller blocks that rotate independently of each other, but in the same direction (after van der Pluijm and Marshak, 1997; Nelson and Jones, 1987).

A more complex small block model is the ball bearing model (Figure 3.2C). Blocks experiencing rotation are typically on the order of a few kilometers or smaller and the amount of rotation experienced by each small block is directly related to the proximity of the block to the fault zone (Figure 3.2B) (Beck, 1976). Blocks closer to the fault zone experience more rotation and distant blocks rotate less. Rotations are regionally variable, but there is a uniform sense of rotation within a larger medium undergoing simple shear (Sonder et al., 1994). It is difficult in places to distinguish between the different models of block rotation because of geologic complexity, limited paleomagnetic sampling, and magnetic overprinting. In addition, the size and the distribution of individual rotating blocks are not known and the physical controls that determine block size are poorly understood. Therefore, we look for evidence of small block rotations through a paleomagnetic study of Carmen Island, Baja California Sur.

Vertical-axis block rotations have been recognized in the Gulf of California (Hagstrum et al., 1987; Hausback, 1984; Lewis and Stock, 1998). Spreading in the Gulf of California has caused clockwise rotation $<3^{o}$ and northward translation $\sim3^{o}$ of latitude of the entire Baja California peninsula (Stock and Hodges, 1989). In northeastern Baja California, paleomagnetic evidence from Lewis and Stock (1998) shows a 30^{o}-40^{o} clockwise rotation within their reference area. These clockwise rotations are interpreted by Lewis and Stock (1998) as resulting from simple shear being taken up by a combination of strike-slip and dip-slip faulting during extension at the plate margin. Shear may then have transferred northward to faults associated with the San Andreas fault system and contributed to the late Miocene to recent rotation of the Western Transverse Range in southern California (Lewis and Stock, 1998). Vertical-axis rotations

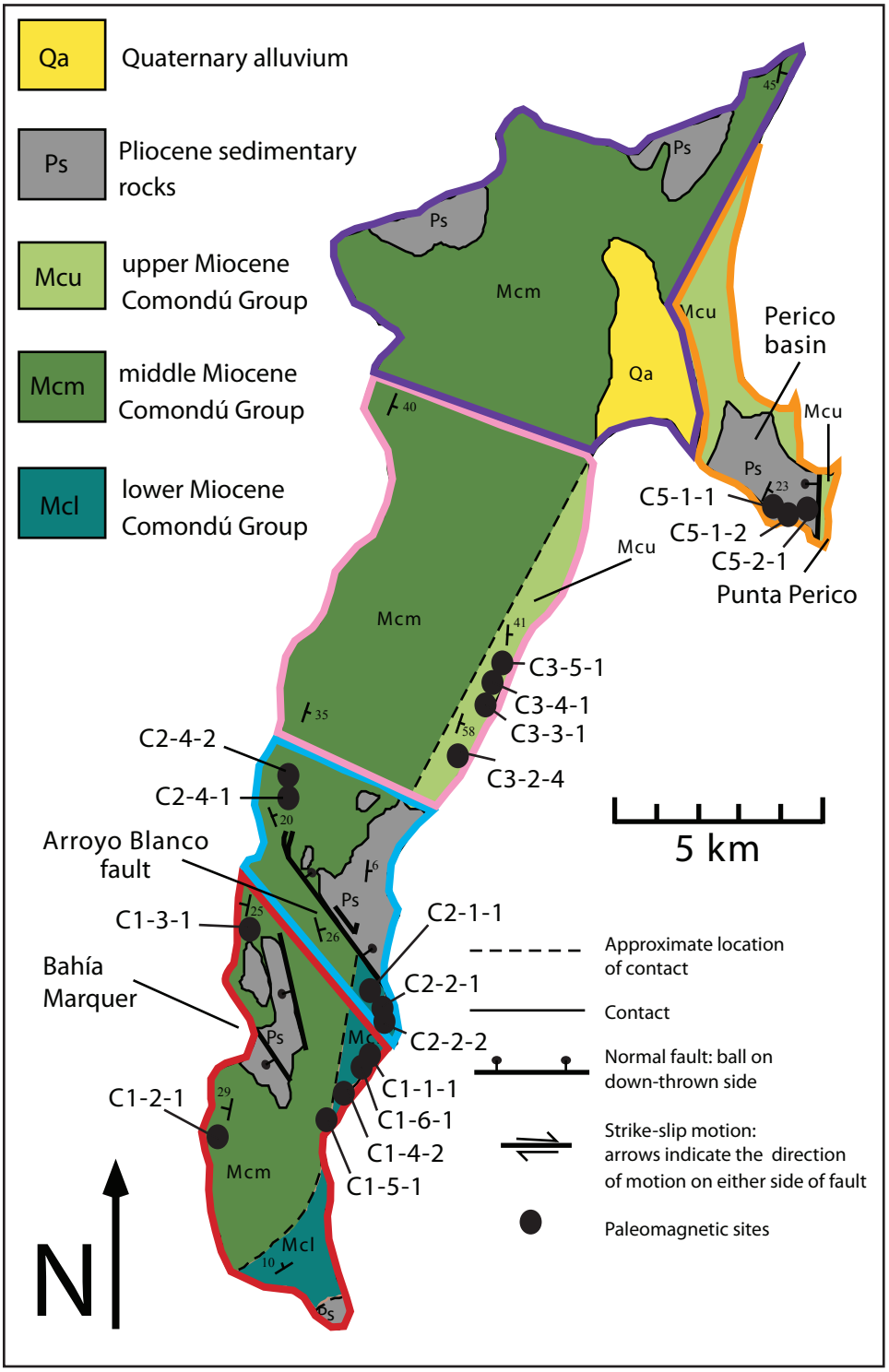

Figure 3.3: Geologic map of Carmen Island with paleomagnetic sampling locations. Paleomagnetic domains are designated by color outline; red = domain 1, blue = domain 2, pink = domain 3, purple = domain 4, and orange = domain 5 (geologic map after Vlad, 2001).

have been a part of the formation of the Gulf of California and work on Carmen Island further supports that observation.

Proposed Rotation of Carmen Island

Carmen Island exhibits an anomalous NNE-SSW trend. Umhoefer et al. (2002) suggested that Carmen Island may have rotated ~35-40^{o} clockwise. Bedding orientation in Miocene rocks on Carmen Island and onshore on the Baja California peninsula are consistent over large areas because deformation in these domains are dominated by simple normal faults which, do not change the bedding strike significantly (Umhoefer et al., 2002). Mean bedding in Miocene rocks on Carmen Island strikes ~008^{o} and dips 18^{o} E, approximately parallel to the trend of the island and was therefore used to check for rotations. Mean bedding in Miocene rocks onshore in the Loreto rift segment strikes 328^{o} and dips 25^{o} (Umhoefer et al., 2002). The average strike of the four main Loreto rift-bounding structures is 335^{o}. Comparison of the mean bedding on Carmen Island and onshore suggests ~40^{o} of clockwise rotation (Figure 3.4). Comparing mean bedding on Carmen Island to the average strike of rift-bounding structures suggests ~33^{o} of clockwise rotation (Figure 3.4) (Umhoefer et al., 2002).

Another explanation for anomalous bedding on Carmen Island could be attributable to normal faulting offshore. Normal faults have been mapped to the west of Carmen Island (Nava-Sanchez et al., 2001) (Figure 3.5). Normal faults may also be present to the east or southeast of Carmen Island based on recent bathymetric profiles (Umhoefer et al., 2002; Umhoefer, personal communication, 2005) (Figure 3.5). These faults exist underwater and there are limited data on their attitude. If normal faults to the

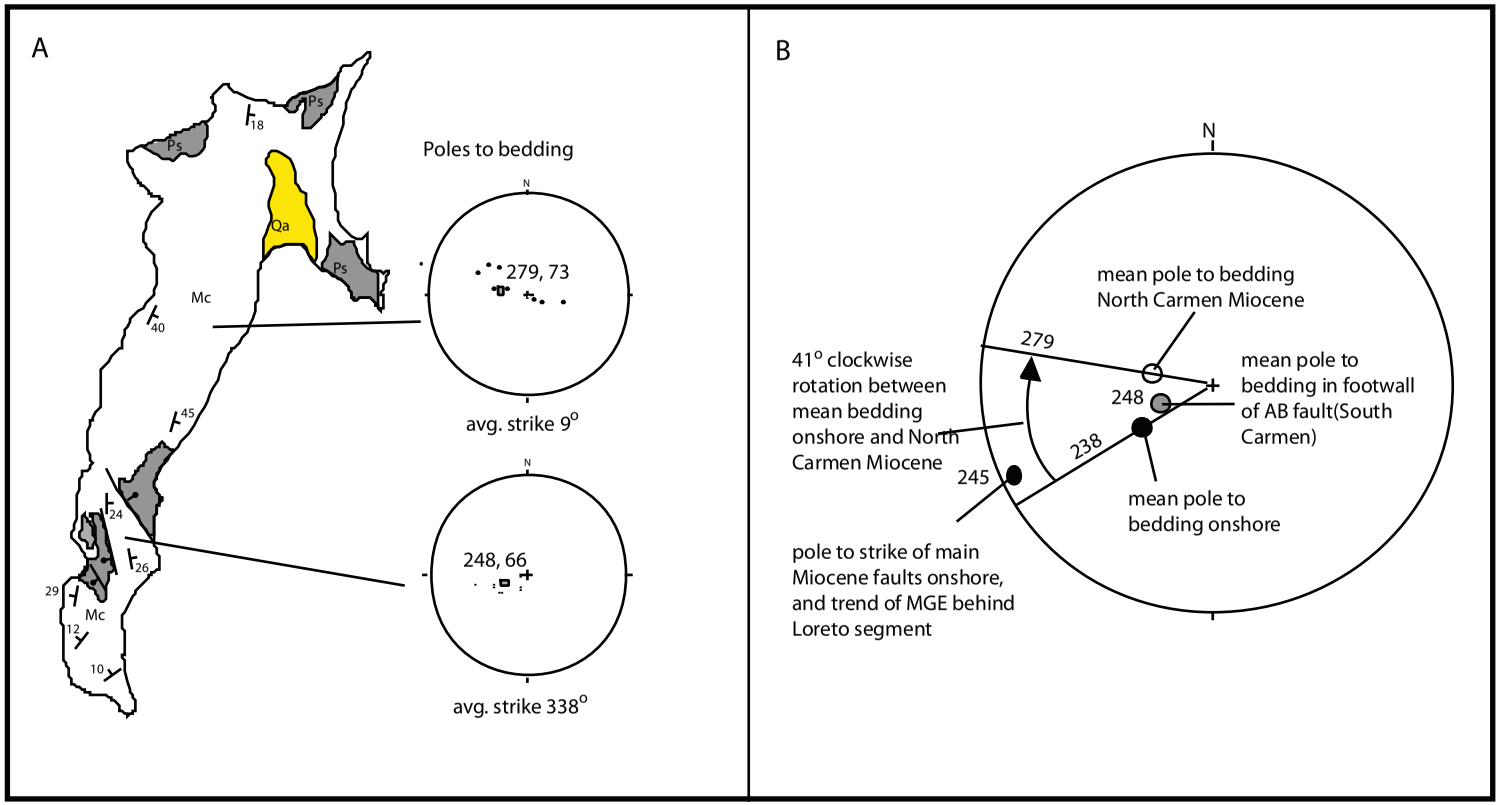

Figure 3.4: (A) Poles to bedding and average strike of bedding is illustrated for northern two-thirds of Carmen Island and near Arroyo Blanco Fault, southern Carmen Island. (B) Stereonet plot of difference between mean pole to bedding on Carmen Island and mean pole to bedding from onshore Loreto segment. MGE = Main Gulf escarpment (after Umhoefer et al., 2002).

northeast and southwest of Carmen Island strike in approximately the same NNE-SSW direction as the island itself, then beds on Carmen Island could have been deformed during Miocene - Pliocene time by normal faulting. The extension direction during mid to late Miocene time was WNW-ESE, approximately perpendicular to the proposed direction of normal faulting (Figure 3.5). The horizontal axis of deformation from these faults would strike NNE-SSW, perpendicular to extension direction, and Carmen Island would essentially be a horst oriented at an oblique angle to the adjacent mainland Baja California peninsula.

The movement of Carmen Island starts with the formation of proto-Gulf of California normal faults at ~12 Ma (Umhoefer et al., 2002). From 12 to 8/6 Ma, there was widespread normal faulting occurring along the margin of the Gulf of California in the Loreto region (Umhoefer at al., 2002). The regional extension direction during this time was east-northeast - west-southwest (Figure 3.5). Average extension direction measured by Umhoefer et al. (2002) for the Loreto region is 244^{o}-64^{o}. This is perpendicular to the 335^{o} overall strike of the main down-to-the-east structures that bound the Loreto segment.

At ~8 – 6 Ma, extension direction distinctly changed from northeast-southwest to west-northwest - east-southeast (Atwater and Stock,1998; Umhoefer et al., 2002). Large offset strike-slip faulting began in the Gulf of California during this time (Oskin et al., 2001). From 6 Ma to 2 Ma, the Loreto fault may have linked to a system of faults offshore that included northwest-striking dextral faults and north- to north-northwest-striking normal faults. Two of the dextral strike-slip faults linked to the Loreto fault may have been the early north and south Pescadero faults (Figure 3.5). The transtensional

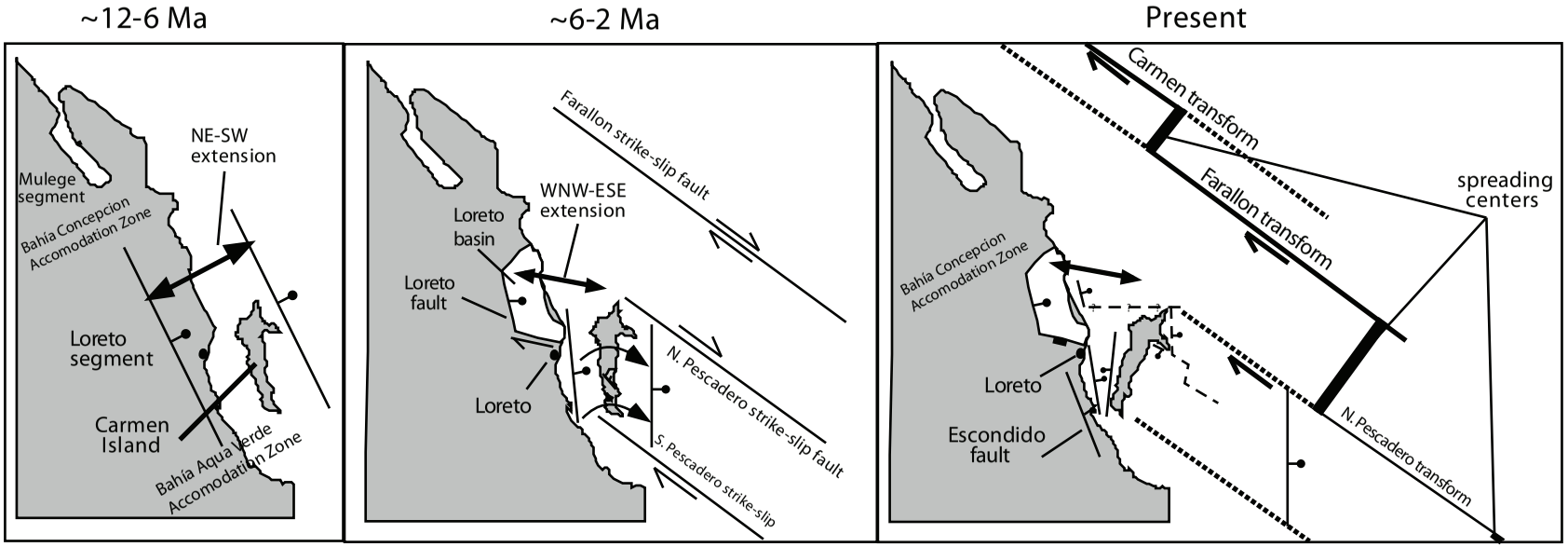

Figure 3.5: Evolution of the rotation of Carmen Island as proposed by Umhoefer et al. (2002). Double-sided arrows indicate extension direction. Solid lines are active faults and dashed lines are projections of active faults in the Gulf (after Umhoefer et al., 2002).

Loreto basin formed and Carmen Island rotated, which are both interpreted to have been linked to the formation of strike-slip faults in the Gulf of California (Figure 3.5). The north and south Pescadero strike-slip faults can be projected from modern transform faults to form two bounding structures between which Carmen Island is thought to have rotated (Figures 1.3 and 3.5) (Umhoefer et al., 2002). Carmen Island could then be treated as a block bounded by major strike slip faults to the north and south and bounded by normal faults to the east and west (Figure 3.5).

From ~2 Ma to the present, faulting has mainly jumped from the Loreto fault and related faults to modern transform faults and spreading centers in the Gulf of California (Umhoefer et al., 2002). Minor normal faults are still active near Carmen Island and near the onshore Baja California peninsula. The northern Loreto and Escondido faults are still active today. Presently, Carmen Island is experiencing uplift between normal faults as a horst (Figure 3.5) (Nava-Sanchez et al., 2001). Sub-bottom surveys using ground-penetrating echo-sounders from Nava-Sanchez et al. (2001) showed active normal faults at the peninsular margin. The extension direction continues in a west-northwest to east-southeast manner, but Carmen Island is interpreted to have stopped rotating and is only experiencing uplift (Umhoefer et al., 2002).

Carmen Island's anomalous trend and geologic history suggest that the island rotated during Miocene to Pliocene time. Bedding on the island and onshore support evidence of rotation, but paleomagnetic work is necessary to test this idea. This study will present the results of paleomagnetic work on Carmen Island and develop a structural evolution of the island.

Paleomagnetic Sample Collection

I divided Carmen Island into structural domains for paleomagnetic analysis. Five domains were defined, one south of the Arroyo Blanco fault and four north of the fault (Figure 3.3). Nomenclature for naming samples was based on five structural domains (Figure 3.3). Twenty-one sites were originally sampled. Paleomagnetic sampling began by drilling cylindrical cores from rock samples at each site; after sampling three locations, the paleomagnetic drill seized up and was no longer operable. Therefore, oriented rock samples were collected and brought back to Flagstaff, AZ, for drilling of 4 to 12 cores per sample. Eighteen oriented rock samples were collected from Carmen Island (Table 3.1). One large oriented rock sample using a Brunton compass was taken from each site (Table 3.1). Only one oriented rock sample was collected from a single rock outcrop and multiple samples from the same outcrop were not collected. Multiple samples were not taken in either the horizontal or vertical direction at a single site. Therefore, possible secular variation within a single site was not eliminated with certainty.

The attitude and azimuth of strike was recorded for a unique face of each sample. Many different rock types were sampled including volcanic sandstones, tuffaceous sandstones, volcanic breccia, and Pliocene sedimentary rocks. The original plan was to sample red volcanic sandstone beds, which would have the most stable magnetic remanence and record a magnetic signature that has been averaged out over thousands of years of deposition. The plan, however, changed to sampling rock types that were accessible and had good bedding surfaces. Magnetic limitations of rocks that were sampled include inherent limitations found in certain lithologies such as tuffs and breccia.

Tuffs record a near instantaneous magnetic record and therefore could be recording some magnetic anomaly. The natural remnant magnetization of a tuff is not reflective of averaging over many thousands of years. A volcanic breccia is another rock type that has inherent problems with its magnetic signature. Breccia are composed of clasts that may carry a secondary magnetic signature and are not preferred for paleomagnetic analysis.

Sampling was limited by transportation around Carmen Island and access to rock exposures. A small inflatable water craft was used to travel the south and southeastern sides of the island. This watercraft was also used to collect samples from the northern Punta Perico area, but travel was too dangerous on the northeastern and northwestern sides of the island. Hiking allowed for sampling of the western side of Carmen Island, but oriented rock samples had to be hiked back to base camp and therefore only limited sampling could occur.

Of the 18 oriented rock slab samples collected, six samples were collected south of the Arroyo Blanco fault in paleomagnetic domain one, six samples came from the middle of the island in paleomagnetic domains two and three, three samples were from the northern part of the island in paleomagnetic domain five, and three samples were taken from onshore the Baja California peninsula (Figure 3.3). Each sample collected was considered a single site.

The six samples taken from south of the Arroyo Blanco fault were primarily red to red-brown volcanic sandstones (Figure 3.6). One of the samples (C1-4-2) was a gray to grayish-purple volcanic breccia. Samples collected from the middle portion of Carmen Island, where exposures and access to the exposures were good, were a volcanic sandstone and a volcanic breccia. Four samples were collected from middle-eastern

Carmen Island and included red to tan-brown volcanic sandstone, gray volcanic sandstone, gray to green tuffaceous sandstone, and pink to white tuff (Figures 3.7 and 3.8). Samples from northern Carmen Island were limited to Pliocene mudstone and marlstones from the Perico basin (Figure 3.3).

Table 3.1: Paleomagnetic site locations, bedding attitude, and rock type.

Site #	UTM North	UTM East	Bed Strike degree	Dip Direction degree	Bed Dip degree	Rock Type
C1-1-1[a]	0481702	2860631	229	319	01	Volcanic Sandstone
C1-2-1	0476774	2858305	160	250	52	Volcanic Sandstone
C1-3-1[b]	0479768	2860677	162	252	25	Volcanic Sandstone
C1-4-2	0480749	2859749	275	05	44	Volcanic Breccia
C1-5-1[c]	0480322	2859585	115	205	10	Volcanic Breccia
C1-6-1[d]	0480888	2859975	FLAT LYING	180		Volcanic Sandstone
C2-1-1[a]	0481593	2861652	247	337	02	Volcanic Breccia
C2-2-1	0481630	2861633	300	030	10	Volcanic Sandstone
C2-2-2[a]	0481630	2861633	335	065	54	Volcanic Sandstone
C2-4-1	0478344	2863255	050	140	20	Volcanic Sandstone
C2-4-2	0478575	2863268	325	055	45	Volcanic Sandstone
C3-2-4	0484335	2867734	020	110	58	Sandstone
C3-3-1	0484289	2867869	015	105	44	Tuffaceous Sandstone
C3-4-1	0484285	2867925	001	091	41	Tuff
C3-5-1	0484290	2867975	321	051	53	Welded Tuff
C5-1-1	0492526	2872557	080	170	04	Mudstone/Marlstone
C5-1-2	0492526	2872557	115	205	05	Mudstone/Marlstone
C5-2-1[d]	0493028	2872583	144	234	44	Mudstone/Marlstone
SJ1-1	0452978	2872995	350	080	25	Volcanic Sandstone
SJ1-2	0452978	2872995	350	080	25	Volcanic Sandstone
E1-2[b]	0465797	2853469	327	057	45	Sandstone

[a] Drill core diameter too large
[b] No stable primary magnetization
[c] Could not drill into rock face geometry
[d] Broke while drilling

Figure 3.6: Red to red-brown volcanic sandstone of the lower Comondú Group, site C2-4-1.

Figure 3.7: Green tuffaceous sandstone of the middle Comondú Group, site C3-3-1.

Figure 3.8: Pink to white welded tuff of the middle Comondú Group, site C3-4-1.

Figure 3.9: Pliocene beige mudstone/marlstone from the Perico basin, site C5-1-1.

Paleomagnetic sampling on the Baja California peninsula was necessary to establish a local control by which samples on Carmen Island could be compared. Two samples of red volcanic sandstone of the Comondú Group were collected along San Javier road about 10 km west of Loreto (Figures 1.4 and 3.10). Samples from San Javier road were collected west of all major normal faults of the Loreto rift segment and beds were near flat lying. Therefore, I felt San Javier road sites were stable and a good reference point from the Baja California peninsula. A sample of red-brown volcanic sandstone was taken near Puerto Escondido (Figure 1.4). Samples from the Baja California peninsula are similar in age to samples from Carmen Island and all samples except Pliocene mudstone/marlstones are from the late Oligocene to middle Miocene Comondú Group (Figures 1.4 and 3.3).

Figure 3.10: Red volcanic sandstone of the Comondú Group found along San Javier road, site SJ1-1.

Laboratory Procedures

In the laboratory, all samples were set in plaster of paris so the oriented face was horizontal. Each sample was drilled into at 90^{o} using a drill press and paleomagnetic drill bit. As many as four to twelve cores were drilled from each rock sample. Cores were named with the sample name followed by an alphabetical letter. Multiple cores from a single rock sample signified a single site. During the drilling process, a sample of mudstone, C5-2-1, was too friable and crumbled when it was drilled and therefore it was not used in the analysis (Table 3.1). Similarly a sample of volcanic sandstone, C1-6-1, cracked into many pieces and was not used (Table 3.1). A sample of volcanic breccia (C1-5-1) was not drillable due to the shape of the sample (Table 3.1). Three of the samples that were originally drilled on Carmen Island, C1-1-1, C2-1-1 and C2-2-2, were also discarded because the drill used on Carmen Island produced cores of greater diameter than the paleomagnetic equipment could process (Table 3.1). Cores that were viable were then analyzed in the paleomagnetic laboratory at Northern Arizona University.

All demagnetization and measurements were carried out using a Molespin minispin magnetometer and an alternating field (AF) shielded demagnetizer. AF demagnetization was performed at varying steps, but aimed at 10% steps according to total magnetic intensity (Butler, 1992). Before analysis began each day, the Molespin magnetometer was calibrated to the given calibration sample, 843 $mA.m^{-1}$. A maximum of 1000 oersteds demagnetization was applied to core samples and a minimum of 200 oersteds was necessary to obtain stable primary magnetization. Each core was subjected

to demagnetization according to its rock type. Marlstones and mudstones required fewer demagnetization steps, while more indurated volcanic rocks required more. Volcanic rocks have a high magnetic stability compared to marlstone and mudstones and magnetic components of rocks with high magnetic stability can only be removed at high levels of demagnetization.

During the demagnetization process, some cores exhibited magnetic properties that were not consistent with primary magnetization. Three samples did not show stable magnetization and were therefore discarded. Of the eighteen original samples, thirteen had good cores and stable magnetic properties, and so were used for the paleomagnetic analysis.

Paleomagnetic Sample Analysis

Stable primary magnetization was achieved when all secondary magnetization was removed and only scatter plus primary magnetization was remaining. This was recognized by examining Zijderveld diagrams (Z-plots) for each core and noting properties of each core such as Z-plot vectors that pointed toward the origin. As secondary magnetizations were removed, the Z-plot vector would point more toward the origin, revealing the primary magnetization (Figures 3.11 and 3.12). Intensity diagrams were included with Z-plots to aid in determining primary magnetization. Intensity curves show a parabolic curve and primary magnetization usually occurs as the parabolic curve begins to flatten. Primary magnetization was based on the two criteria of Z-plot properties and intensity properties (Butler, 1992). Most cores from a single sample exhibited the same demagnetization patterns (Figure 3.11). Therefore, a measured

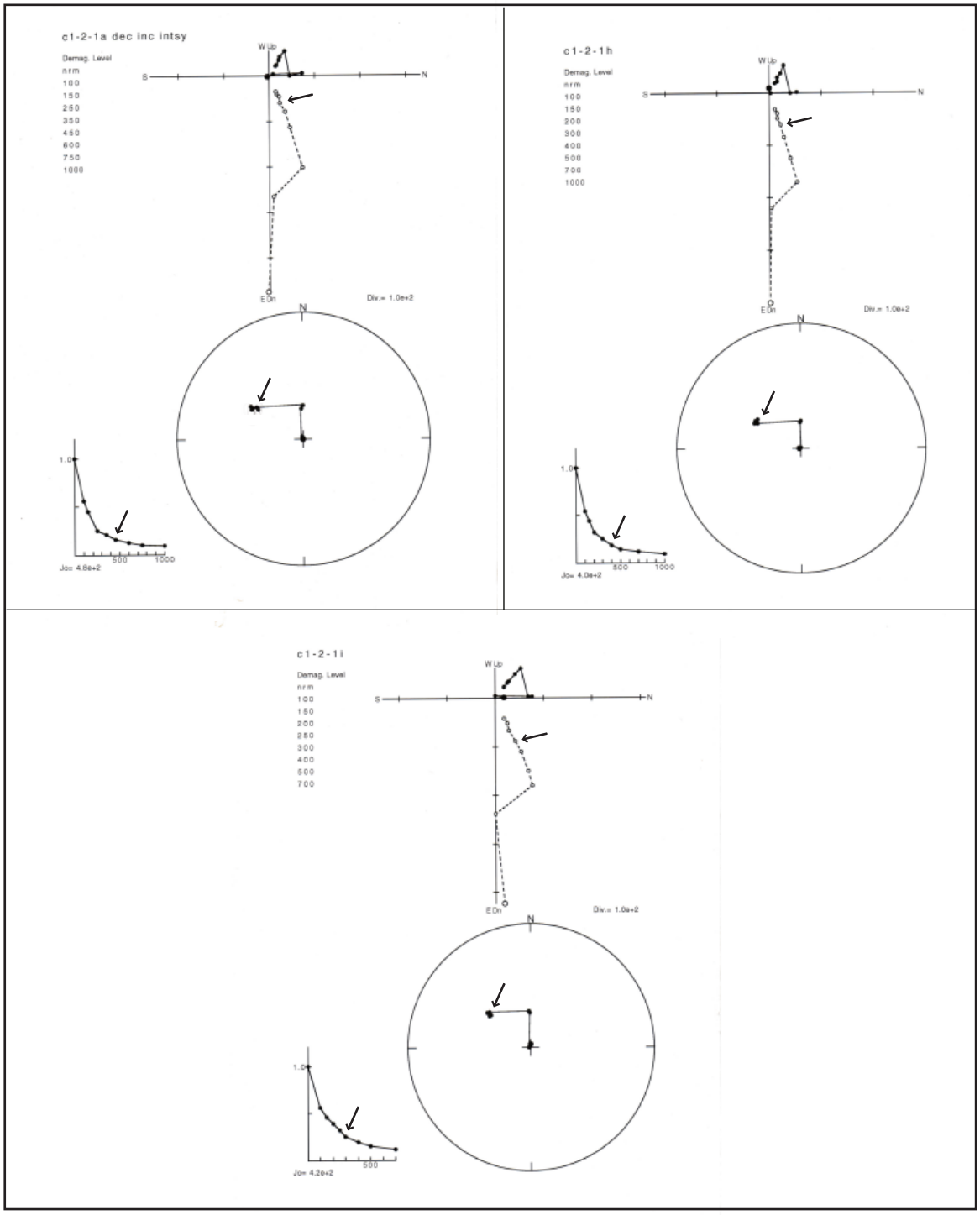

Figure 3.11: Ziljderveld diagrams with intesity curves for three cores (a, h, i) from sample, C1-2-1. Cores demagnetization properties were very consistent within this sample. Black arrows indicate demagnetization level where all secondary magnetization was stripped away and natural remnant magnetization was reached.

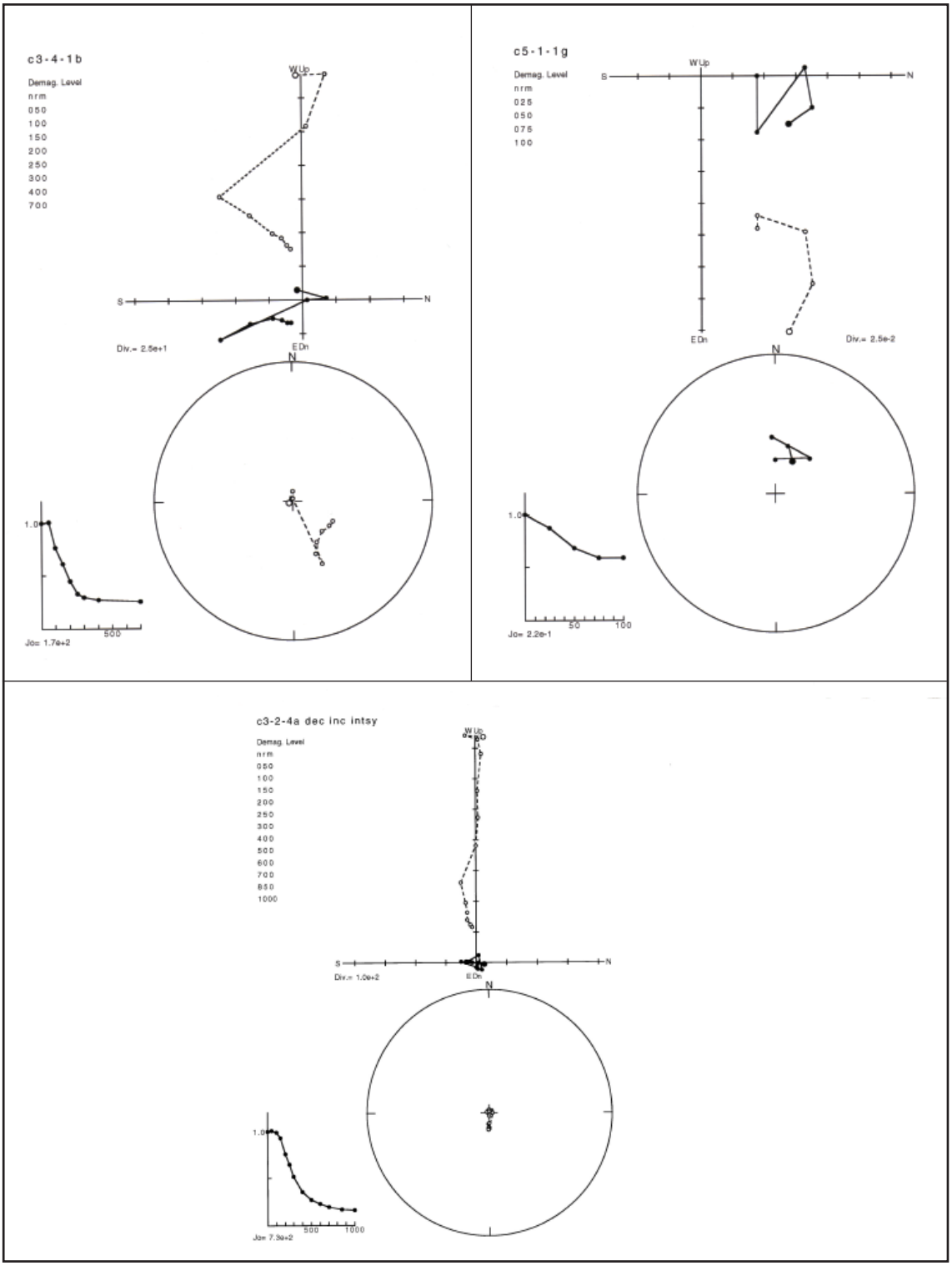

Figure 3.12: Ziljderveld diagram with intensity curve for demagnetization for one representative core from three different samples. C3-4-1b is a core from a green to white tuff, C5-1-1g is a core from a mudstone/marlstone, and C3-2-4a is from a red-tan sandstone.

magnetic intensity and demagnetization level during the demagnetization process was the indicator of primary magnetization. For example, sample C1-2-1 showed its primary magnetization when the magnetic intensity dropped to ~60% of original intensity and that coincided with a demagnetization level of about 400 oersted. Therefore, the inclination and declination at 400 oersted and ~60% intensity level was designated as primary magnetization for C1-2-1 and these criteria were applied to all cores from that sample. The same criteria were used to determine the level of demagnetization for each sample and intensity of primary magnetization (Figure 3.11).

Inclination and declination were recorded for each core's primary magnetization (Table 3.2) and all cores for a given sample were plotted on a pole diagram and the mean pole with 95% confidence interval was recorded. All cores from every sample were used in the analysis and there were not any cores discarded after demagnetization. The only cores not used were ones that were cut too short and would not sit in the molespin magnetometer correctly. Within each sample, cores behaved similarly, probably because they were drilled so close to one another (within a few centimeters). The average declination and inclination for each sample were next entered into a tilt correction program to correct for bedding attitude. In this manner, all samples were returned to paleo-horizontal and could be compared to one another (Figure 3.13).

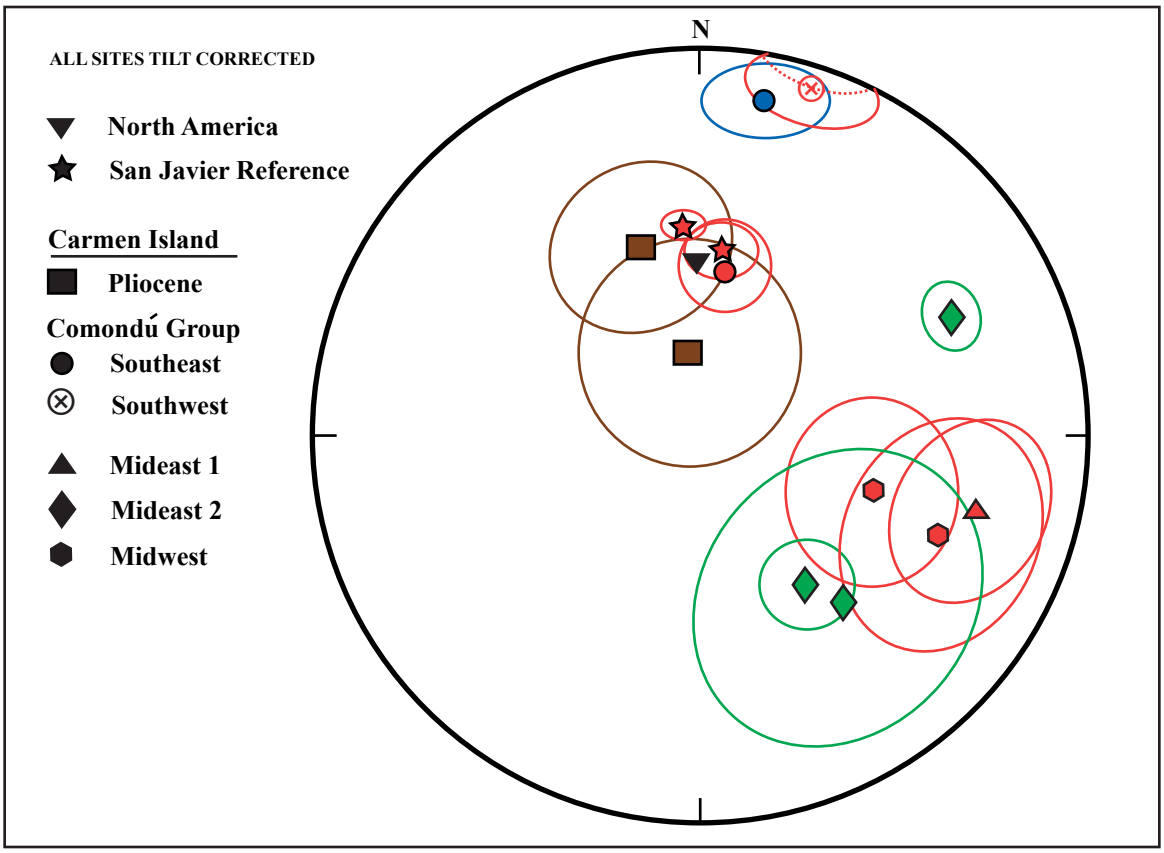

Figure 3.13: Pole position of mean tilt-corrected paleomagnetic analysis of sites and references. Colors indicate rock type; red = volcanic sandstone, brown = mudstone/marlstone, blue = breccia, and green = tuff. Cone of 95% confidence is shown as circle.

Table 3.2: Tilt corrected magnetic poles for sites and individual cores. All cores from each sample were used in calculated average declination (Dec) and inclination (Inc) and no cores were discarded. Difference in declination (Dec) is with respect to San Javier road reference site.

Tilt Corrected								
Site #	Rock Type	Core #	Dec degrees	Inc degrees	alpha 95	k	R	Difference in Dec degrees
C121	Volcanic sandstone	Average	17.5	5.6	10.2	26.4	8.7	25 +/- 16
		121a	13.2	2.9				
		121b	28.7	-0.6				
		121c	12	5.2				
		121d	344.6	11.6				
		121e	20.2	6.8				
		121f	24.6	3				
		121g	41.6	7.3				
		121h	9.7	6.9				
		121i	21.3	6				
C142	Volcanic breccia	Average	11.2	12.1	10	24.5	9.6	10 +/- 10
		142a	21.4	24.5				
		142b	16.8	13.6				
		142c	35.5	12.6				
		142d	346.4	22.8				
		142e	18.6	14.2				
		142f	14.5	2.9				
		142g	14.7	6.2				
		142h	10	15.2				
		142i	348.6	3.2				
		142j	4.9	2.2				
C221	Volcanic sandstone	Average	8.8	53.6	9.5	50.9	5.9	7 +/- 13
		221a	13.9	63.7				
		221b	4.3	52.9				
		221c	22.4	56.4				
		221d	4.1	34.8				
		221e	355.7	59.4				
		221f	14.7	52.4				
C241	Volcanic sandstone	Average	107.3	51.5	19.1	6.7	9.5	111 +/- 14
		241a	125.3	55.4				
		241b	114.7	42				
		241c	124.1	55.1				
		241e	123.2	58.6				
		241f	128.2	48.9				
		241h	122.3	56.8				
		241i	81.9	31.3				
		241j	102	49				
		241k	127.6	51.6				
		241l	123.3	39.6				
C242	Volcanic sandstone	Average	111.9	33.7	22.7	6.9	6.98	113 +/- 29
		242a	142.9	32.6				
		242b	87.1	16.6				
		242c	109.1	46.7				
		242d	57.8	32.2				
		242e	165	29.9				
		242f	93.9	14.2				
		242g	107.7	25				
		242h	139.5	38.9				
C324	Sandstone	Average	105.1	28.0	18.2	7.2	9.61	109 +/- 8
		324a	109.9	22.4				
		324b	130.9	31				

Table 3.2: (continued)

		324c	116.2	26.9				
		324d	112.7	22.9				
		324e	106.8	26.4				
		324f	97.9	27				
		324g	99.1	30				
		324h	114.8	27.8				
		324i	115.3	28.9				
		324j	110.6	25.2				
C331	Tuffaceous sandstone	Average	144.7	51.3	9.3	43	6.86	143 +/- 15
		331a	135.5	32.1				
		331b	142.1	53.9				
		331c	138.9	57.6				
		331d	159.5	46.3				
		331e	131.2	62				
		331f	149.5	59.7				
		331g	153.3	44.3				
C341	Tuff	Average	64.0	28.9	6.5	63.1	8.87	65 +/- 9
		341a	70.9	31.4				
		341b	75.1	23.4				
		341c	61.5	29.2				
		341d	43.2	33.1				
		341e	52.5	30				
		341f	65.8	31.1				
		341g	68.7	34.7				
		341h	72.9	24.2				
		341i	63.9	19.8				
C351	Welded tuff	Average	139.7	42.4	30.6	3.2	7.86	138 +/- 8
		351a	127.9	29.3				
		351b	124.7	28.3				
		351c	221.5	28.6				
		351d	120	28.6				
		351e	117.8	28.7				
		351f	67.4	28.4				
		351g	215.7	29.2				
		351h	148	28.9				
		351i	129.8	29.1				
		351j	110.2	28.8				
		351k	275.7	28.8				
C511	Mudstone/ marlstone	Average	342.1	46.3	18.3	14.3	5.65	-18 +/- 21
		511a	311.4	28.3				
		511b	345.9	31.2				
		511c	341.2	40.6				
		511e	30.5	54				
		511f	333.8	57.3				
		511g	346.3	52.2				
C512	Mudstone/ marlstone	Average	350.0	72.0	24	15.7	3.8	-10 +/- 39
		512a	17	58.3				
		512b	359.1	74				
		512c	9.6	64.9				
		512d	264.8	64.8				
SJ11	Volcanic sandstone	Average	6.4	49.1	6.3	66.8	8.88	
		sj11a	17.6	52.3				
		sj11b	4.3	50.7				
		sj11d	9.4	51.4				
		sj11e	13.6	50.4				
		sj11g	8.3	51.6				

Table 3.2: (continued)

		sj11h	6.6	53.3				
		sj11i	357.5	49.6				
		sj11j	354.4	26.3				
		sj11k	11.5	53.9				
SJ12	Volcanic sandstone	Average	355.2	44.2	3.7	197.1	8.95	
		sj12a	2.7	45				
		sj12c	354.1	45.1				
		sj12b	357.4	44.3				
		sj12d	5.1	46.5				
		sj12e	349.1	43.6				
		sj12f	0.3	44.7				
		sj12g	339.8	43.1				
		sj12h	357.5	42.4				
		sj12i	351.9	41				

Paleomagnetism Results

This study is interested in looking at the difference between observed tilt-corrected declinations and inclinations versus expected declinations and inclinations. During Miocene time, the stable magnetic pole of North America was at 357.1^{o} declination and 52.4^{o} inclination (Figure 3.13) (Irving and Irving, 1982) and similarly the Baja California peninsula's magnetic pole was at 357.9^{o} declination and 43.1^{o} inclination (Hagstrum et al., 1987). Inclination for the Baja California magnetic pole is shallower than North America because the Baja California peninsula is located at lower latitude. The Baja California peninsula magnetic pole inclination matches the San Javier reference site, further supporting San Javier as a stable reference. Mid-Miocene stable North American craton exhibited a magnetic pole at 358^{o} declination and 55^{o} inclination, similar to the modern North America pole (Mankinen et al., 1987). For the purpose of this study, we will use the Irving and Irving (1982) stable Miocene North America craton magnetic pole properties of 357^{o} declination and 52^{o} inclination. We should expect that all Miocene rocks from North America would exhibit the same magnetic orientation properties unless they underwent deformation after deposition. Irving and Irving's (1982) stable Miocene North American pole takes into account apparent polar wander,

and secular variation over the last 100 Ma in Baja California has not exceeded 12^{o} (Lund and Bottjer, 1991). Therefore, we can compare observed tilt-corrected magnetic properties of samples from Carmen Island to results from onshore Baja California peninsula, and both of those to expected magnetic properties from Miocene rocks of North America.

When comparing magnetic orientation properties of rock samples of this study from Baja California peninsula to magnetic properties of the Miocene of North America, we see a strong resemblance. Samples from San Javier road, on the Baja California peninsula, have mean magnetic properties within 5-10^{o} of the Miocene North America and Baja California peninsula geomagnetic pole (Figure 3.13). Therefore, I determined that within the Loreto segment in the area of the footwall of the Nopolo structure (Willsey et al., 2002) there is no appreciable rotation since Miocene time.

Paleomagnetic results from Carmen Island are variable (Figure 3.14). In the middle of Carmen Island, samples from the Comondú Group have calculated clockwise rotations that range from 65^{o} to 143^{o} (Table 3.2). South of the Arroyo Blanco fault, paleomagnetic results showed a small amount of rotation, only about 7^{o} to 25^{o} of clockwise rotation. Two of the three sites from the southern paleomagnetic domain showed no rotation within errors. The northernmost part of Carmen Island, near Punta Perico, had small counter-clockwise to no rotation in samples from Pliocene strata, both sites with no rotation are within the 95% confidence interval. All error analysis was calculated by using the rotation and flattening in direction space technique of Butler (1992). Varying amounts of rotation were separated into their own sub-domains.

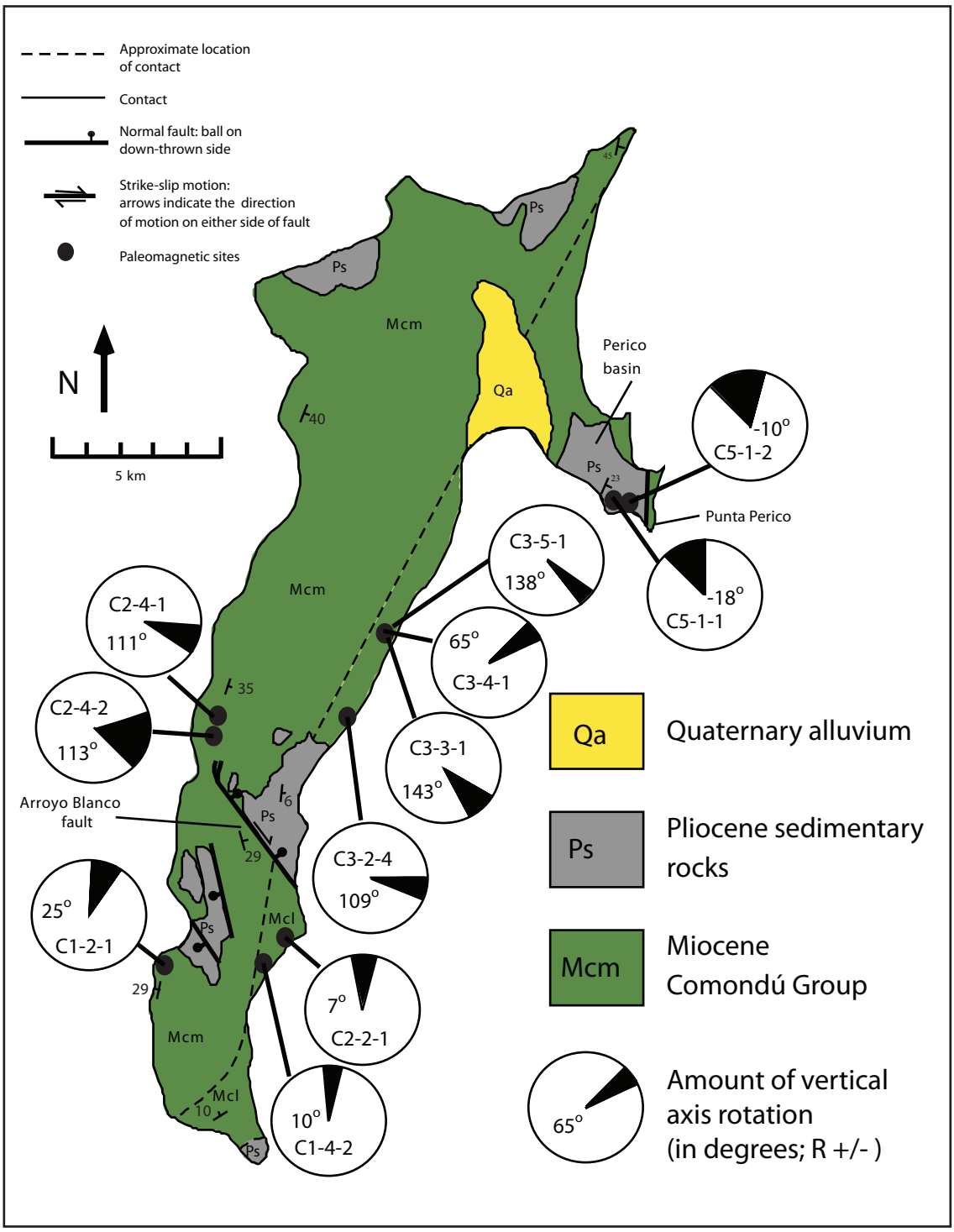

Figure 3.14: Geologic map of Carmen Island with paleomagnetic sites. Amount of vertical-axis rotation relative to site on San Javier road for each sample is shown in circle plot. Black area represents error calculated by using Butler (1992) approach for rotation and flattening in direction space.

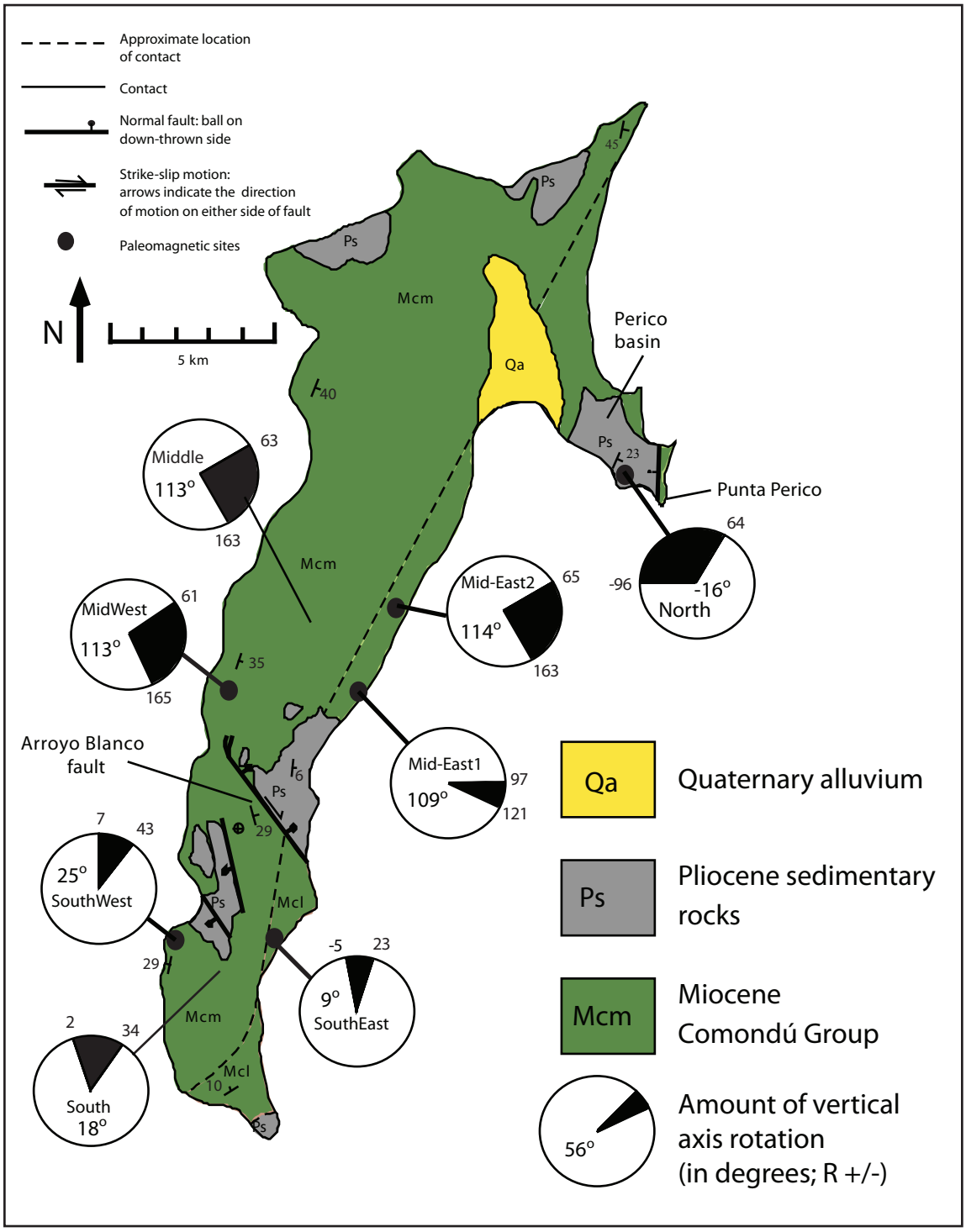

Figure 3.15: Mean paleomagnetic rotations for domains on Carmen Island. Amount of vertical axis rotation is shown in circle plot and black area represents error with maximum and minimum errors noted next to black area. Each domain shows consistency

After looking at the paleomagnetic results, I re-evaluated the division of Carmen Island created for this study. I started by grouping together samples that were from proximal localities to each other (Figure 3.15) (Table 3.3). Mean paleomagnetic results from proximal localities were also plotted on a stereonet (Figures 3.16 and 3.17). All samples from southeastern and southwestern Carmen Island, and from northern Carmen Island Pliocene strata, exhibit little or no rotation when compared to the samples from San Javier road (Baja California peninsula) (Table 3.3). Samples from both the middle-east and middle-west of Carmen Island exhibit similar rotation with large errors. Therefore, instead of five paleomagnetic domains, Carmen Island is now divided into two major domains separated by the Arroyo Blanco fault and a sub-domain, younger in age, from the Pliocene Perico basin.

Another comparison of paleomagnetic samples on Carmen Island with samples from San Javier road involves observed inclinations. After determining the amount of declination rotation for each sample with respect to San Javier road, I then removed that rotation amount from each sample and compared inclinations with respect to San Javier road (Figure 3.18). Inclinations from the middle domains and northern Pliocene rock, on Carmen Island were within the 95% confidence cone of inclinations from San Javier road (Figure 3.18A, B and E). Inclinations from the southern domain on Carmen Island had two samples, C1-4-2 and C1-2-1, that were not within the 95% confidence cone of San Javier. These two samples show not only a vertical-axis rotation, but also have a component of horizontal-axis rotation associated with them. C1-4-2 has ~33^{o} and C1-2-1 has ~40^{o} difference in inclination from samples from San Javier road.

Summary

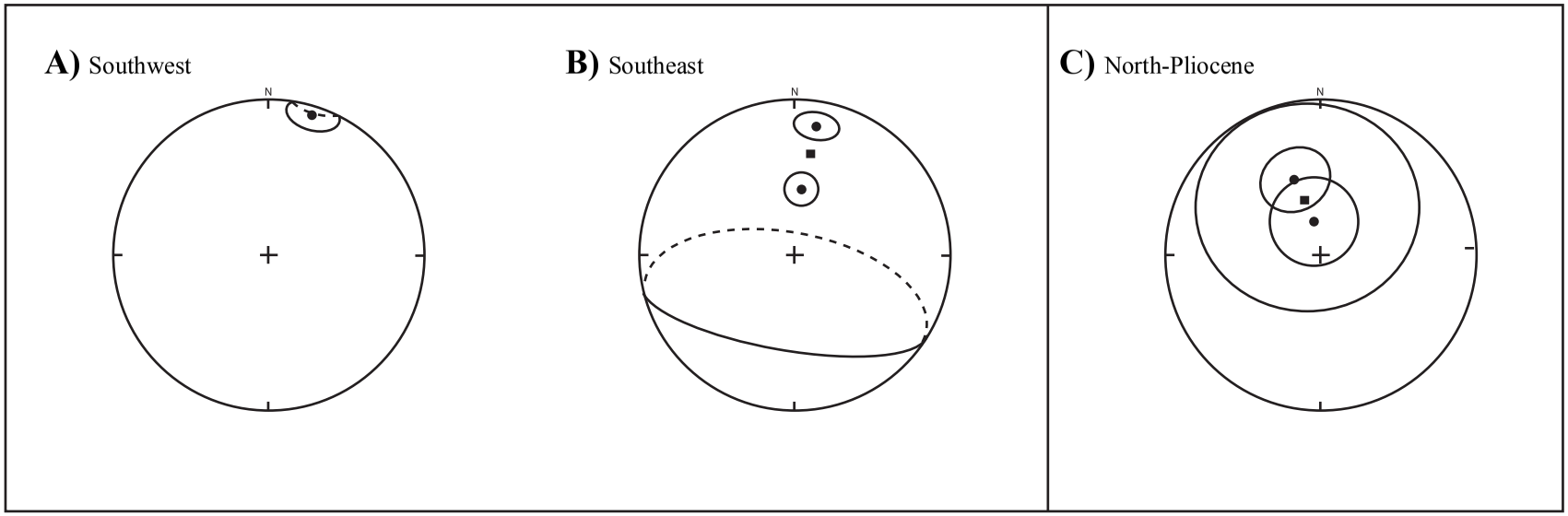

Figrue 3.16: Mean tilt corrected magnetic poles from samples from the southwest (A), southeast (B) and north (Pliocene) (C) domains on Carmen Island. Mean poles measured for the southwest and southeast domains are similar and show little rotation. Black circles are individual sites from each domain and squares are the mean pole position for that domain. 95% confidence cone is circle around points.

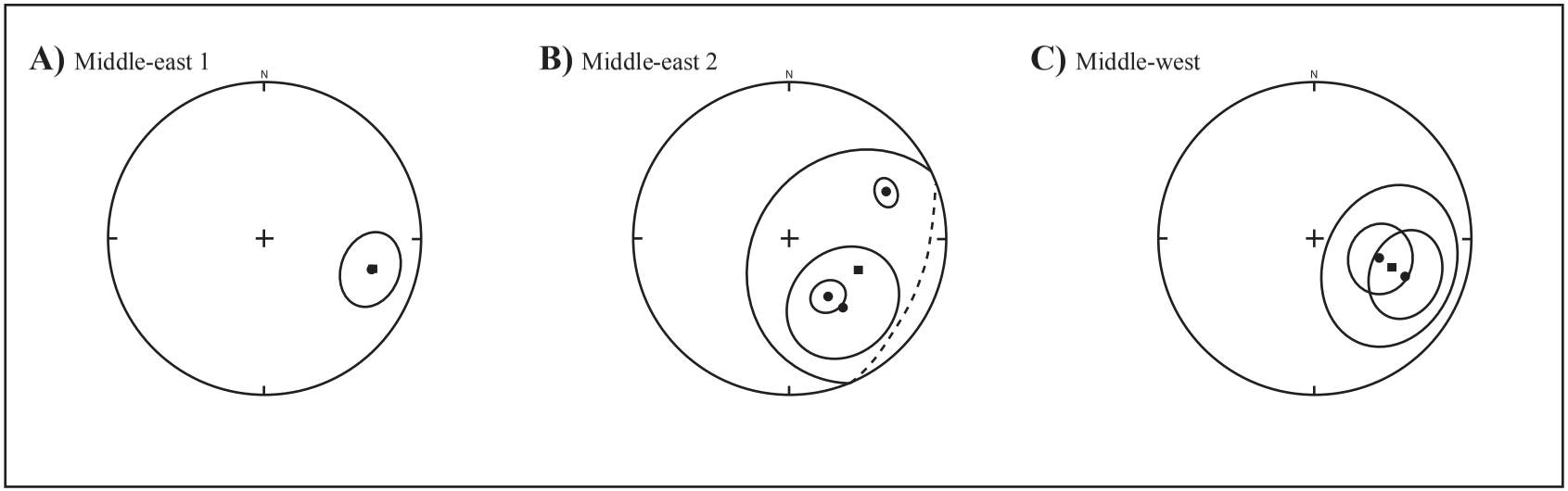

Figure 3.17: Mean tilt corrected magnetic poles from samples from the middle of Carmen Island domain. The middle of Carmen Island domain is divided into three sub-domains, middle-east 1 (A), middle-east2 (B), and middle-west (C). Black circles are individual sites and black squares are the mean for that sub-domain. 95% confidence cone is circle around points.

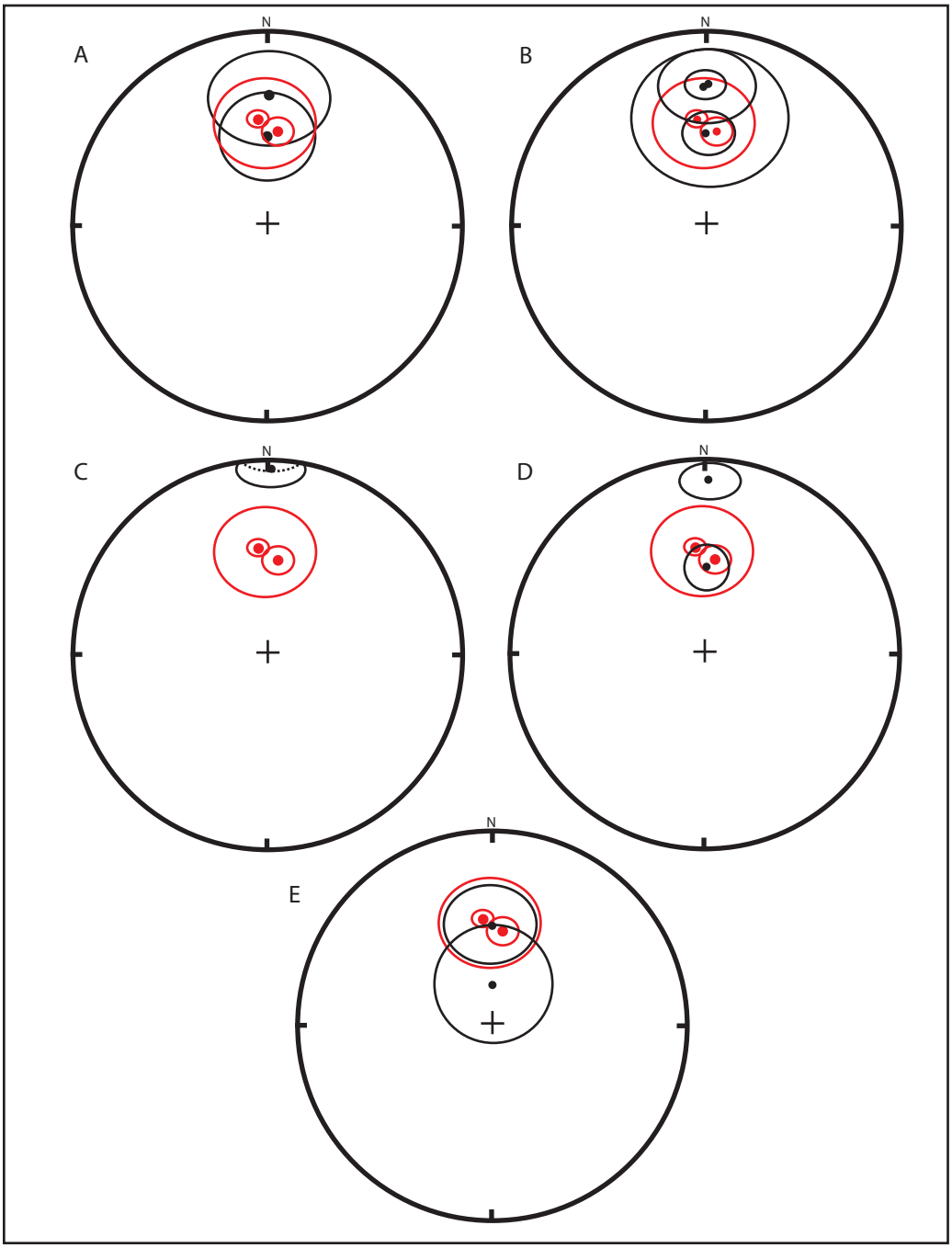

Figure 3.18: Stereonet plot of the paleomagnetic samples from Carmen Island after they have been rotated counterclockwise back to reference sample on San Javier road. Plot compares inclinations if all samples had similar declination. San Javier road is plotted in red and 95% confidence between San Javier sites is larger red circle. All 95% confidence cones are shown as circles surrounding individual points. A) Sample from middle-west paleomagnetic domain on Carmen Island. B) Sample from middle-east paleomagnetic domain. c) Samples from southwest paleomagnetic domain. D) Samples from southeast paleomagnetic domain. E) Samples from northern Pliocene paleomagnetic domain.

The domain on southern Carmen Island shows little vertical-axis rotation, with a mean of ~16^{o}. The eastern part of the southern Carmen Island domain only had ~9^{o} of clockwise vertical-axis rotation (Table 3.3). According to work done by Vlad (2001), the Arroyo Blanco fault may have accommodated some of the rotation of Carmen Island and little to no rotation would be expected for areas on Carmen Island south of the Arroyo Blanco fault (Figures 3.15 and 3.16).

Table 3.3: Mean magnetic poles for domains on Carmen Island. Rotation relative to San Javier road sites.

Mean Rotations						
Sample#	**Dec**	**Inc**	**Alpha95**	**K**	**Amount Rotation**	**Rotation Error +/-**
SouthEast	10	33	10.9	7.8	8.8	14.6
SouthWest	25.9	3	14.1	12.7	24.7	18.6
South Average	18	18	12.5	9	16	16
MidWest	114.6	39.7	45.3	32.6	113.4	51.7
MidEast1	110.3	26.9	1.7	803.6	109.1	12.2
MidEast2	115.2	42.6	66.7	4.5	114	49
Middle Average	113	36	52	150	110	50
NorthPlio	-15.5	58.8	58.2	20.6	-16.7	80
SanJavier	1.2	46.7	10.7	547	0	

The domain north of the Arroyo Blanco fault, however, demonstrated larger than expected and variable rotations. Although the rotations exhibited by the middle domain on Carmen Island were larger than expected, they were internally consistent with a mean of ~110^{o} clockwise rotation (Figures 3.15 and 3.17) (Table 3.3).

The sub-domain on Carmen Island of Pliocene strata in Perico basin also shows consistent paleomagnetic results with a mean of -16^{o} +/- 29^{o} clockwise rotation, statistically indicating no rotation or counterclockwise rotation relative to San Javier road (Figures 3.15 and 3.16) (Table 3.3).

The results from the division of Carmen Island into two major domains and a sub-domain of Pliocene strata in the north are used to produce a modified evolution of the rotation of Carmen Island described in chapter 5. Paleomagnetic results were variable, but consistent within each domain and therefore they help explain Carmen Island's rotation over the last ~12 million years. Paleomagnetic and geologic data suggest Carmen Island did not rotate as a uniform block, but either rotated as a couple of smaller blocks or as a couple of ball bearing-like blocks (Figure 3.2). There are not enough paleomagnetic data to suggest many small blocks rotating independently of one another. Also, the lack of structural mapping on Carmen Island presents insufficient structural controls to test if small blocks rotated independently. Limited mapping on Carmen Island shows consistent bedding attitudes north of the Arroyo Blanco fault, making small-block rotation less likely unless they occurred before tilting of beds. The Arroyo Blanco fault is the only structural control on Carmen Island and it divides the northern two-thirds from the southern third of the island. The large amount of vertical-axis rotation observed from paleomagnetic data from the northern two-thirds of Carmen Island versus small amounts of vertical-axis rotation observed from paleomagnetic data from the southern third of Carmen Island confirm the island is not rotating as a coherent block. Paleomagnetic data also support some tilting and rotating of blocks from the southern paleomagnetic domain on Carmen Island. Our best scenario is one where Carmen Island is rotating clockwise away from Loreto, but Carmen Island is rotating as two blocks and the Arroyo Blanco fault is accommodating the varying amounts of rotation.

CHAPTER 4

QUATERNARY UPLIFT OF CARMEN ISLAND

Marine terraces have been used as indicators of tectonic uplift in coastal settings (Broecker et al, 1968; Chappell, 1983; Merritts and Bull, 1989). Coastal marine platforms and coral reefs form within a few meters of sea level. A flight of emergent marine terraces record a tectonic component from the rising landmass and a glacioeustatic component from the sea-level changes of the world's oceans (Lajoie, 1986). It has been inferred by researchers that the ongoing opening of the Gulf of California was accompanied by vertical motions related to active normal faulting along the peninsula and islands (Mayer and Vincent, 1999; Umhoefer et al., 2002). Uplifted marine terraces found on Carmen Island at Bahía Marquer (Figure 2.4) were surveyed to determine the vertical movement associated with the tectonics of the Loreto region (Figure 2.3). Shells and corals collected from terraces were analyzed using amino acid racemization and U-Th series dating to establish a time frame in which uplift occurred.

Background

The accommodation of strain between the North American plate and the Pacific plate has been partially recorded across the eastern Baja California peninsula and the Gulf of California. There are many segmented areas along the rift axis that accommodate partitioned strain from the plate motion. The Loreto segment has experienced much tectonic movement associated with transtension in the Gulf of California (Umhoefer et al., 2002). Most importantly for this study, the Loreto segment has recorded tectonic

activity since Pliocene time that helps constrain the timing and development of the oblique-rift margin of Gulf of California. Quaternary tectonic movement along the Loreto segment is more poorly understood than Pliocene tectonism, but it is important because tectonic activity continues today in the Loreto area and reflects the change in strain within the active margin of Baja California.

Quaternary faults are active in the Loreto area. The Escondido fault is a 14-km long down-to-the-east normal fault (Figure 2.4) (Umhoefer et al., 2002) that juxtaposes sedimentary and volcanic rocks of the lower Comondú Group in its footwall with Quaternary alluvium and local belts of middle to upper Comondú Group in the hanging wall (Vlad, 2001). Movement of parts of the Escondido fault is recorded by offset of Quaternary gravels, supporting recent activity in the Loreto segment (Mayer and Vincent, 1999).

Pliocene to Quaternary fault movement in the Loreto segment is also associated with subsidence of the Loreto basin. The transtensional Loreto basin developed along the dextral-oblique normal Loreto fault during the Pliocene (Figure 2.4) (Umhoefer et al., 1994). The development of the Loreto basin is estimated to have begun after ~5 to 6 Ma (Dorsey and Umhoefer, 2000). During the middle stages of the Loreto basin development , at ~2.4 to 2.3 Ma, the Loreto fault may have accommodated a significant portion of the plate motion. The northern Loreto fault is active in Pliocene to Quaternary time (Mayer and Vincent, 1999). Strain on the southern Loreto fault began to decrease at ~2.0 Ma and by Pleistocene time, the southern Loreto basin was experiencing uplift as faulting shifted offshore and became dominantly normal slip (McLean, 1988; Dorsey and Umhoefer, 2000). During Quaternary, time the northern Loreto basin has been

characterized by slow slip rates and subsidence (Mayer and Vincent, 1999). The main active faults since ~2 Ma are offshore and related to the uplift of Carmen Island.

This study supports previous work that shows Quaternary fault movement in the Loreto region. This section will focus on uplifted marine terraces found on Carmen Island that are associated with tectonic activity offshore in the Loreto segment.

Coastal uplift

Marine terraces are important markers of paleo coastlines and can be used to measure coastal uplift rates. The west coasts of North and South America are rising as a result of plate tectonics and uplifted marine terraces record this episodic movement. Marine terraces are wave-cut platforms that form when sea level is stable long enough to form an erosion feature (Ortlieb, 1991; Keller and Pinter, 2002). The terrace inner edge is the intersection of the sea cliff or riser with an abrasion platform (Figure 4.1). The elevation of a terrace inner edge records the position of sea level (Figure 4.1). This sea level marker can be compared to other chronologies such as oxygen isotope records and U-Th series dating to determine high stands of sea level (Mayer and Vincent, 1999; Keller and Pinter, 2002). The abrasion platform is commonly covered by rounded cobbles, gravel, shell hash, and sand (Figure 4.2).

The nomenclature used to discern between terraces on Carmen Island is as follows. The abrasion platform is the marine surface cut into the Pliocene strata and is commonly composed of calcarenite or limestone (Figures 4.1 and 4.2). The inner edge is surveyed as the elevation of a particular abrasion platform (Figure 4.1). Abrasion platforms can be covered by debris, making it more difficult to find the true shoreline

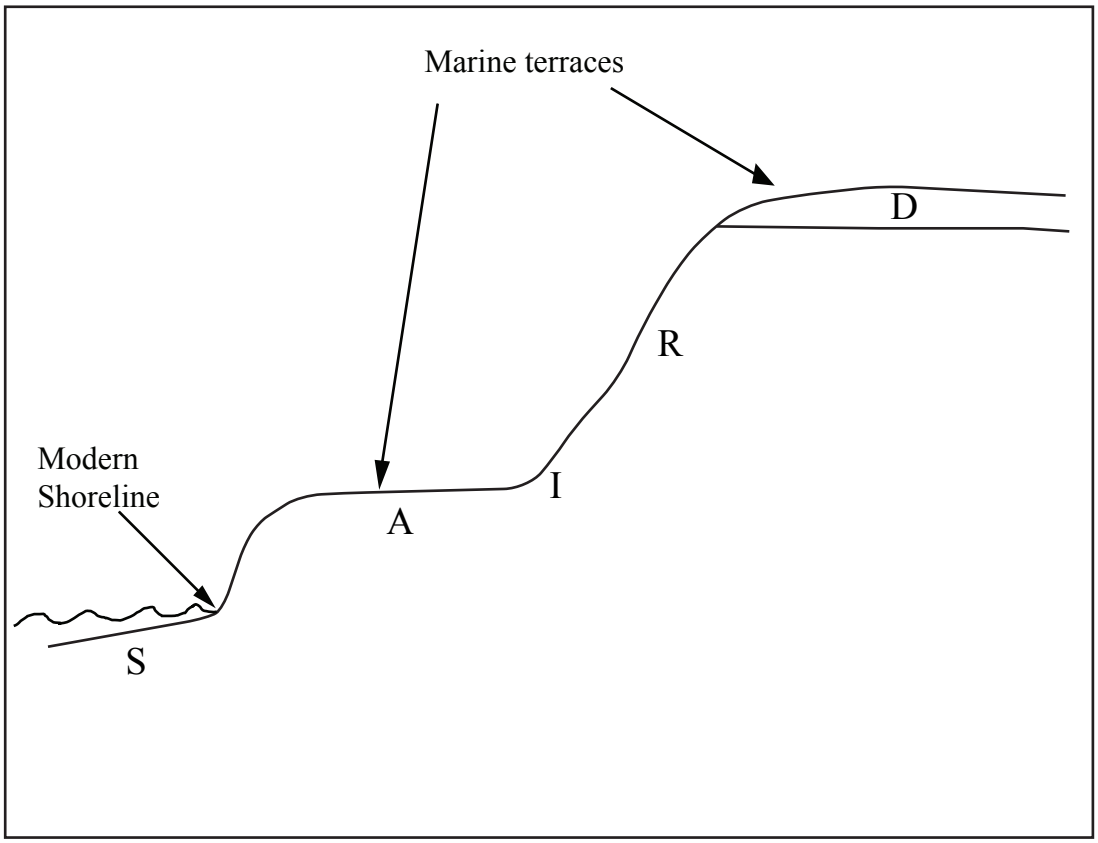

Figure 4.1: Drawing of hypothetical uplifted terraces and nomenclature used to describe terrace features. S = Shoreline angle; A = Abrasion platform; I = Inner edge; R = Riser; D = Deposit on abrasion platform.

angle and inner edge. On each platform surveyed, the degree of dissection from flat to more undulating, the type of cover, the presence or absence of shells and corals, and the vegetation density was noted (Figure 4.1). On risers and abrasion platforms, the slope material and type of cover was noted as well as the type of weathering. Because it is difficult to survey every inner edge, some inferences have to be made using a shoreline angle. The elevations of some inner edges had to be estimated using the projection of an abrasion platform and a riser surface.

Figure 4.2: Photograph of abrasion platform from Bahía Marquer. Broken, weathered gray Pliocene sedimentary rocks dominate these platforms.

Coastal geomorphology and the formation of marine terraces are closely related to sea-level fluctuations. Sea level during the last interglacial highstand, about 120 ka or Oxygen Isotopic Stage 5e, was about 6 m higher than present (Chappell, 1983). That highstand has not been exceeded in elevation since (Shackleton and Opdyke, 1973;

Mayer and Vincent, 1999). Each oxygen isotopic stage represents a sea-level highstand or lowstand and marine terraces are markers of those highstands (Figure 4.3) (Chappell, 1983). The oxygen isotopic stage (I.S.) 5e terrace is the only terrace above modern sea level (+6 m) and therefore should be the only terrace exposed today unless the area has experienced tectonic coastal uplift (Figure 4.3) (Chappell, 1983). Coastal uplift is verified by surveying shoreline angles across a flight of marine terraces and a eustatic component of the terrace elevation is subtracted out (Lajoie, 1986; Mayer and Vincent, 1999).

The age of a marine terrace can be determined by dating materials found in abrasion platforms such as shells and corals. Amino Acid Racemization (AAR) is a technique by which shells can be relatively dated. AAR is not an absolute dating technique, but it is a powerful correlation tool. When an organism is alive it is producing known ratios of amino acids. When that organism dies and then becomes fossilized, it loses some of its amino acids, but approximately 40-60% of those original amino acids remain (Wehmiller and Miller, 2000). AAR uses the ratio of the decomposition of amino acids in a fossilized organism by comparing D/L ratios in a fossilized organism to other D/L ratios in the same species of organism from similar climatic regions. The amino acid racemization method relies upon the conversion of L-amino acids in living organism to L and D-forms of amino acids in fossilized organisms (Wehmiller and Miller, 2000). The ratio D/L (D-alloisoleucine/L-isoleucine, or A/I for alloisoleucine/isoleucine) measures the extent of racemization or “epimerization” in the case of isoleucine (Wehmiller and Miller, 2000; Hearty and Kaufman, 2000). When an organism is living, the ratio D/L is 0 and after it dies racemization/epimerization occurs and can change that D/L ratio to as

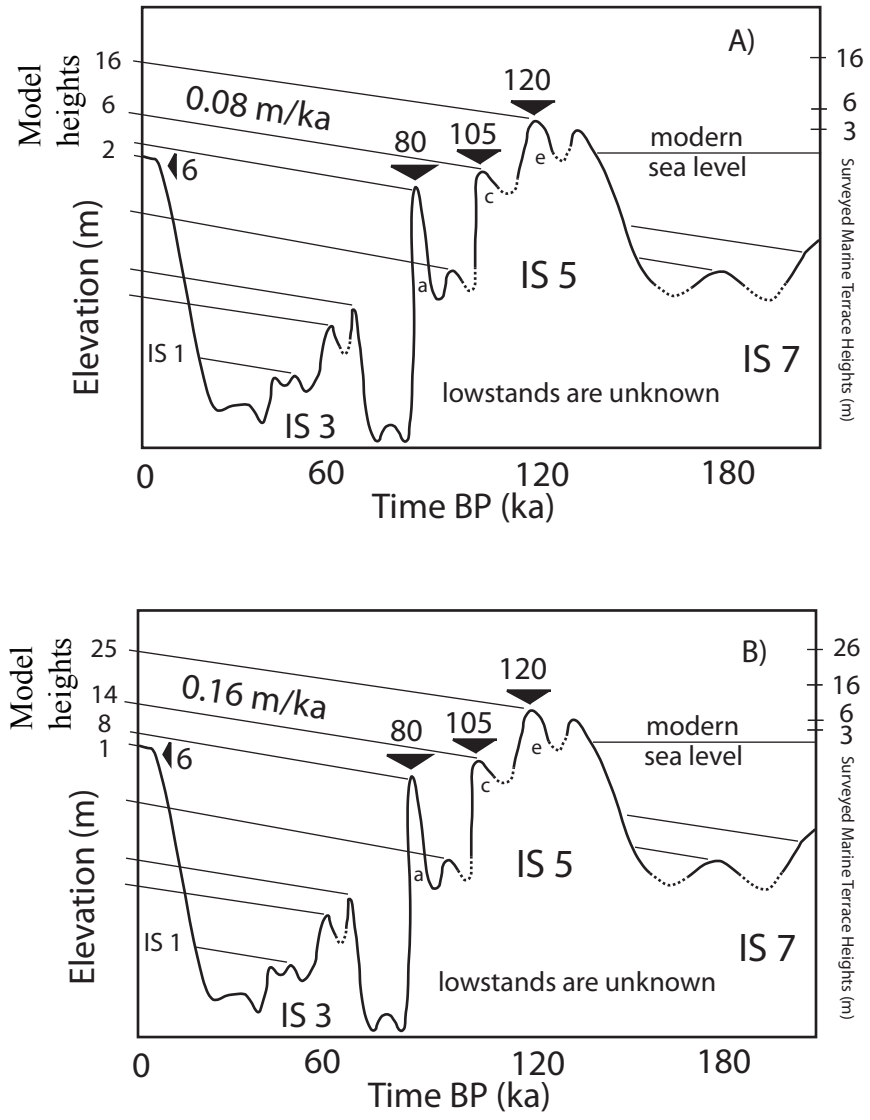

Figure 4.3: Graph showing fluctuation of sea-level with the modeled altitudinal spacing of Pleistocene marine terraces at Punta El Bajo; under conditions of constant uplift compared to surveyed marine terrace elevations. Dashed line indicates unknown lowstands of sea-level. A) Uplift rate of 0.08 m/ka produces three exposed terraces: 80 ka = 2 m; 105 ka = 6 m 120 ka = 16 m B) Uplift rate of 0.16 m/ka produces four exposed terraces: 6 ka = 1 m; 80 ka = 8 m; 105 ka = 14 m; 120 ka = 25 m (sea-level curve after Chappell, 1983; Mayer and Vincent, 1999).

much as 1.3 (Hearty and Kaufman, 2000). The rate of the racemization/epimerization reaction is dependent on the ambient temperature of the organism. One expect to see higher racemization rates closer to the equator and lower rates at higher latitudes (Wehmiller and Miller., 2000; Hearty and Kaufman, 2000). Also as this study has confirmed, speciation has an effect on D/L ratios. For the purpose of this study, AAR was used to correlate shells from terraces at Bahía Marquer on Carmen Island and shells from terraces at Punta El Bajo on the mainland Baja California peninsula.

Previous Work

Some work has been done throughout the Gulf of California concerning uplifted marine terraces. Emerged Pleistocene shorelines in Baja California were first noted by Gabb (1868), Lindgren (1888), and Emmons and Merrill (1894). Ortlieb (1980, 1991) studied evidence of Quaternary movement along both coasts of Baja California and western Sonora, contributing greatly to the understanding of vertical movement along the Baja California peninsula. Ortlieb (1991) surveyed marine terraces around the Baja California peninsula and determined an average uplift rate of about 0.1 m/ka for the past million years. Ledesma-Vazquez and Johnson (1993) supported Ortlieb's claims of uplift rates of approximately 0.1 m/ka with studies just north of Loreto, Baja California Sur, in the Arroyo de Arce. They reported uplifted terraces and rocky shorelines with an age of 1.8 Ma at about 175 m above sea level.

Ortlieb (1991) also examined the area between Punta Chivato and Loreto (Figure 1.1) determining that terraces with an age of 150-130 ka were found at elevations of 9 and 13 m and showed uplift rates of ~0.09 m/ka (Ortlieb, 1991). Around Concepción

Peninsula (Figure 1.1), terraces of similar age were found even higher, at elevations of about 15 and 18 m. Between Bahía Concepción (Figure 1.1) and Punta El Bajo (Figure 1.4), Ortlieb (1991) reported middle Pleistocene marine terraces (I.S. 11) at elevations from 30 to 50 m (Ortlieb, 1991).

Mayer and Vincent (1999) surveyed marine terraces at elevations of 6, 16, and 26 m at Punta El Bajo and noted a low level terrace at 3 m. Mayer and Vincent's work agreed with Ortlieb's (1991) results confirming a 6 m terrace during isotopic stage 5c, but ages on the 16 and 26 m terraces varied between the two studies. Mayer and Vincent (1999) concluded the average coastal uplift rates for the Loreto area were between 0.08 and 0.16 m/ka since 120 ka. They cited offset rocky shoreline points as further evidence that a rate of 0.08 m/ka may be most exemplary of the Quaternary. Mayer and Vincent (1999) also used evidence from a model based on predicted uplift rates and sea level fluctuations (Figure 4.3). Surveyed terrace elevations by Mayer and Vincent (1999) agreed with modeled terrace elevations using a steady uplift rate of 0.08 m/ka (Figure 4.3). A model based on an uplift rate of 0.16 m/ka predicts four emergent terraces that did not match surveyed terraces (Figure 4.3). Later U-Th series dating of a coral from the 6 m terrace indicated the terrace was 107 ka and the 0.08 m/ka uplift rate is correct (Mayer et al., 2002).

Work at Punta El Bajo is important to this study because its location, 10 km to the west of Carmen Island, allows correlation of uplifted terraces on Carmen Island. Shells were collected for this study from the 6 m terrace surveyed by Mayer and Vincent (1999) and analyzed using amino acid racemization to try to correlate terraces onshore at Punta El Bajo to terraces offshore on Carmen Island.

Methodology - Marine Terrace Surveys on Carmen Island

Uplifted marine terraces are cut into Pliocene sedimentary rocks on Carmen Island in approximately six locations (Figure 3.3). This study will concentrate on the area near Bahía Marquer, located on the southwest end of Carmen Island and terraces found near Arroyo Blanco, eastern Carmen Island (Figures 3.3 and 4.4). Marine terraces found at the northern and southern most areas of Carmen Island will not be addressed because it was logistically too difficult to survey and study these terraces. Terraces at Bahía Marquer and Arroyo Blanco were surveyed to determine the number and elevations of the terraces. Shells and corals were collected from terraces where possible. The following describes techniques and processes used to determine the elevations of uplifted marine terraces on Carmen Island and subsequent uplift rates for Carmen Island.

Uplifted marine terraces on Carmen Island are characterized by wave cut platforms found on gray to tan Pliocene sedimentary rocks (Figure 4.2). Some higher terraces are characterized by highly pitted grayish Pliocene limestone, whereas lower terraces are cut into a tan sandy calcarenite. The modern beach on Carmen Island is a calcarenite platform backed by a sea cliff. The modern beach is covered by sand, shell hash, and an abundance of well rounded volcanic cobbles and pebbles. The modern beach and shoreline are also a high energy environment where cobbles and pebbles can be heard rolling against one another like a rock tumbler. The modern beach environment is important because we look for similar characteristics on uplifted marine platforms to distinguish them.

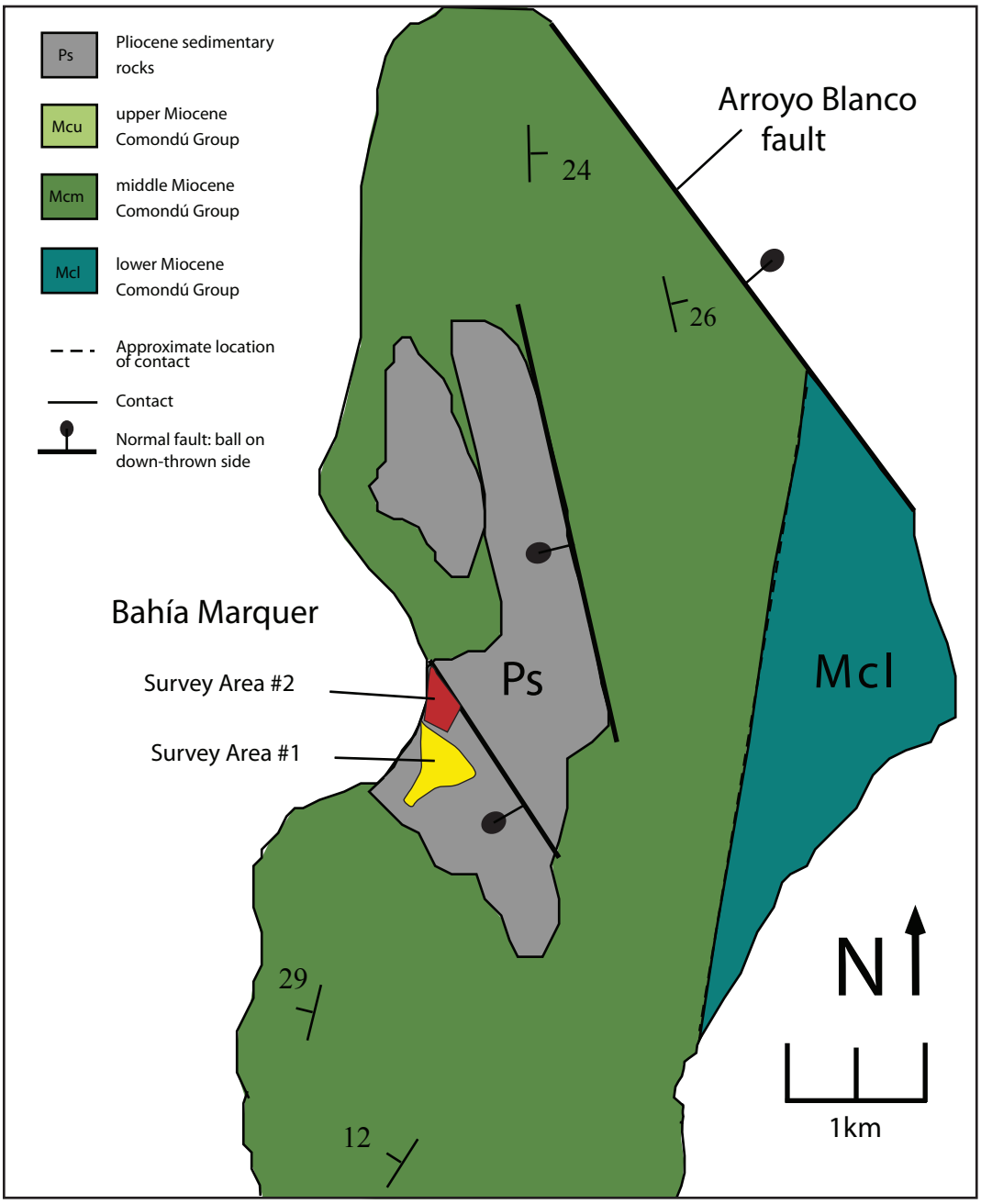

Figure 4.4: Geologic map of area ~5 km southwest of Arroyo Blanco fault on Carmen Island (after Umhoefer et al., 2002).. Bahía Marquer survey areas #1 and #2 are designated with polygons. See figure 3.3 for location of this map on Carmen Island.

I surveyed marine terraces at Bahía Marquer and Arroyo Blanco in March of 2000 using a Sokkia Set 6E total station (Figure 4.4). Because of the difficulty of identifying the inner edge of a marine terrace, I surveyed the abrasion platforms, debris on abrasion platforms, risers, and inner edges where visible. Observing and surveying all of these characteristics of a marine terrace allowed us to make inferences about inner edge locations where one was not visible. Approximately 110 spot elevations were measured at Bahía Marquer (Figure 4.4) and 50 at Arroyo Blanco to define shoreline angles and inner edges of terraces. Daily sea level elevation was also surveyed and adjusted for tide variation by a constant of 0.5 m to equal mean sea level.

This study will focus on the western side of Carmen Island at Bahía Marquer. The survey from the eastern side of Carmen Island at Arroyo Blanco was found to have many errors and I discarded survey data from Arroyo Blanco. Based on observation and limited survey from this study and Mayer and Dorsey's survey in 1996, we have estimated 5-6 terraces on the eastern side of Carmen Island (Figure 4.5). There are no terrace ages at Arroyo Blanco or the eastern part of Carmen Island, but the numerous terraces and relatively high elevation of the terraces suggest a fast rate of uplift.

Figure 4.5: Photograph of three uplifted marine terraces (arrows) near Arroyo Blanco, on the eastern side of Carmen Island.

Based on the survey at Bahía Marquer on the western side of Carmen Island, maximum paleo-sea level markers were established for two to three terraces. Profiles were made from the survey data at Bahía Marquer using Surfer contouring and surface mapping software (Figures 4.6, 4.7, 4.8, and 4.9). Surfer profiles and further study of survey data revealed approximately three uplifted terraces at elevations of 18, 25, and 55 m (Figures 4.6, 4.7, 4.8, and 4.9). The 55 m terrace was not studied, however, because there was no material from this terrace for relative age dating. Timing and formation of the 55 m terrace will be discussed later when uplift rates can be established for western Carmen Island. The 18 and 25 m terraces were examined further and found to have shell material or coral suitable for dating (Figure 4.10).

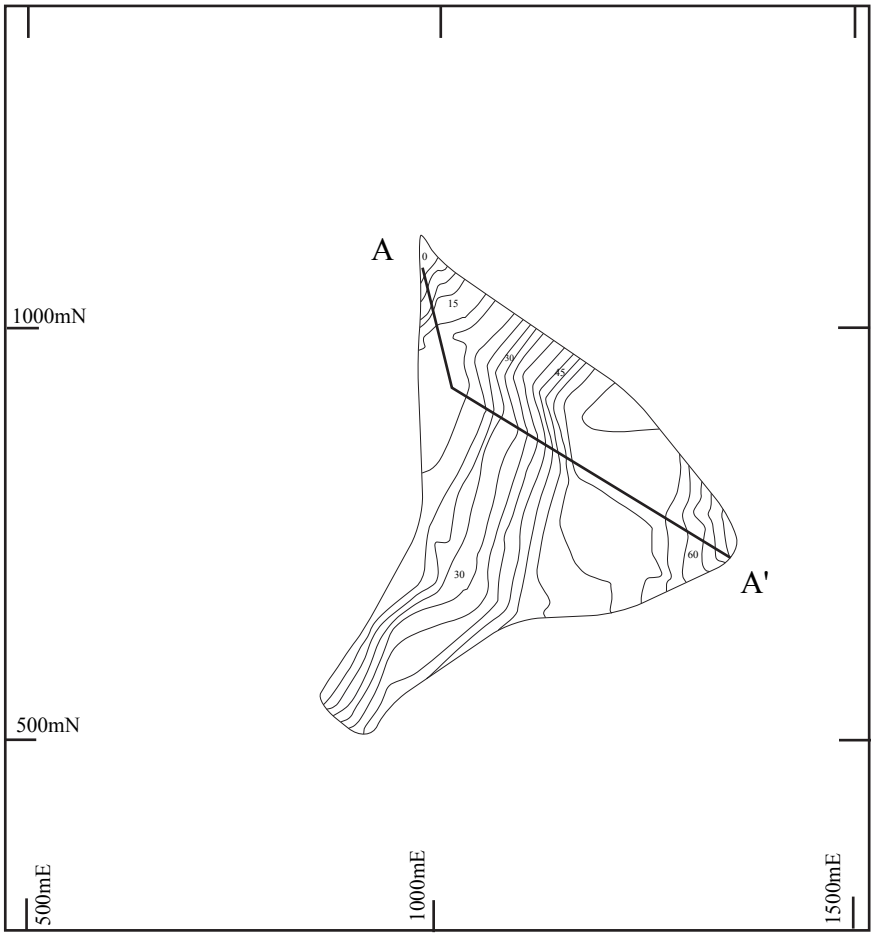

Figure 4.6: Elevation contour profile from Bahia Marquer survey area #1. All data are relative to an arbitrary point. Cross section A - A' is shown in figure 4.7.

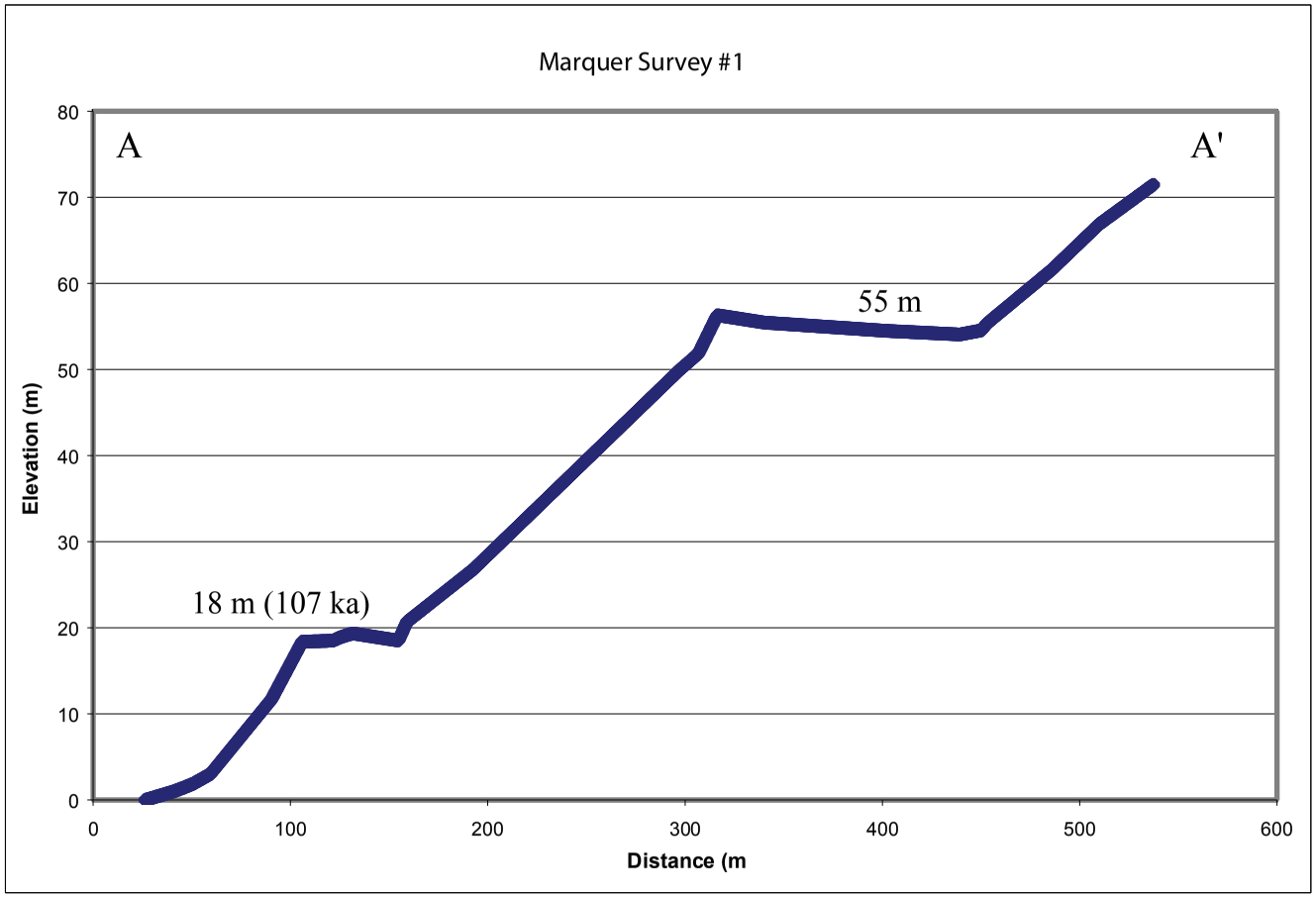

Figure 4.7: Profile of cross-section A-A' from figure 4.6 with 5x vertical exaggeration. 18 m (107 ka) terrace is visible and the unstudied terrace at 55 m.

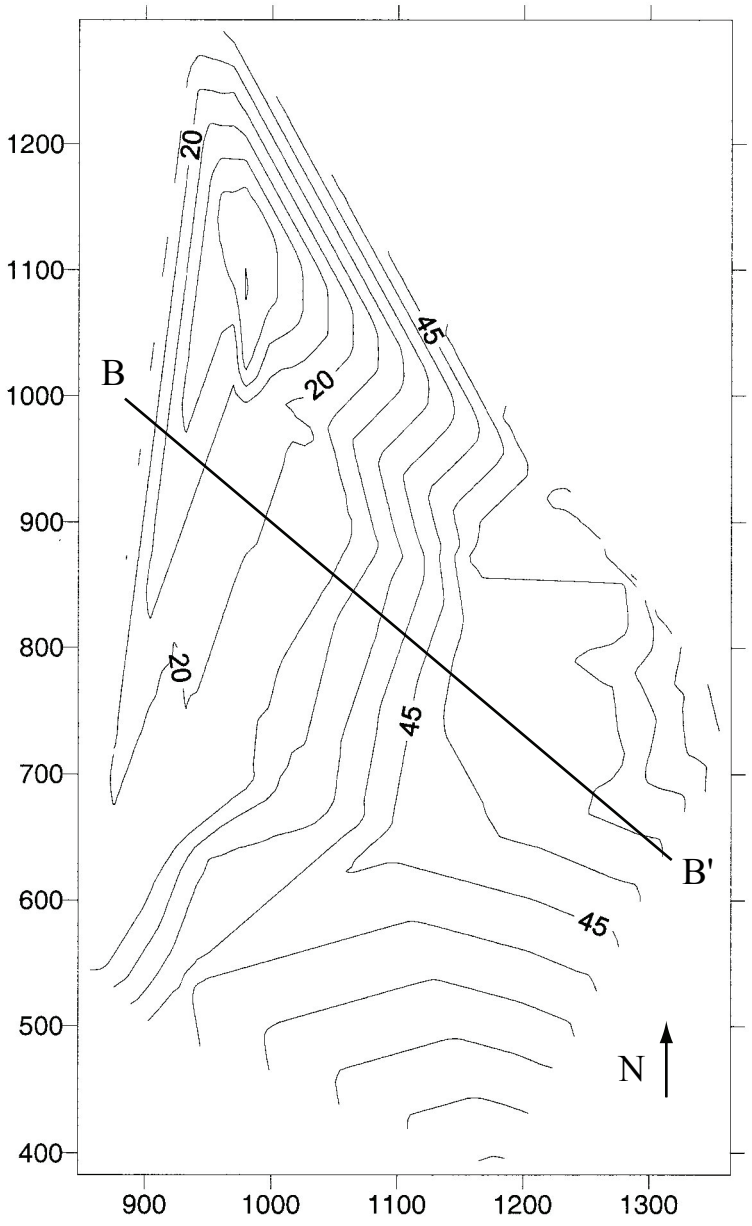

Figure 4.8: Elevation contour map of Bahia Marquer survey area #2. All dats are relative to an arbitrary point. The 25 m (125 ka) terrace and 55 m terrace are visible. Cross-section B to B' is shown in figure 4.9.

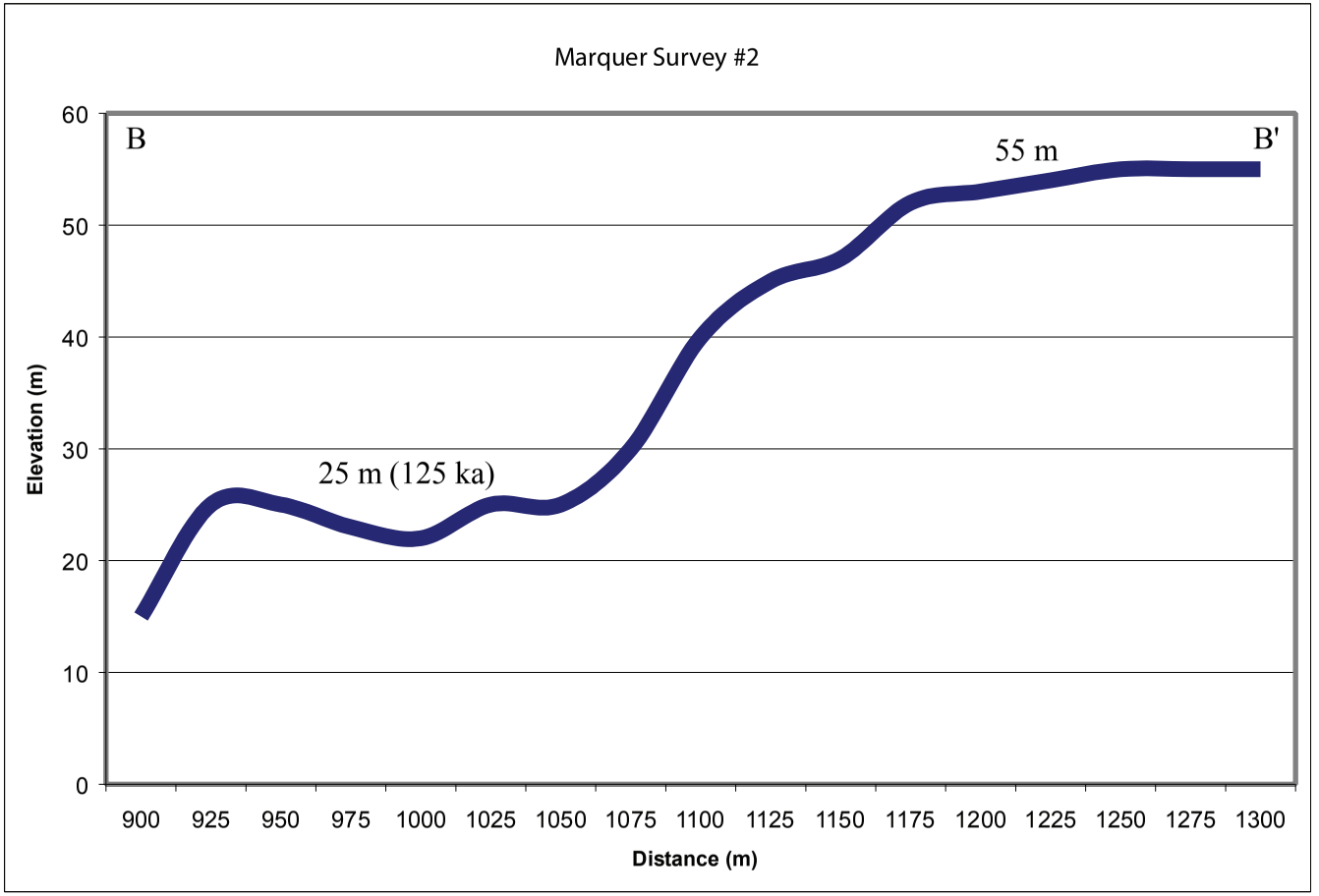

Figure 4.9: Cross-section B-B' from figure 4.8 with 4x vertical exaggeration. The 25 m (125 ka) terrace and unstudied 55 m terrace are visible. The dip in the 25 m (125 ka) terrace is an erosional feature.

Figure 4.10: A) Photograph of view from north looking south over 2-3 flights of uplifted marine terracs at Bahia Marquer. B) Same photograph with terraces outlined in color; 18 m (107 ka) terrace outlined in yellow, 25 m (125 ka) terrace outlined in red, and 55 m (not dated but interpreted to be 320 ka based on modeling) terrace outlined in black.

Methodology - Geochronology of marine platforms

Shell material was gathered from the 18 and 25 m terraces for dating by amino acid racemization to correlate the uplifted marine terraces (Figure 4.11).

All amino acid racemization analysis was performed at the Northern Arizona University in Dr. Kaufman's Amino Acid Racemization lab in Flagstaff, AZ. Shell material was collected on Carmen Island and the Baja California peninsula from depths of 1 m or greater so that local temperature fluctuations would not affect the sample (Figure 4.11). Shell samples were prepared under the guidance of Darrell Kaufman for analysis. Shells were broken into multiple pieces and a grinding tool was used to clean outer edges of modern contamination and then using 2M HCl. Pieces of the shell closest to the beak were preferred for analysis although some pieces of outer shell were also used. Broken pieces of cleaned shell were additionally cleaned.

Figure 4.11: Photograph of collecting shell samples at 1 m depth to account for regional temperature fluctuations. Sample collection site MS-1, located on 18 m terrace.

There were two shell collection sites (MS-1 and MS-2) on the 18 m terrace and one site on the 25 m terrace on Carmen Island at Bahía Marquer and one site at Punta El Bajo, ~10 km north of Loreto (Table 4.1; Figures 1.4, 4.11 and 4.12). Site MS-1 had 10 sub-samples collected from 5 shells (Table 4.1; Figure 4.11). All sub-samples from MS-1 were used in the analysis. MS-2 yielded 12 sub-samples that were analyzed from 6 shells (Table 4.1). Two sub-samples from MS-2 were not used in the analysis because they both showed low A/I ratios when compared to other sub-samples from the same shell which is indicative of modern contamination. In total there were 22 sub-samples from 11 shells and only two of those sub-samples were discarded for modern contamination from the 18 m terrace. Modern contamination was often detected as discoloring in the sample after it was prepared or unreliably low A/I ratios when compared to other sub-samples from the same shell. All shells from the 18 m terrace used in this analysis were of the species *Chione californiensis*. The average A/I ratio for *Chione californiensis* from the 18 m high terrace is 0.833 +/- 0.085 (Table 4.1).

Table 4.1: Shell collection sites, locations, burial depth, and AAR analysis. All sub-samples with contamination and in red and were not used when calculating average A/I ratios.

	Location									
Site #	Easting	Northing	Sample	Burial Depth (M)	Sub-Sample	A/I Ratio	A/I Ratio	A/I Ratio	A/I Ratio	
					UAL	Run 1	Run 2	Run 3	average	stdev
MCAS	0478600	2861307	1	3.00	3743 A	0.632	0.631		0.632	0.001
					3743 B	0.617	0.613		0.615	0.003
			3	3.00	3743 C	0.901	0.746	0.898	0.848	0.089
					3743 D	0.687	0.709		0.698	0.016
			4	3.00	3743 E	0.713	0.714		0.714	0.001
					3743 F	0.634	0.613		0.624	0.015
			5	3.00	3743 G	0.711	0.691		0.701	0.014
					3743 H	0.763	0.771		0.767	0.006
			7	3.00	3743 I	0.104	0.103		0.104	0.001
					3743 J	nd	0.382	0.374	0.378	0.006

Table 4.1: Continued

			21	1.50	3743 K	0.469	0.477		0.473	0.006
					3743 L	0.372	0.405	0.373	0.373	0.001
			2	3.00	3473 M	0.607	0.617		0.612	0.007
					3743 N	0.566	0.579		0.573	0.009
					3743 O	0.152	0.147		0.150	0.004
					3743 P	0.552	0.576		0.564	0.017
			19	1.50	3743 Q	0.328	0.324		0.326	0.003
					3743 R	0.155	0.156		0.156	0.001
					3743 S	0.088	0.090		0.089	0.001
					3743 T	0.464	0.479		0.472	0.011
			16	1.50	3743 U	0.149	0.146		0.148	0.002
					3743 V	0.360	0.358		0.359	0.001
					3743 W	0.604	0.613		0.609	0.006
					3743 X	0.602	0.610		0.606	0.006
			8	3.00	3743 Y	0.684	0.688		0.686	0.003
					3743 Z	0.720	0.727		0.724	0.005
Average									0.652	0.062
MS-1	0478267	2860672	1	0.89	3744 A	0.814	0.795		0.805	0.013
					3744 B	0.941	0.925		0.933	0.011
			2	0.89	3744 C	0.723	0.756	0.761	0.759	0.004
					3744 D	0.731	0.737		0.734	0.004
			4	0.89	3744 E	0.885	0.898		0.892	0.009
					3744 F	0.830	0.878	0.879	0.879	0.001
			23	1.02	3744 G	0.983	0.963		0.973	0.014
					3744 H	0.964	0.934		0.949	0.021
					3744 I	0.840	0.838		0.839	0.001
					3744 J	0.964	1.000		0.982	0.025
Average									0.874	0.088
MS-2	0478300	2860643	17	1.02	3745 A	0.823	0.830		0.827	0.005
					3745 B	0.809	0.795		0.802	0.010
			19	1.02	3745 C	0.789	0.733	0.799	0.794	0.007
					3745 D	0.828	0.814		0.821	0.010
			28	0.97	3745 E	0.704	0.689		0.697	0.011
					3745 F	0.760	0.771		0.766	0.008
			31	1.02	3745 G	0.752	0.714	0.731	0.732	0.019
					3745 H	0.761	0.762		0.762	0.001
			36	1.12	3745 I	0.764	0.738		0.751	0.018
					3745 J	0.750	0.713	0.728	0.730	0.019
			37	1.14	3745 K	0.954	0.927		0.941	0.019
					3745 L	0.349	0.346		0.348	0.002
Average									0.792	0.062
MS-1 & 2	Average								0.833	0.085

Table 4.1: Continued

Punta El Bajo			1		3871 A	0.811	0.755	0.756	0.756	0.001
					3871 B	0.844	0.847		0.846	0.002
					3871 C	0.806	0.805		0.806	0.001
					3871 D	0.848	0.853		0.851	0.004
			2		3871 E	0.750	0.739		0.745	0.008
					3871 F	0.709	0.712		0.711	0.002
					3871 G	0.763	0.772		0.768	0.006
					3871 H	0.741	0.751		0.746	0.007
Average									0.778	0.051

Figure 4.12: Photograph of deposit on 18 m (107 ka) terrace at Bahía Marquer.

The 25 m terrace at Bahía Marquer had only one collecting site, MCAS that had both shells and corals deposited together (Figures 4.13 and 4.14). Shells were analyzed using AAR and corals were dated using U-Th series. There were 12 sub-samples from 6 shells found at MCAS were initially run for AAR. Of those 12 sub-samples, 5 either showed signs of contamination or the results exceeded two standard deviations of the other sub-samples values. Therefore, it was decided to run 14 more sub-samples from 4 shells and, of those, another 7 sub-samples were discarded for contamination or falling

outside of two standard deviations. It is important to note that all shells from MCAS are of the species *Cardita californica* and not *Chione californiensis*, as in the 18 m terrace (Figure 4.15). The problems with modern contamination could be attributable to the different species of shell. The shells from the 25 m terrace had an average A/I ratio of 0.652 +/- 0.062 (Table 4.1; Figure 4.16).

At Punta El Bajo, there was one shell collection site on the 6 m terrace and only two *Chione californiensis* shells were found, yielding a total of 8 sub-samples. All sub-samples from El Bajo were used and none were contaminated or discarded. The average A/I ratio for the two *Chione californiensis* shells at El Bajo is 0.778 +/- 0.051 (Table 4.1; Figure 4.17).

Figure 4.13: Photograph of shells and corals within the 25 m (125 ka) terrace deposit.

Figure 4.14: Photograph of shells and corals of the 25 m (125 ka) terrace with tan calcarenite matrix of platform.

Interpretations of Geochronology and Correlation of Terraces

The AAR A/I ratios should increase as shells become older, but the results from Carmen Island give a lower A/I ratios (0.652) on the samples higher in elevation versus a higher A/I ratios (0.833) on the lower terraces (Figures 4.16 and 4.18). I found the reason for the discrepancy to be speciation between shells. The difference in shell species greatly changed the A/I ratios and therefore correlation could not be made between different shell species (Figure 4.15).

Chione californiensis shells found on the 18 m terrace at Bahía Marquer and the 6 m terrace at Punta El Bajo exhibited very similar A/I ratios, 0.833 +/- 0.085 and 0.778 +/- 0.051 respectively (Figures 4.16, 4.17, 4.18, and 4.19). Therefore, I imply a correlation of both terraces as having deposits of equal age (Figure 4.18). Previous work at Punta El Bajo by Mayer et al. (2002) revealed corals from the 6 m terrace that were dated using U-Th series and determined to be 107 ka (Mayer et al., 2002). I conclude that the 18 m

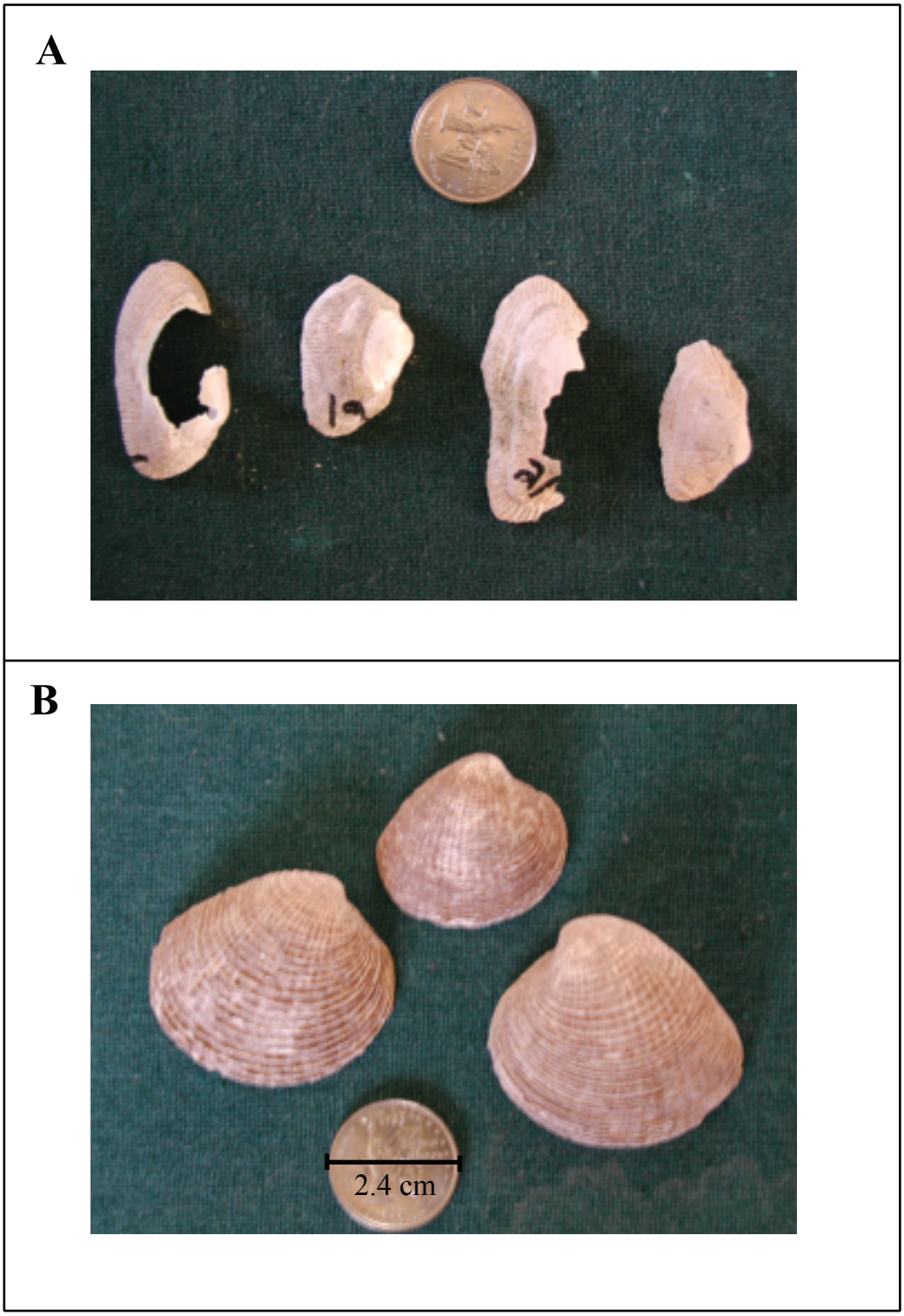

Figure 4.15: Two types of shell species from Bahía Marquer and Punta El Bajo. A) *Cardita californica*, found on 25 m (125 ka) terrace at Bahía Marquer. B) *Chione californiensis*, found on 18 m (107 ka) terrace at Bahía Marquer and 6 m (107 ka) terrace at Punta El Bajo.

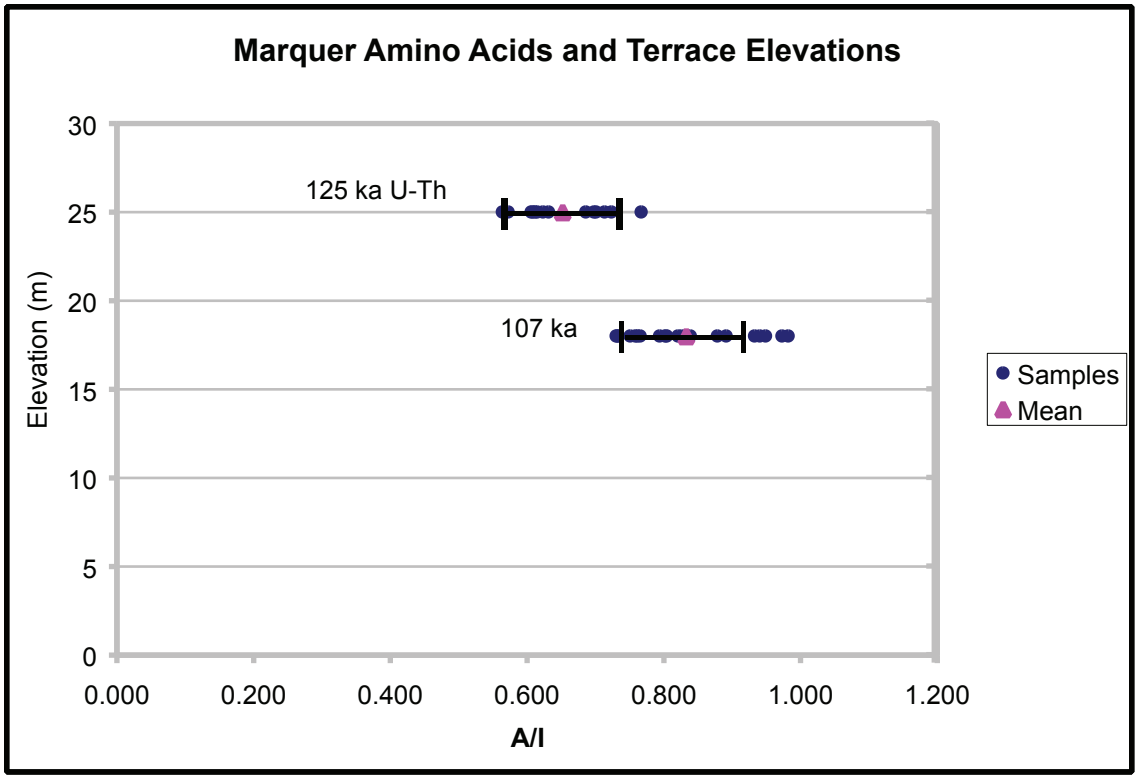

Figure 4.16: Graph of Bahia Marquer samples with A/I ratios and their associated elevation terrace. Mean A/I ratio is plotted as triangle. Note that different species *Cardita californica* was found on the 25 m (125 ka) terrace, and *Chione californiensis* was found on 18 m (105 ka) terrace. 125 ka date is U-Th series by Kathleen Simmons (USGS) and 107 ka age is correlated from Punta El Bajo (Mayer et al., 2002).

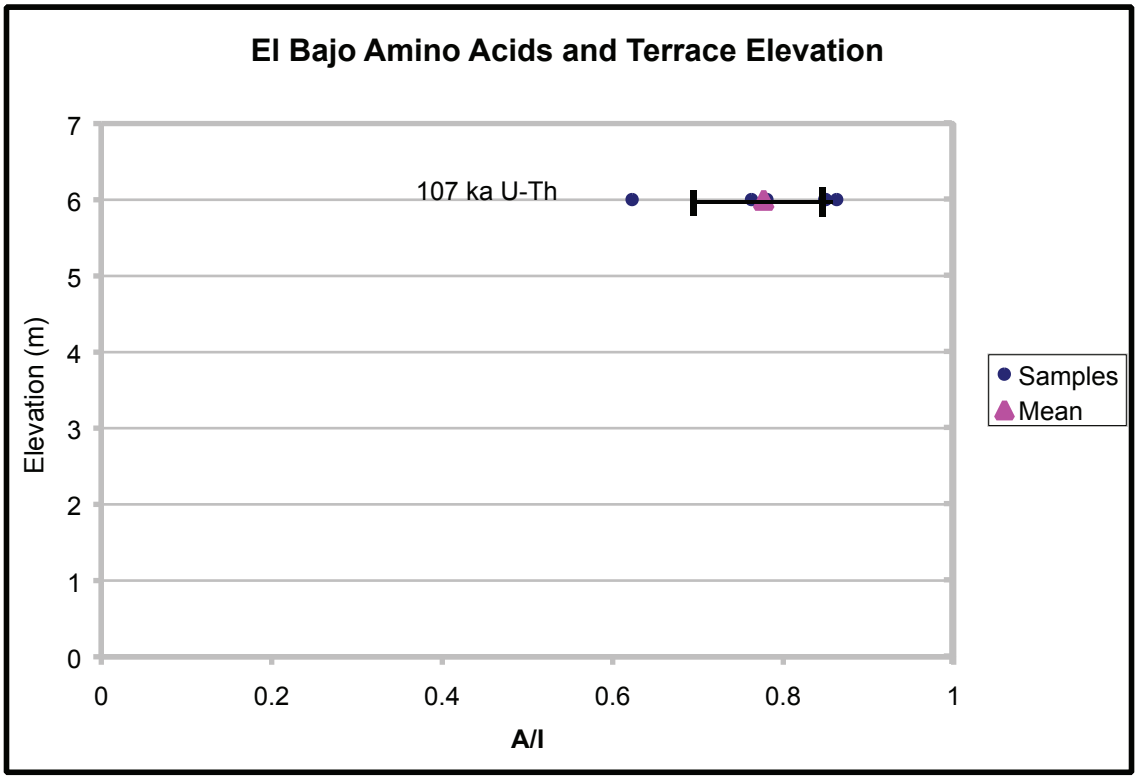

Figure 4.17: Graph plotting shell samples collected at Punta El Bajo with A/I ratios and the elevation at which the shells were collected. Note species *Chione californiensis* was found on 6 m terrace. 107 ka date is U-Th series (Mayer et al., 2002).

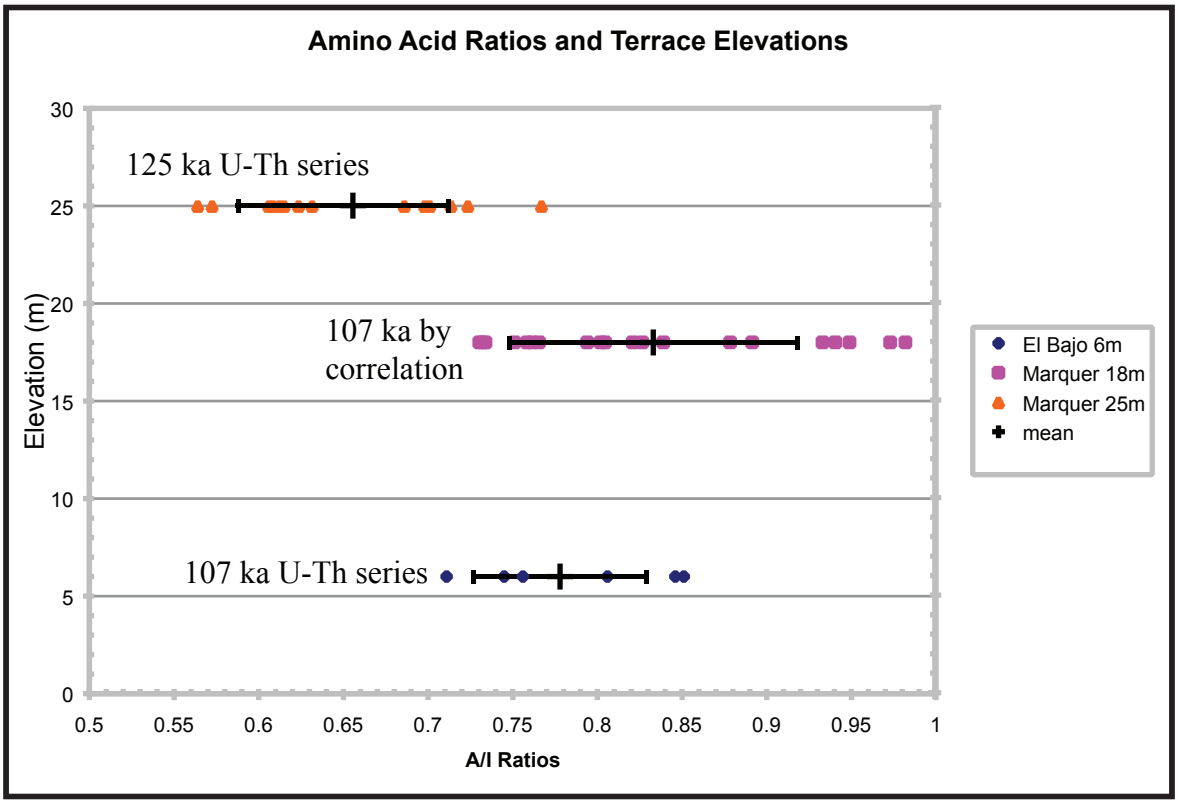

Figure 4.18: Graph plotting A/I ratios of shell samples from Punta El Bajo 6 m terrace, Bahia Marquer 18 m terrace, and Bahia Marquer 25 m terrace. Mean A/I ratio are plotted with + symbol and one standard deviation is designated by error bars.

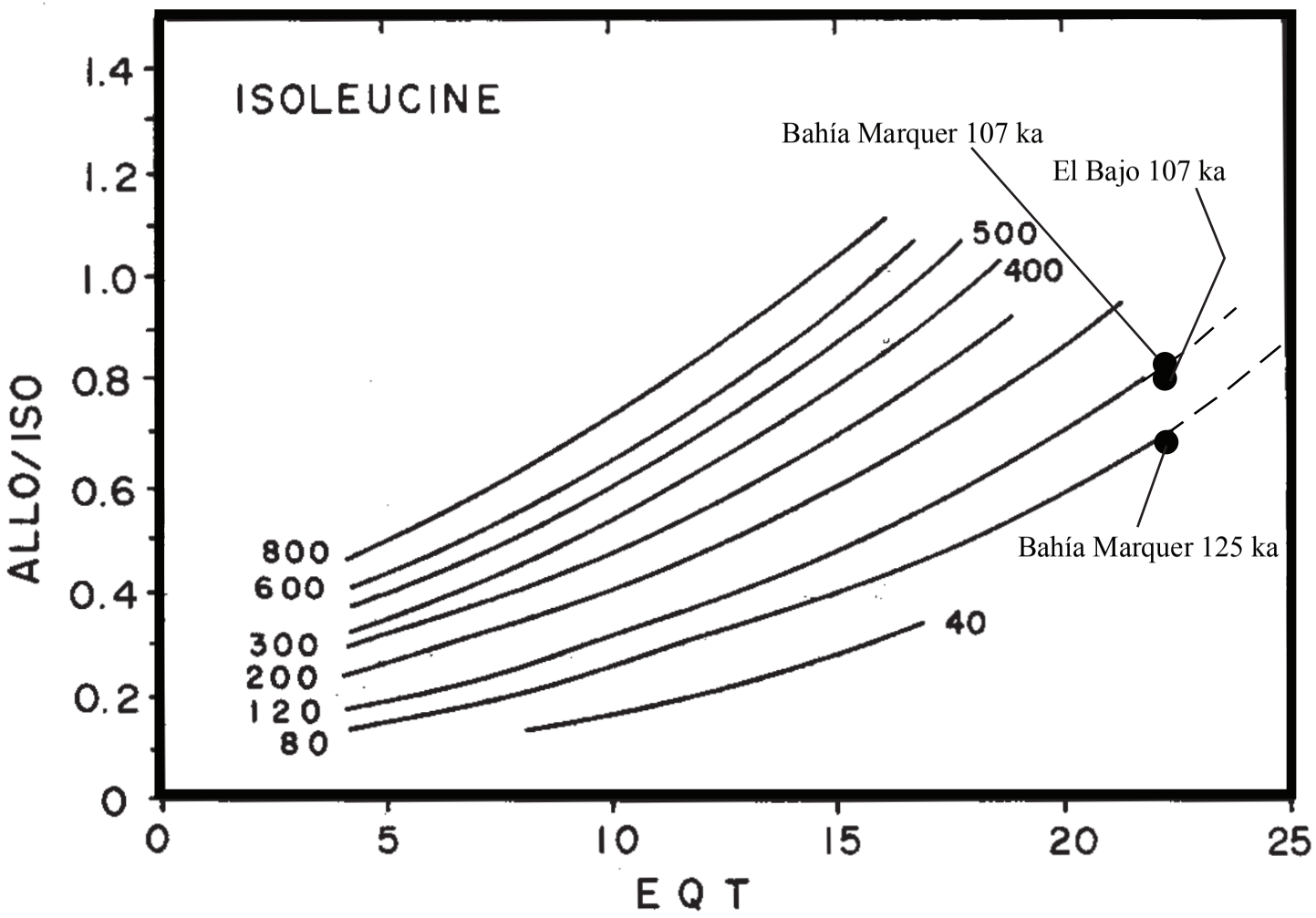

Figure 4.19: Expected epimerization/racemization of isoleucine for given ambient temperatures (Wehmiller and Miller, 2000). Marquer 125 ka data point was subject to species problems and exhibited lower thatn expected A/I ratios. Higher than expected A/I ratios for Marquer 107 ka and El Bajo 107 ka could be attributable to warm climate and demonstrate that upper end of predicted A/I ratios may be erroneous and should be shifted higher.

terrace at Bahía Marquer on Carmen Island is also 107 ka and was formed during the I.S. 5c. Sea-level during the I.S. 5c has been subject to revisions by many researchers. Chappell and Shackleton (1986) showed sea-level at ~-9 m below modern sea-level based on work in Papua New Guinea (Table 4.2). Studies of marine terraces along the Pacific coast of North America by Rockwell et al. (1989) (cited in Mayer and Vincent, 1999) and Muhs et al. (1994) indicate that sea-level during the I.S. 5c was probably at ~-2 m below modern sea level (Table 4.2). Uplift rates for Bahía Marquer were calculated using both sea-levels and I found the -2 m sea-level for I.S. 5c indicated by Rockwell et al. (1989) as more probable for the Carmen Island study area because they indicate a near steady uplift rate. Uplift rates for the 18 m terrace at Bahía Marquer using Chappell and Shackleton (1986) sea-level curve are ~0.26 m/ka, whereas uplift rates based on Rockwell et al. (1989) are ~0.19 m (Figure 4.20; Table 4.2). Estimated uplift rates from other terraces at Bahía Marquer suggest the ~0.19 m/ka is preferred (Table 4.2).

Table 4.2: Isotopic stage ages and uplift rates for Bahía Marquer terraces based on surveyed marine terraces and eustatic sea level.

I.S. Age	Ancient Sea-level elevation from modern (m)	Surveyed Terrace (m)	Inferred Uplift (m)	Uplift Rate m/ka
320 ka	+4(1)	55	51	0.16
120 ka	+6(1)(2)	25	19	0.15
105 ka	-2(2)	18	20	0.19
105 ka	-9(1)	18	27	0.26

(1) Chappell and Shackleton, 1986
(2) Rockwell et al., 1989

The 25 m terrace at Bahía Marquer was dated by U-Th series from a coral collected by Becky Dorsey, University of Oregon, and were found to have a U-Th series

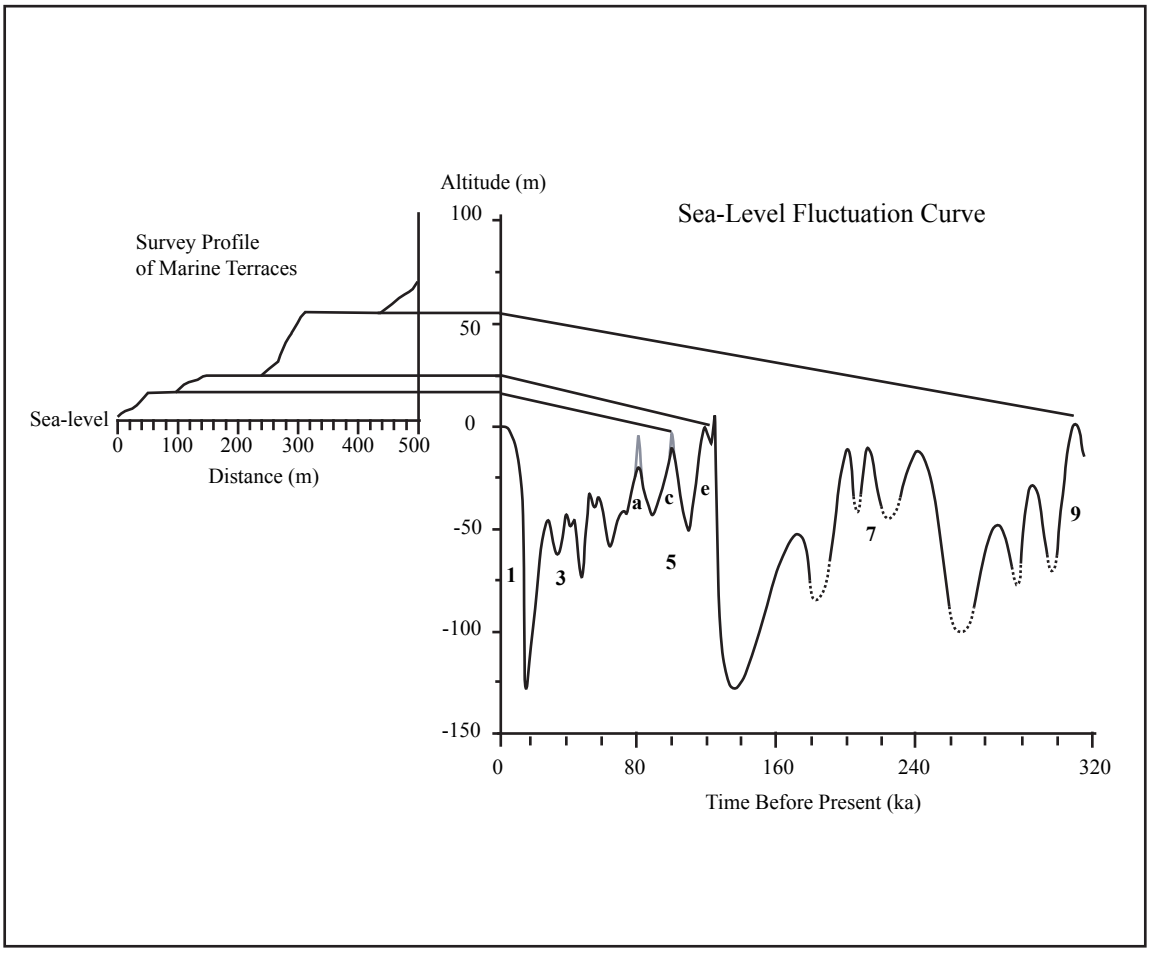

Figure 4.20: Prediction diagram with sea-level fluctuation curve and altitude of marine terraces from Bahia Marquer. Gray extensions on sea-level curve represent sea-level determinations from Muhs et al., 1994. Dashed lines represent uncertainty of lowstands of sea-level (after Chappell and Shackleton, 1986; Muhs et al., 1994).

age of 125 ka (Mayer et al., 2002). The 25 m terrace on Carmen Island was formed during the I.S. 5e. Sea-level during the I.S. 5e was ~6 m higher than present sea-level (Chappell and Shackleton, 1986; Rockwell et al., 1989; Muhs et al., 1994). Although the amino acid chronology could not be correlated for the 25 m terrace, the U-Th series date given to this terrace can be used with the *Cardita californica* A/I ratio of 0.652 for correlation of further studies. The 125 ka U-Th series age on the coral from the 25 m terrace at Bahía Marquer suggests an uplift rate of ~0.15 m/ka (Figure 4.20; Table 4.2).

Modeling a constant uplift rate of between ~0.15 and 0.19 m/ka would place the formation of the Bahía Marquer 55 m terrace during the I.S. 9, at 320 ka (Table 4.2). Therefore, the 55 m terrace would suggest uplift rates of ~0.16 m/ka and is likely correlated to the 26 m terrace at Punta El Bajo surveyed by Mayer and Vincent (1999). If we use a regression analysis on all three terraces at Bahía Marquer, then we see an average uplift rate of ~0.15 m/ka with an R^2 relationship of 0.99 (Figure 4.21). Another line of evidence supporting formation of the 55 m terrace at Bahía Marquer during I.S. 9 is the relationship between terraces at Bahía Marquer and Punta El Bajo (Table 4.3). At both locations there are uplifted marine terraces from I.S. 5c (105 ka), 5e (125 ka), and 9 (320 ka). Punta El Bajo has an additional I.S. 5a (80 ka) terrace, but that is a low-lying terrace that could have been removed at Bahía Marquer. We have a strong correlation between terrace formation at Bahía Marquer and Punta El Bajo and justifiably so because they are close in location to one another, ~30 km apart. I used the same approach as Mayer and Vincent (1999) when looking at paleo-sea-levels from I.S. 5c, 5e, and 9. Mayer and Vincent (1999) adopted the sea-level curve from Rockwell et al. (1989) for I.S. 5c, but chose to accept I.S. 9 sea-level from work by Chappell and Shackleton

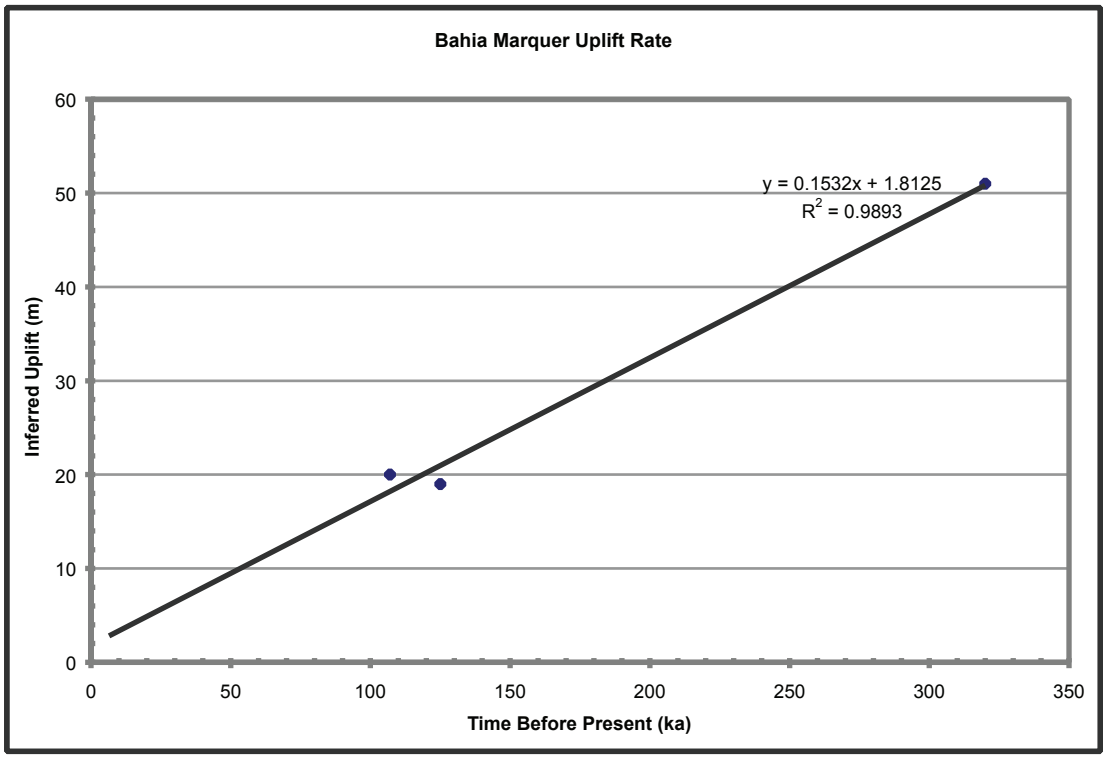

Figure 4.21: **I**nferred uplift versus time at Bahia Marquer. Equation besides curve is determined from linear regression analysis and indicates an average uplift rate of ~0.15 m/ka.

(1986), and used the accepted sea-level, + 6 m, for I.S. 5e from both Rockwell et al. (1989) and Chappell and Shackleton (1986). Uplift rates on Carmen Island are determined to be ~0.15 m/ka for the last 320 ka at a steady rate. Mayer and Vincent (1999) estimated uplift rates of ~0.08 m/ka for the Loreto region at Punta El Bajo. The results demonstrate that Carmen Island has been uplifting at almost twice the rate of the coastal belt near Loreto.

Table 4.3: Comparison of surveyed uplifted marine terraces at Punta El Bajo and Bahía Marquer with uplift rates.

	Location	
I.S. Age	**Punta El Bajo Surveyed Terraces (m)**	**Bahía Marquer Surveyed Terraces (m)**
320 ka	26	55
120 ka	16	25
105 ka	6	18
80 ka	3	na
Uplift rates	0.08 m/ka	0.15 m/ka

CHAPTER 5

DISCUSSION

This study has reported evidence for rotation of Carmen Island from paleomagnetic data and uplift of Carmen Island from surveyed marine terraces and a geochronology of those marine terraces. This study is an initial examination of the timing and style of tectonics on Carmen Island and the relationship of Carmen Island to the Loreto rift segment.

Tectonic Evolution of Carmen Island

As previously discussed in chapter 3, Umhoefer et al. (2002) proposed a tectonic evolution of Carmen Island. This study supports much of the model of Umhoefer et al. (2002), but modifies the estimates of Carmen Island's rotation and timing.

The period of ~6 to 2 Ma saw the Loreto fault probably linked to a system of offshore faults including northwest-striking dextral faults and north to north-west-striking normal faults (Figure 5.1) (Umhoefer et al., 2002). The timing on the initiation of the Loreto fault is poorly constrained. Two of these dextral-strike slip faults are the Farallon and North Pescadero strike-slip faults that evolved to the Farallon and North Pescadero transform faults. Carmen Island was rotated between these two strike-slip faults to the northwest and southeast and normal faults to the east and west (Nava-Sanchez et al., 2001) and as a result rotated (Figure 5.1). The amount of rotation and style of block rotations can be evaluated in a number of scenarios. What must be true of any scenario is that any rotations occurred after ~12 Ma, and rotations after 3 Ma are likely to be $<10^{o}$.

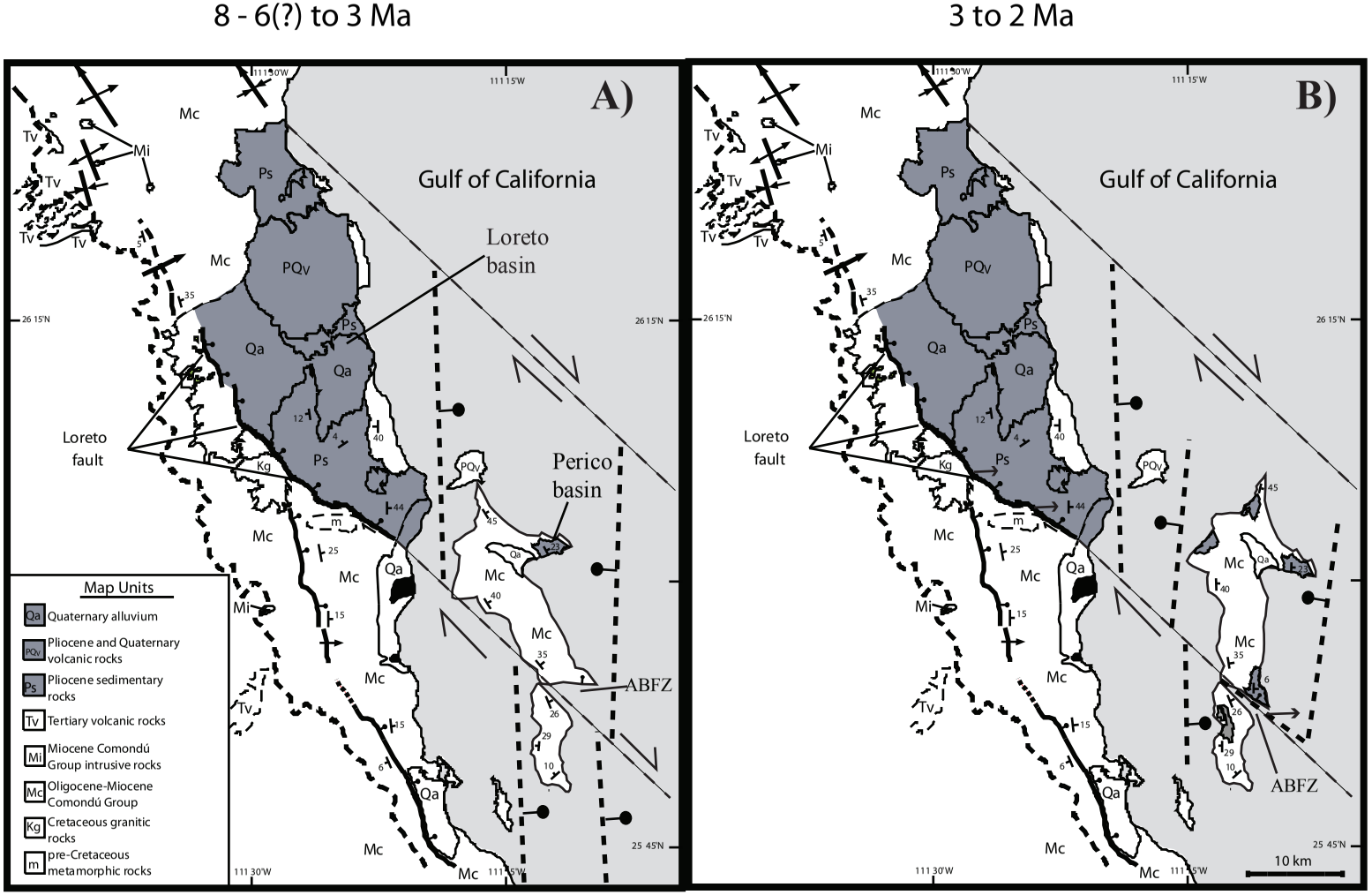

Figure 5.1: Reconstruction of rotation and uplift of Carmen Island. A) Northern two-thirds of Carmen Island is restored counterclockwise 60° and southern third is restored counterclockwise 7° back to hypothesized original position. Southern strike-slip fault is offshore extension of the Loreto fault and divides Carmen Island as a proto-Arroyo Blanco fault. This fault system is an extension of the South Pescadero fracture zone shown in (D). Northern strike-slip fault is extension of North Pescadero fracture zone shown in (D). Normal faulting, located to the east and west of island rotated beds that dip to the east for the northern two-thirds of the island and to the west for the southern thrid of the island. B) Northern two-thirds of Carmen Island has rotated ~50° clockwise from A. Normal fault movement continues east and west of Carmen Island and a graben forms between Carmen Island and the Loreto Basin. Dashed lines are inferred faults from onshore features and bathymetric escarpments. ABFZ = Arroyo Blanco fault zone.

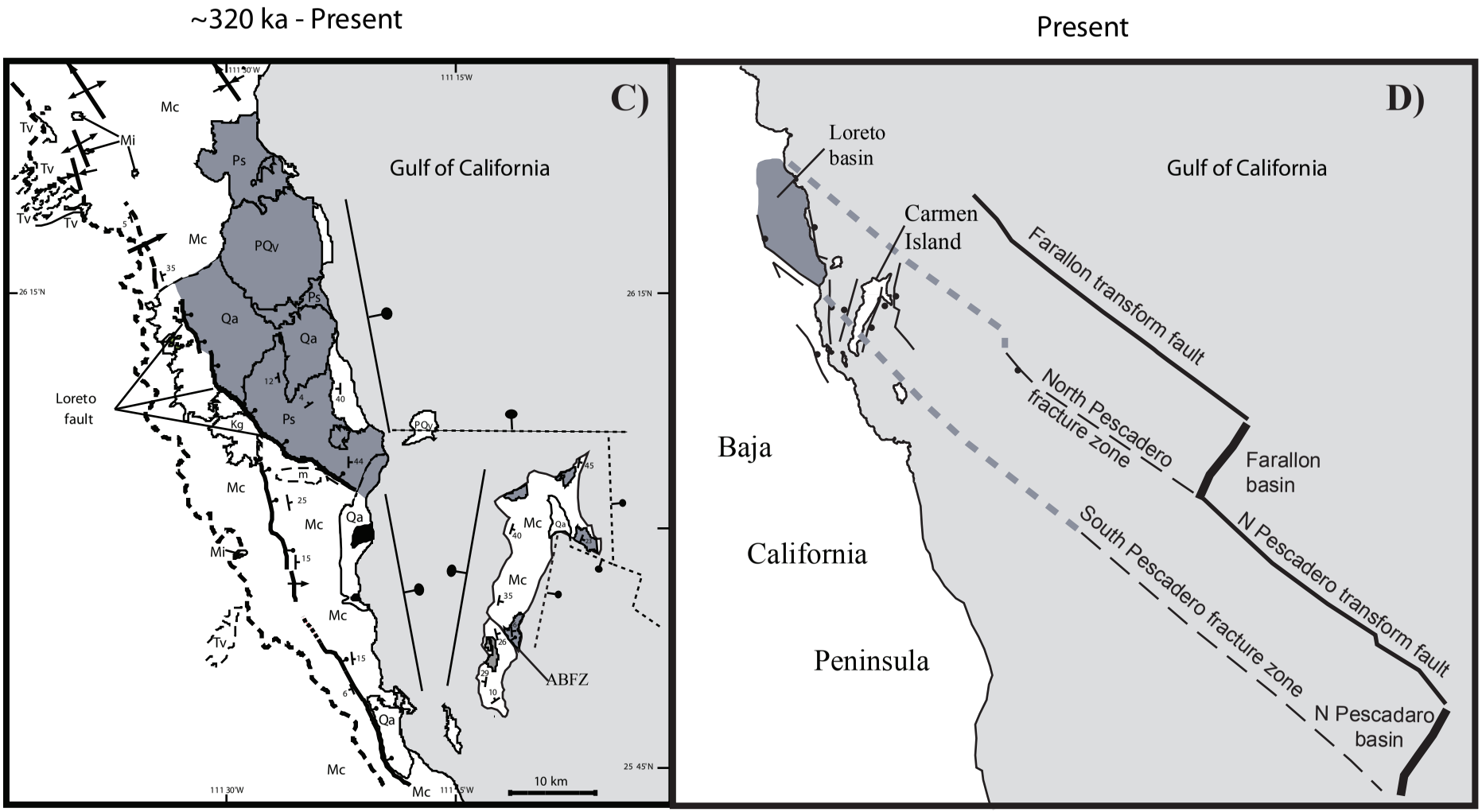

Figure 5.1: (Continued) C) Strike slip faulting has stopped and Carmen Island is uplifting between normal faults as a horst. D) Larger view of present Carmen Island and relationship to Pescadero and Farallon fracture zones and transform faults. Dashed lines are inferred faults from onshore features and bathymetric escarpments. Farallon and North Pescadero basins are topographic basins with a spreading center in the middle of the basin.

Scenario 1: No Rotation

If Carmen Island has experience no rotation, then all beds and faults would be in the same position today as they were originally. Geologic evidence from bedding and faults of the Loreto rift segment suggest otherwise. The strike of bedding in the Loreto rift segment and bedding on Carmen Island should be parallel if the island did not rotate. Bedding on Carmen Island strikes approximately NNE-SSW and bedding in the Loreto rift segment strikes approximately NNW-SSE. Also, it would be expected to see parallel structures on Carmen Island and in the Loreto rift segment. Structural data from Umhoefer et al. (2002) show that in domain P on north Carmen Island are faults in Miocene rocks that record an extension direction of 120^{o}-300^{o}, not compatible with extension directions found in faults of Miocene rocks from domains L, M, N and O of the onshore Loreto segment. If there was no rotation, then normal faults from the southern portion of Carmen Island along Pliocene strata would be expected to record an extension direction of E-W and strike N-S, which they do not (Umhoefer et al., 2002). Paleomagnetic data would also yield 0^{o} of rotation and even with the largest amount of error calculated from the northern domain, paleomagnetic data yields some rotation. There is no evidence to support no rotation of the whole island.

Scenario 2: Northern two-thirds of Carmen Island rotated clockwise ~100^{o} and southern third rotated clockwise ~10^{o} from 12 to 3 Ma and there was no rotation after 3 Ma.

Scenario two is based on paleomagnetic evidence from Carmen Island. Paleomagnetic data suggest the northern two-thirds of Carmen Island rotated clockwise between ~60^{o} and 140^{o}. If Carmen Island is rotated back 100^{o} to its original position at ~12 Ma, then it becomes obvious that this scenario is not possible because land masses would overlap (Figure 5.2). Large rotations are possible if northern Carmen Island has many independently rotating domains of variable rotation, but consistent bedding attitudes make this unlikely. Other lines of evidence that dispute large amounts of rotation include the differences in fault orientations and bedding attitude on Carmen Island and on the Baja California peninsula. Scenario 2 would produce bedding on the northern two-thirds of Carmen Island that would originally strike almost E-W and would be perpendicular to bedding in the Loreto segment if some of the tilt was before rotation (Figure 5.2). Bedding on the southern third of Carmen Island would also be near perpendicular to bedding from northern Carmen Island (Figure 5.2).

Comparing primary and secondary faults from Carmen Island and the Loreto segment would also produce erroneous results for scenario 2. Faults from Miocene rocks in the Loreto rift segment show an extension direction between 245^{o}-250^{o}, perpendicular to the rift axis. These faults are demonstrated in domains L, M, N, and O from Umhoefer et al. (2002). Faults from Miocene rocks in domain P, on Carmen Island have an extension direction of ~120^{o} -300^{o} (Umhoefer et al., 2002). If Carmen Island has rotated 110^{o} then the original extension direction of faults in Miocene rocks would be almost N-S and would not be compatible with early faulting from the Loreto rift segment if these faults formed before rotation. Calculated extension directions for faults in Miocene and Pliocene rocks for the southern third of Carmen Island are between 255^{o} and 265^{o}. An

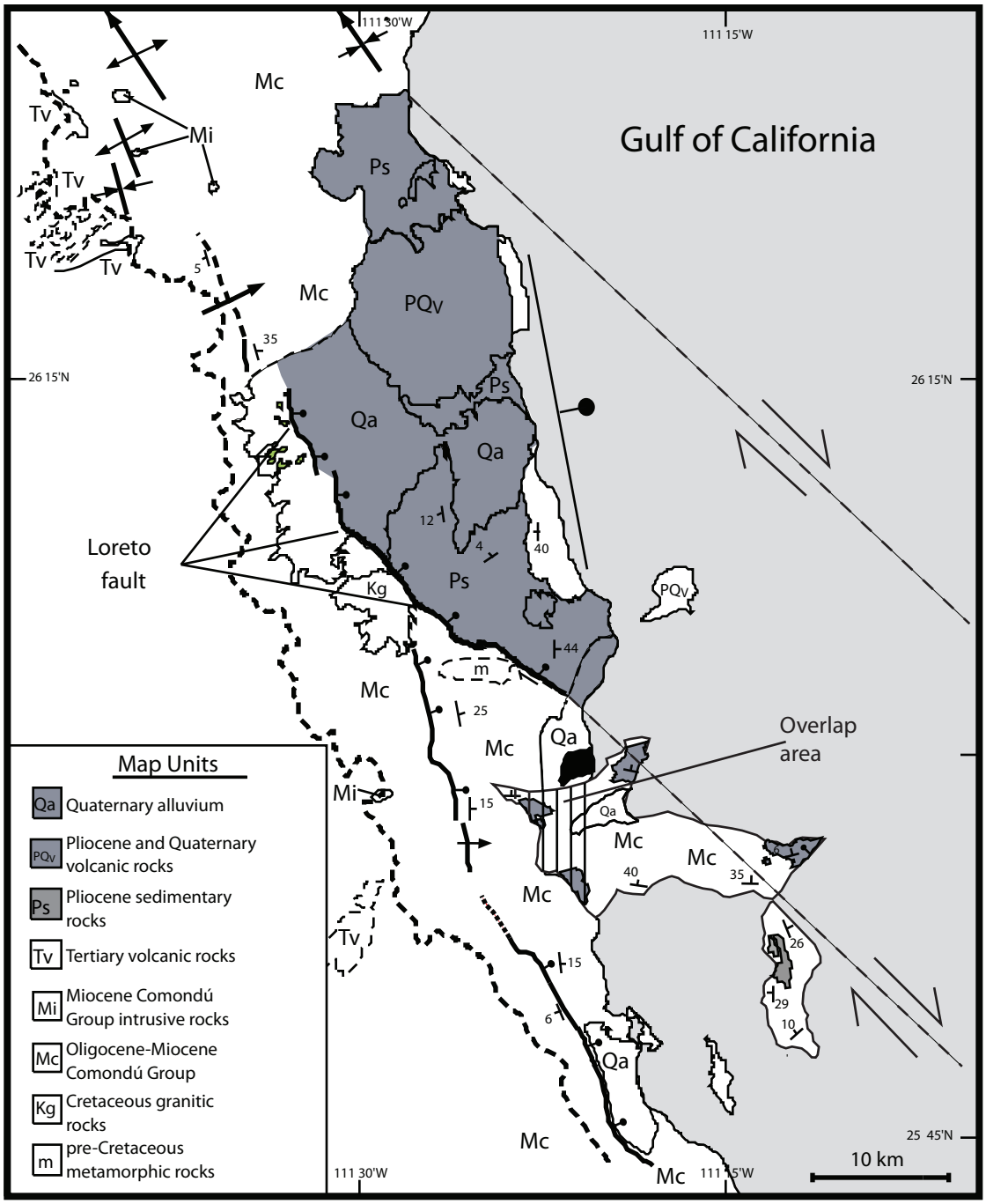

Figure 5.2: Northern two-thirds of Carmen Island is restored counterclockwise ~100º as one domain and southern third is restored counterclockwise ~10º. Northern two-thirds of Carmen Island substantially overlaps onshore Loreto segment. Dashed lines are inferred faults from onshore features and bathymetric escarpments.

extension direction between 255^{o} - 265^{o} is similar to that found in faults from domains L, M, N, and O (245^{o} – 250^{o}) and support no rotation for the southern third of the island (Umhoefer et al., 2002).

Pliocene rocks of the Perico basin are dated between 2 and 3 Ma and paleomagnetic evidence from these rocks shows little to no rotation. Therefore, it is concluded that rotations would have stopped by this time period, and geologic evidence from faults in Pliocene rocks (Domain Q) support this claim. Faults in Pliocene rocks in domain Q show a similar extension direction as faults in Miocene rocks from both Carmen Island domains Q and R, and the Loreto segment domains L, M, N, O (Umhoefer et al., 2002). We would expect to see a difference between Pliocene and Miocene faults if rotation had occurred. Scenario 2 fits the paleomagnetic evidence from this study, but geologic evidence invalidates this scenario.

Scenario 3: Northern two-thirds of Carmen Island rotated clockwise the minimum ~60^{o}, and southern third rotated clockwise ~10^{o} from 12 to 3 Ma and there was no rotation after 3 Ma.

Paleomagnetic evidence shows that the northern two-thirds of Carmen Island may have rotated clockwise a minimum of ~60^{o} within errors and the southern third of the island may have rotated ~10^{o} from 12 to 3 Ma. Paleomagnetic data also support little to no rotation for Pliocene age strata at about 3 to 2 Ma. If the northern two-thirds of Carmen Island is restored ~60^{o} counterclockwise back to its original position at ~12 Ma, then there are many lines of evidence in support (Figure 5.1). Bedding on the northern two-thirds of Carmen Island would strike within 10^{o} to 15^{o} of same age rocks in the

Loreto segment. Extension direction of faults in Miocene rocks on Carmen Island in domain P is ~120^{o} -300^{o} (Umhoefer et al., 2002). Rotating these faults counterclockwise 60^{o} would result in an extension direction of ~240 ^{o} which is compatible with extension directions for faults in Miocene age rocks from domains L, M, N, and O (Umhoefer et al., 2002). Umhoefer et al. (2002) showed that normal faults with ~245^{o} extension direction are likely Miocene and formed before the Loreto fault. The agreement for the restoration domain P suggests those faults are pre-rotation and also Miocene.

The southern third of Carmen Island has experienced little to no rotation and is supported not only by paleomagnetic data, but also by faults in Miocene and Pliocene age strata from domain R (Umhoefer et al., 2002). Faults from domain R record a similar extension direction when compared to faults in domains L, M, N, and O, ~240 to 260^{o}. Pliocene paleomagnetic data and structural data from domain Q support little or no rotation for strata after ~3 to 2 Ma as discussed in scenario 2.

Scenario 4: Northern two-thirds of Carmen Island rotated clockwise ~40 to 50^{o} from 12 to 3 Ma and rotated clockwise ~10 to 20^{o} from 3 Ma to present. Southern third rotated 5 to 7^{o} clockwise from 12 to 3 Ma and 3 to 5^{o} from 3 Ma to present.

Scenario 4 is similar to scenario 3, but the estimate of the timing of rotation and amount of rotation are different. If the northern two-thirds of Carmen Island rotated ~40^{o} to 50^{o} from 12 to 3 Ma, then it would be expected to see differences in orientation between faults from Miocene age rocks on Carmen Island and in the Loreto rift segment. In domains L, M, N, and O of the Loreto rift segment, there is an average extension direction between 245^{o} -250^{o}. Extension direction for domain P on Carmen Island is

120° -300°. Restoring domain P counterclockwise by ~40° -50° gives an extension direction of about 250° -260° and is compatible with domains L, M, N and O. Bedding attitude on Carmen Island supports ~45° of rotation based on mean strike of bedding of Miocene rocks on the northern two-thirds of the island versus mean strike of bedding from Miocene rocks in the Loreto segment. Paleomagnetic evidence from the northern two-thirds of Carmen Island also suggests rotations. Although paleomagnetic evidence shows more rotation (65° -110°) than expected (35° -45°) from geologic models, this evidence supports clockwise rotation of the island. Scenario 4 also differs from scenario 3 because the rotation of Carmen Island is not complete by 3 Ma. The northern two-thirds of Carmen Island still experiences small amounts of rotation into late Pliocene time, ~2 Ma. Pliocene strata found on Carmen Island are depositing at the end of rotation and record the last 10° of rotation. The mean paleomagnetic result from Pliocene rocks in the northern Perico Basin show a small amount of rotation within error, ~20° or less. Pliocene strata used for paleomagnetic analysis may not have been dated correctly based on misinterpretation of foraminifera and could be closer to 2.5 Ma than the previously thought 3 to 3.5 Ma (Umhoefer, personal communication, 2005). These lines of evidence allow for Carmen Island to have rotated until ~2 Ma. The southern third of Carmen Island has experienced little rotation, about 10°. Following the argument that Carmen Island may be experiencing rotation until 2 Ma leads to the following scenario. The southern third of Carmen Island would have experienced only ~5° - 7° of rotation from 12 to 3 Ma. This is confirmed with paleomagnetic data that within error allows for 5° - 7° of rotation and from bedding on the southern third of Carmen Island. Structural data from domain R on southern Carmen Island shows similar extension direction to faults in rocks

in Miocene, Pliocene and Quaternary time (Umhoefer et al., 2002). Average extension direction for domain R is 255^{o} to 265^{o}, ~10^{o} more westerly than domains L, M, N, and O of the Loreto Segment. Structural data supports minimal rotation as suggested by paleomagnetic data. The rotation of the southern third of Carmen Island continues until about 2 Ma as suggested by Pliocene data from the Perico basin.

Based on the above scenarios I have reconstructed a tectonic evolution of Carmen Island that modifies the Umhoefer et al. (2002) model (Figure 5.1). Between 8 and 6 Ma there is a change in plate motion (Atwater and Stock, 1998) and the Gulf moves from orthogonal rifting to oblique rifting. At 8 - 6 Ma the northern two-thirds of Carmen Island was likely ~60^{o} counterclockwise of its position today and the southern third of the island was ~10^{o} counterclockwise from its current position (Figure 5.1A). Significant normal faulting had likely already occurred from 12 – 8 Ma in the Loreto segment so that some of the tilting of beds on Carmen Island had already occurred before 8 Ma. The southern Loreto fault is a northwest-southeast striking dextral-normal fault that has many jogs and bends (Figure 5.1). If the southern Loreto fault is extended offshore, then we can project the fault zone through the area of the current Arroyo Blanco fault (Figure 5.1A and D). This area will be informally named the proto-Arroyo Blanco fault zone and may not have behaved like the current Arroyo Blanco fault, but may be a larger fault zone that has been overprinted by the current Arroyo Blanco fault. The projection of the Loreto fault offshore lines up along the western edge of 8-6(?) to 3 Ma Carmen Island and forms the southern of two strike-slip faults responsible for the rotation of Carmen Island (Figure 5.1A). To the north, there is another area of strike-slip faulting that is associated with the North Pescadero fracture zone (Figure 5.1D). Projecting the North

Pescadero fracture zone from the central Gulf of California to the Loreto rift segment forms the northern strike-slip fault that borders Carmen Island (Figure 5.1A and D). Projection of the North Pescadero fracture zone to the Loreto rift segment also lines up with synclines found at the north end of the Loreto rift segment (Figure 5.1C) (Umhoefer personal communication). Two parallel, projected strike-slip faults isolate Carmen Island into a northern two-thirds and southern third block at the area called the Arroyo Blanco fault zone (Figure 5.1A). To accommodate the rotation and tilting of bedding on Carmen Island it is necessary for normal faulting to the east and west. Also, south of the Arroyo Blanco fault zone, there is normal faulting that accommodates modest rotation in this fault zone.

Scenarios 3 and 4 for the rotation of Carmen Island are favored. Although there are still some conclusions to be reached about the exact timing of the completion of rotation, scenario 4 is the most favored by this study. Paleomagnetic, geologic bedding, and structural data support scenario 4 as the possible rotation of Carmen Island. Another important aspect about scenario 4 is the dip of bedding on Carmen Island. As previously mentioned, bedding north of the Arroyo Blanco fault dips east and south of the Arroyo Blanco fault bedding dips west (Figures 2.4 and 5,1). To account for the different dips in bedding we have a period from ~3 to 2 Ma where Carmen Island is still experiencing a small amount of rotation, but normal faulting becomes more dominant and beds are tilted (Figure 5.1B). There is still an area called the Arroyo Blanco fault zone, which divides the island and allows both domains to dip in different directions. Normal faulting in the northern two-thirds of Carmen Island is greater in magnitude than in the south as seen by beds that dip 29^{o} or less in the southern third and 35^{o} to 45^{o} in the northern two-thirds

(Figures 2.4 and 5.1). By ~2 Ma all rotation of Carmen Island has stopped. The good evidence for cessation of strike-slip faulting in the Loreto fault at ~2 Ma supports this conclusion (Dorsey and Umhoefer, 2000). Normal faulting continues from 2 Ma into the Quaternary, but strike-slip faulting offshore of the Loreto segment has moved into transform faults in the central Gulf of California (Figure 5.1C and D). The proto Arroyo Blanco fault zone likely ended by ~2 Ma and the dextral-normal Arroyo Blanco fault we see today became active and overprints the proto Arroyo Blanco fault zone. The secondary faults in the footwall of the Arroyo Blanco fault are complex with evidence of different extension directions (Vlad, 2001) and support this complex 2-stage faulting history.

Normal faulting in Quaternary time along the Loreto segment resulted in uplifted marine terraces on Carmen Island and at Punta El Bajo. Uplift rates are ~0.08 m/ka for the coastal belt near at Punta El Bajo and ~0.15 m/ka for the western side of Carmen Island as concluded from surveyed and dated uplifted marine terraces. From 320 ka to the present, Carmen Island has been uplifting between two normal faults. Nava Sanchez et al. (2001) mapped a graben ~4 km west of Carmen Island between the island and the city of Loreto (Figure 5.1C). There is a low-lying salt deposit (Qa) on the northern part of Carmen Island and it is suspected that down-to-the-east normal faulting is associated with it (Figure 5.1). Projecting a fault south from the salt deposit provides a second normal fault by which to uplift Carmen Island (Figure 5.1C). Based on the greater number and higher elevation marine terraces on eastern Carmen Island at Arroyo Blanco, Quaternary slip rates on the eastern side of Carmen Island are interpreted to greater than on the western side of Carmen Island (Figure 5.1C). The Pliocene Perico basin is also

uplifting on Carmen Island and that may be connected to additional normal faulting near Punta Perico (Figure 5.1C) (Dorsey et al., 2001). In Quaternary time, the southern Loreto fault is not active and is thought not to extend further southeast offshore, ~5 km north of Loreto, but is linked to normal faults east of Loreto and speculated to link to a complex east-striking fault zone north of Carmen Island (Figure 5.1) (Umhoefer et al., 2002). This east-striking fault zone projects under Coronado Island and the uplifted marine terraces at Punta El Bajo and along the northern shores of Carmen Island suggest that this fault zone is active.

Recommendations for Future Studies

This study supports, and begins to quantify, the ideas that Carmen Island has experienced Miocene to Pliocene rotation and Quaternary uplift. This study used a broad approach when examining Carmen Island, where very little work had been done. A general tectonic framework was established, but many questions concerning the amount of rotation are still unanswered. An important result of the work of this study concerns the knowledge gained about the possible complexity of rotation of Carmen Island. In the northern two-thirds of Carmen Island there were variable and large paleomagnetic rotations suggested for Miocene rocks. The reasons why there were large paleomagnetic rotations warrants further study. There were only two sites used for the paleomagnetic analysis in Pliocene-age rocks, in which negligible rotation was found, and that also warrants further study. Future studies are necessary to determine the amount of rotation and details of the complex rotation history.

Improvements could be made on paleomagnetic sampling and analysis for future studies of Carmen Island. Paleomagnetic results yielding varying degrees of rotation could be attributable to errors in the collection process and rock types chosen for analysis.

As previously stated, paleomagnetic rock drilling equipment malfunctioned while this study was in progress and I had to use oriented rock slabs to be drilled back in the laboratory. Inherently, collecting oriented rock slabs will have larger orientation errors than drilling cores in the field. Rock slabs were oriented using a Brunton compass and the compass could have been affected by the rock magnetic properties. Back in the laboratory, an oriented rock face from each rock sample was drilled into at 90^{o} or as close to 90^{o} as possible. Rock faces were squared against the paleomagnetic drill press using multiple leveling devices, but some cores may not have been drilled perfectly square.

Rock types collected for paleomagnetic analysis may have caused the variable paleomagnetic results. Volcanic sandstones carried the most stable and easily deciphered magnetic signal. Alternating field demagnetization of volcanic sandstones was also very consistent and reliable.

Welded tuffs and tuffs were used for paleomagnetic samples, but tuffs record an instantaneous record of the geomagnetic field. Therefore, paleomagnetic results from tuffs may not be representative of the Earth's magnetic field for a long enough time period to average secular variation. Tuffs are very useful for chronologies because tuffs have a unique magnetic signature that allows correlation to other tuffs. Stock et al. (1999) demonstrated that the tuff of San Felipe has a unique, low inclination, reversed magnetization, which may record a field transition or a geomagnetic excursion within

reversed polarity subchron C5Ar.2r (12.401 to 12.678 Ma). Tuffs on Carmen Island were difficult to temporally constrain in this study because there is limited geologic mapping of the island and the number and ages of tuffs are unknown. Paleomagnetic evidence from tuffs on Carmen Island would be beneficial after mapping and dating these tuffs. After tuffs are mapped on Carmen Island, then they could be used for paleomagnetic analysis to test whether different exposures of the same tuff have different declinations and inclinations, and whether there is evidence of secular variation within the tuff. If samples were analyzed from beds immediately below and above the tuffs, secular variation could be averaged. It would be most powerful if the same tuff could be indentified in the footwall of the Loreto rift segment and on Carmen Island so paleomagnetic comparisons of the same deposit could be made.

Another rock type used in the paleomagnetic analysis was volcanic breccia and clasts within the breccia could contain some remanent magnetization. Larger breccia clasts could contain some secondary magnetizations and may not have been fully removed during demagnetization processes. I only collected a few breccias, and I only collected those with good bedding and with small to no clasts. However, breccias are not preferred for this type of study and should be avoided in future studies.

Mudstone/marlstone carried weak, but usable magnetic signatures. Mudstone/marlstone had inconsistent demagnetization properties and it was often difficult to decipher their magnetic signal.

Better testing for secular variation among paleomagnetic samples on Carmen Island is a suggestion for future studies. This study was limited to single, large oriented rock samples from stratigraphic exposures to form a site. I would suggest taking multiple

samples both horizontally and vertically from a single location. Rock samples should be tested vertically through multiple lithologies to average secular variation over time. It is recommended that at least 100,000 yrs of rock strata are tested in a single area to rule out secular variation (Butler, 1992). This is ~10 m of section in the Comondú Group (Umhoefer, personal communication, 2005). This was not done on Carmen Island and is necessary to fully evaluate the variability in the rotation measurements. I would also suggest testing rock units laterally to look for variation within a single stratigraphic unit.

The paleomagnetic analysis process was limited in the way demagnetization was performed. Alternating field demagnetization was the only method available at the NAU lab. Other methods of demagnetization, such as thermal or chemical, would have been a good alternative to judge the effectiveness of alternating field demagnetization on different rock types from Carmen Island.

Other recommendations for refining a paleomagnetic study of Carmen Island include a study just on the Comondú Group rocks from the paleomagnetic domain immediately south and north of the Arroyo Blanco fault. I would sample many lithologies, both vertically and horizontally, located in the same stratigraphic column to test for secular variation and variability between rock types. More work is needed particularly at the northwest end of the Arroyo Blanco fault, where it does not rupture the western side of the island. This area is the hinge around which Carmen Island rotated and there are no paleomagnetic or detailed geologic data from that area.

A better understanding of Carmen Island neotectonism would be gained through further study of the Arroyo Blanco fault. Vlad (2001) is the only study regarding the Arroyo Blanco fault and her study showed complex and mixed results. It would be

beneficial to understand the mixed fault patterns and the amount and timing of rotation as recorded in the fault. A better understanding of fault patterns could lead to support for a proto-Arroyo Blanco fault zone as hypothesized in the present study.

Future studies of uplifted marine terraces along the eastern side of Carmen Island at Arroyo Blanco may determine if eastern Carmen Island is uplifting at the same rate as western Carmen Island. There are 5 to 6 observed terraces from Arroyo Blanco on eastern Carmen Island. Because we found only 3 sets of terraces at Bahia Marquer on western Carmen Island, then it is possible that eastern Carmen Island could be uplifting much faster than western Carmen Island.

Knowledge gained from this thesis will be important to understand the complexity of rotation of Carmen Island and implications for tectonics of the Loreto rift segment.

CHAPTER 6

CONCLUSIONS

The major conclusions of this study are addressed below.

- Paleomagnetic data from Carmen Island consisted of 11 sites from three paleomagnetic domains. The average paleomagnetic rotation with reference to San Javier road for sites from southern Carmen Island are ~18^{o}. The average paleomagnetic rotation in the middle part of Carmen Island with respect to San Javier road is ~113^{o}. The northern part of Carmen Island in Pliocene age rocks showed no rotation to possible counter-clockwise rotation with respect to San Javier road.
- Paleomagnetic data suggest variable and complex rotation of Carmen Island. Paleomagnetic data from the northern two-thirds of Carmen Island show large variations in rotation that are not consistent with 30-40^{o} of predicted rotation. Carmen Island rotated from ~6 to 3 Ma in a complex fashion between two major strike-slip faults that linked to transform faults in the central Gulf of California. Paleomagnetic and geologic evidence from the northern two-thirds of Carmen Island suggest both rotation of the island and possible small-block rotations. Paleomagnetic data from the southern two-thirds of Carmen Island show little to no rotation, consistent with the geologic model. Carmen Island may be undergoing smaller more localized rotations than predicted and the southern island may not be rotating at all. Pliocene paleomagnetic analysis confirms that Carmen Island is not currently experiencing rotation.

- There are 3 sets of uplifted marine terraces on the western side of Carmen Island and shells and corals were used to establish a time frame in which the terraces were uplifted. Marine terraces were surveyed at Bahia Marquer on Carmen Island at 18 m, 25 m, and 55 m. The geochronology of uplifted marine terraces at Bahia Marquer are determined through U-Th series dates and amino acid correlation. U-Th series dates on the 25 m terrace at Bahia Marquer lend an uplift rate of ~0.20 m/ka. Correlation using amino acid racemization ratios from the 18 m terrace at Bahia Marquer and the 6 m terrace at Punta El Bajo give us an age of 107 ka. This age for the 18 m terrace at Bahia Marquer gives us an uplift rate of ~0.20 m/ka. A Quaternary uplift rate for the western side of Carmen Island, ~0.20 m/ka, is 2.5x or more than that of ~0.08 m/ka from coastal areas near Loreto. Carmen Island continues to experience tectonic uplift as processes associated with the opening of the Gulf of California continue. Shells used for amino acid racemization analysis are important for calibrating a worldwide AAR curve for relative dating.

REFERENCES

Atwater, T., 1970, Implications of plate tectonics for the Cenozoic tectonic evolution of Western North America: Geological Society of America Bulletin, v. 81, p. 3513-3535.

Atwater, T., and Stock, J., 1998, Pacific-North American plate tectonics of the Neogene southwestern United States: International Geology Review, v. 10, p. 375-402.

Axen, G., 1995, Extensional segmentation of the Main Gulf Escarpment, Mexico and United States: Geology, v. 23, p. 515-518.

Beal, C.H., 1948, Reconnaissance of the Geology and oil possibilities of Baja California, Mexico: Geological Society of America, Memoir 31, p. 138.

Beck, M.E., Jr., 1976, Discordant paleomagnetic pole positions as evidence of regional shear in the western Cordillera of North America: American Journal of Science, v. 271, p. 694-712.

Bigioggero, B., Chiesa, S., Zanchi, A., Montraiso, A., and Vezzoli, L., 1995, The Cerro Mencenares volcanic center, Baja California Sur: Source and tectonic control on postsubduction magmatism with the Gulf Rift: Geological Society of America Bulletin, v. 107, p. 1108-1122.

Bosworth, W., 1985, Geometry of propogating continental rifts: Nature, v. 316, p. 625-627.

Broecker, W.S., Thurber, D.L., Goddard, J., Ku, The-Lung, Mathews, R.K., and Mesolella, K.J., 1968, Milankovitch hypothesis supported by precise dating of coral reefs and deep sea sediments: Science, v. 159, p. 297-300.

Burbank, D.W. and Anderson, R.S., 2001, Tectonic Geomorphology: Blackwell Science, Mulden, Massachusetts, 177 p.

Butler, R.F., 1992, Paleomagnetism: Blackwell Scientific Publications, Boston, p. 1-20.

Chappell, J.M., 1983, A revised sea level record for the past 300,000 years from Papua New Guinea: Search 14, p. 99-101.

Chappell, J.M., and Shackleton, N.J., 1986, Oxygen isotopes and sea level: Nature, v. 324, p. 137-140.

Colleta, B., Le Quellec, P., Letouzey, J., and Moretti, I., 1988, Longitudinal evolution of the Suez rift structure (Egypt): Tectonophysics, v. 153, p. 221-233.

Curray, J.R., and Moore, D.G., 1984, Geologic history of the mouth of the Gulf of

California, *in* Crouch, J.K., and Bachman, S.B., eds., Tectonics and Sedimentation along the California Margin, Publication 38: Bakersfield, California, Pacific Section, society of Economic Paleontologists and Mineralogists, p. 17-36.

Dement, A., 1975, Caracteres quimicos principales del vulcanismo terciario y cuaternario de Baja California Sur. Relaciones con la evolution del margin continental pacifico de Mexico. Revista de Instituto de Geologia, UNAM, 1: p. 19-69.

DeMets, C., 1995, A reappraisal of seafloor spreading lineations in the Gulf of California: Implications for the transfer of Baja California to the Pacific plate and estimates of Pacific-North America motion: Geophysical Research Letters, 22, p. 3545-3548.

Dixon, T., Farina, F., Demets, C., Suarez-Vidal, F., Fletcher, J., Marquez-Azua, B., Miller, M., Sanchez, O., Umhoefer, P., 2000, New kinematic models for Pacific-North America motion from 3 Ma to present, II: Evidence for a "Baja California shear zone": Geophysical Research Letters, v. 27, p. 3961-3964.

Dorsey, R.J., and Umhoefer, P.J., 2000, Tectonic and eustatic controls on sequence stratigraphy of Pliocene Loreto basin, Baja California Sur, Mexico: Geological Society of America Bulletin, v. 112, p. 177-199.

Dorsey, R.J, Umhoefer, P.J., Ingle, J.C. Jr., Mayer, L., 2001, Late Miocene to Pliocene stratigraphic evolution of northeastern Carmen Island, Gulf of California: implications for oblique-rifting tectonics: Sedimentary Geology, v. 144, p. 97-123.

Drake, W.R., Umhoefer, P.J., and Peters, L., 2005, Framework stratigraphic evolution and broad correlation of the Comondú Group from San Juan De La Costa to Timbabichi, Baja California Sur, Mexico: Peninsular Geological Society Memoirs, p. 45-46.

Emmons, S.F., and Merrill, G.P., 1894, Geological sketch of Lower California: Geological Society of America Bulletin, v. 4, p. 489-514.

Faulds, J.E. and Varga, R.J., 1998, The role of accommodation zones and transfer zones in the regional segmentation of extended terranes, *in* Faulds, J.E., and Stewart, J.H., eds., Accommodation Zones and Transfer Zones: The Regional Segmentation of the Basin and Range Province: Geological Society of America Special Paper 323, p. 1-47.

Ferrari, L., Lopez-Martinez, M., Aquirre-Diaz, G., and Carrasco-Nunez, G., 1999, Space-time patterns of Cenozoic arc volcanism in central Mexico: From the Sierra Madre Occidental to the Mexican Volcanic Belt: Geology, v. 27, p. 303-306.

Fletcher, J.M., Kohn, B.P., Foster, D.A., and Gleadow, A.J.W., 2000, Heterogeneous Neogene cooling and exhumation of the Los Cabos block, southern Baja California: Evidence from fission-track thermochronology: Geology v. 28, p. 107-110.

Gabb, W.M., 1868, Lower California, in Report of J. Ross and B. Browne on the mineral resources of the States and Territories west of the Rocky Mountains: Washington D.C., US Government Printing Office, p. 630-642.

Gastil, R.G., Krummenacher, D., and Minch, J., 1979, The record of Cenozoic volcanism around the Gulf of California: Geological Society of America Bulletin, v. 90, p. 839-857.

Hagstrum, J.T., Sawlan, M.G., Hausback, B.P., Smith, J.G., and Gromme, C.S., 1987, Miocene paleomagnetism and tectonic setting of the Baja California peninsula, Mexico: Journal of Geophysical Research, v. 92, p. 2627-2639.

Hausback, B.P., 1984, Cenozoic volcanic and tectonic evolution of Baja California Sur, *in* Frizzel, V.A. Jr., ed., Geology of the Baja California peninsula; SEPM, Pacific Section, v. 39, p. 219-236.

Hearty, P.J., and Kaufman, D.S., 2000, Whole-rock amino stratigraphy and Quaternary sea-level history of the Bahamas: Quaternary Research, v. 54, p. 163-173.

Heim, A., 1922, Notes on the Tertiary of southern Lower California: Geological Magazine, v. 59, p. 529-547.

Irving, E., and Irving, G.A., 1982, Apparent polar wander paths Carboniferous through Cenozoic and the assembly of Gondwana, Geophysical Survey, v. 5, p. 141-188.

Karig, D.E., and Jensky, W., 1972, The proto-gulf of California: Earth and Planetary Science Letters, v. 17, p. 169-174.

Keller, E.A., and Pinter, N., 2002, Active Tectonics: Earthquakes, Uplift, and Landscape: Prentice Hall, Upper Saddle River, New Jersey, p. 194-202.

Laj, C., Mitouard, P., Roperch, P., Kissel, C., Mourier, T., and Megard, F., 1989, Paleomagnetic rotations in the coastal areas of Ecuador and northern Peru, *in* Kissel, C., and Laj, C., eds., Paleomagntic Rotations and Crustal Deformation, p. 489-511.

Lajoie, K.R., 1986, Costal tectonics, *in* Wallace, R. E., ed., Active Tectonics: National Academy Press, Washington, p. 95-124.

Lamb, S.H., 1988, Tectonic rotations about vertical axes during the last 4 Ma in part of

the New Zealand plate-boundary zone: Journal of Structural Geology, v.10, p 875-893.

Ledesma-Vazquez, J., and Johnson, M.E., 1993, Neotectonica del area Loreto-Mulege, *in* Delgado-Argote, L. A., Martin-Barajas, A., eds, Contribuciones a la Tectonics del Occidente de Mexico, Union Geofisica Mexicana.

Lewis, C.J., and Stock, J.M., 1998, Paleomagnetic evidence of localized vertical axis rotation during Neogene extension, Sierra San Fermin, northeastern Baja California, Mexico: Journal of Geophysical Research, v. 103, p. 2455-2470.

Lindgren, W., 1888, Notes on the geology of Baja California, Mexico: California Academy of Sciences Proceedings, v. 1, p. 173-196.

Lonsdale, P., 1989, Geology and tectonic history of the Gulf of California, *in* Winterer, E. L., et al., eds., The eastern Pacific Ocean and Hawaii: Boulder, Colorado, Geological Society of America, Geology of North America, v. N, p. 499-521.

Lonsdale, P., 1991, Structural patterns of the Pacific floor offshore of Peninsular California, *in* Dauphlin, J.P., Simoneit, B.R.T., eds, The Gulf and Peninsular Province of the Californias: American Association of Petroleum Geologists Memoir 47, p. 87-125.

Lund, S.P., and Bottjer, D.J., 1991, Paleomagnetic evidence for microplate tectonic development of Southern and Baja California. *in* Dauphin, J.P., and Simoneit, B.R.T., eds., The Gulf and Peninsular Province of the Californias: American Association of Petroleum Geologists Memoir 47, p. 87-125.

Luyendyk, B.P., Kamerling, M.J., Terres, R.R., and Hornafius, J.S., 1985, Simple shear of southern California during Neogene time suggested by paleomagnetic declinations: Journal of Geophysical Research, v. 90, p. 12454-12466.

Mankinen, E.A., Larson, E., Gromme, C.S., Preveot, M., and Coe, R.S., 1987, The Steen Mountain (Oregon) geomagnetic polarity transition, 3, Its Regional Significance: Journal of Geophysical Research, v. 92, p. 8057-8076.

Mayer, L., and Vincent, K.R., 1999, Active tectonics of the Loreto area, Baja California Sur, Mexico: Geomorphology, v. 27, p. 243-255.

Mayer, L., Umhoefer, P.J., Macy, J., Dorsey, R.J., Kaufman, D.S., and Simmons, K.R., 2002, Ages and uplift rates of marine terraces near Loreto and on Isla Carmen, Baja California Sur, VI Reunión Internacional sobre Geologia de la Península de Baja California La Paz, Baja California Sur, April 4-6, p. 59.

McFall, C.C., 1968, Reconnaissance geology of the Concepcion Bay area, Baja

California, Mexico: Stanford University Publications in Geological Sciences, v. 10, p. 1-25.

McKenzie, D., and Jackson, J., 1983, The relationship between strain rates, crustal thinning, paleomagnetism, finite strain and fault movements within a deforming zone: Earth Planetary Science Letters, v. 65, p. 182-202.

McKenzie, D., and Jackson, J., 1986, A block model of distributed deformation by faulting: Geological Society of London, v. 143, p. 349-353.

McLean, H., 1988, Reconnaissance geologic map of Loreto and part of the San Javier quadrangles, Baja California Sur, Mexico: U.S. Geological Survey Map MF 2000, scale 1:50,000.

Merritts, D., and Bull, W.B., 1989, Interpreting Quaternary uplift rates at the Mendocino triple junction, northern California, from uplifted marine terraces: Geology, v. 17, p. 1020-1024.

Moore, D.G., and Buffington, E.C., 1968, Transform faulting and growth of the Gulf of California since the late Pliocene: Science, v. 161, p. 1238-1241.

Muhs, D.R., Kennedy, G.L., and Rockwell, T.K., 1994, Uranium-series ages of marine terrace corals from the Pacific coast of North America and implications for last-interglacial sea level history: Quaternary Research, v. 42, p. 72-87.

Nava-Sanchez, E.H., Gorsline, D.S., and Molina-Cruz, A., 2001, The Baja California peninsula borderland: Structural and sedimentological characteristics: Sedimentary Geology, v. 44, p. 63-82.

Nelson, M.R., and Jones, C.H., 1987, Paleomagnetism and crustal rotation along a shear zone, Las Vegas Range southern Nevada: Tectonics, v. 6, p. 13-34.

Nicholson, C., Sorlien, C.C., Atwater, T., Crowell, J.C., and Luyendyk, B.P., 1994, Microplate Capture, rotation of the western Transverse Ranges, and initiation of the San Andreas transform as a low-angle fault system: Geology, v. 22, p. 491-495.

Nur, A., and Ron, H., 1987, Block rotations, fault domains, and crustal deformation: Annales Tectonicae, v. 1, n. 1, p. 40-47.

Nur, A., Ron, H., and Scotti, O., 1989, Kinematics and machanics of tectonic block rotations, *in* Cohen, S.C. and Vanicek, P., eds., Slow Deformation and Transmission of Stress in the Earth: Geophysical Monogram Series, v. 49, p. 31-46.

Ortlieb, L., 1980, Neotectonics from marine terraces along the Gulf of California, *in*

Morner, ed., Earth Rheology, Isostasy, and Eustasy, Wiley Interscience, p. 497-504.

Ortlieb, L., 1991, Quaternary vertical movements along the coasts of Baja California and Senora, *in* Dauphin, J.P., Simoneit, B.R.T., eds., The Gulf and Peninsular Province of the Californias: American Association of Petroleum Geologists Memoir 47, p. 447-480.

Oskin, M.E., Stock, J.M., and Martin-Barajas, A., 2001, Rapid localization of Pacific-North American plate motion in the Gulf of California: Geology, v. 29, p. 459-462.

Roberts, A.P., 1995, Tectonic rotation about the termination of a major strike-slip fault, Marlborough fault system, New Zealand. Geophysical Research Letters, v. 22, p. 187-190.

Rockwell, T.K., Muhs, D.R., Kennedy, G.L, Hatch, M.E., Wilson, S.H., and Klinger, R.E., 1989, Uranium Series ages faulnal correlations and tectonic deformation of marine terraces within the Agua Blanca fault zone and Punta Banda, northern Baja California, Mexico. *in* Abbott, P. L., ed, Geologic Studies in Baja California, Society of Economic Paleontologists and Mineralogists, Pacific Section, p. 1-16.

Ron, H., Freund, R., Garfunkel, Z., and Nur, A., 1984, Block rotation by strike-slip faulting: Structural and paleomagnetic evidence: Journal of Geophysical Research, v. 89, p. 6256-6270.

Ron, H., Aydin, A., and Nur, A., 1986, Strike-slip faulting and block rotation in the Lake Mead fault system: Geology, v. 14, p. 1020-1023.

Roperch, P., and Carlier, G., 1992, Paleomagnetism of Mesozoic rocks from the central Andes of southern Peru: Importance of rotations in the development of the Bolivian orocline: Journal of Geophysical Research, v. 97, p. 17233-17249.

Rosendahl, B.R., 1987, Architecture of continental rifts with special reference to East Africa: Annual Review of Earth and Planetary Sciences, v. 15, p. 445-503.

Sawlan, M.G., and Smith, J.G., 1984, Petrologic characteristics, age and tectonic setting of Neogene volcanic rocks in northern Baja California Sur, Mexico *in* Frizzel, V.A., Jr., ed., Geology of the Baja California peninsula: SEPM, Pacific section, v. 39, p. 237-251.

Sawlan, M.G., 1991, Magmatic evolution of the Gulf of California *in* Dauphin, J.P., and Simoneit, P. R. T., eds., The Gulf and Peninsular province of Californias: AAPG Memoir 47, p. 301-369.

Shackleton, N.J., and Opdyke, N.D., 1973, Oxygen isotope and paleomagnetic

stratigraphy of equatorial Pacific core V28-238: oxygen isotope temperature and ice volumes on a 105-year and 106-year timescale, Quaternary Research, v. 3, p. 39-45.

Sonder, L.J., Johns, C.H., Salyards, S.L., and Murphy, K.M., 1994, Vertical axis rotations in the Las Vegas Valley Shear Zone, southern Nevada: Paleomagnetic constraints on kinematics and dynamics of block rotations: Tectonics, v. 13, p. 769-788.

Stock, J.M., and Hodges, K.V., 1989, Pre-Pliocene extension around the Gulf of California and the transfer of Baja California to the Pacific plate: Tectonics, v. 8, p. 99-115.

Stock, J.M., and Lee, J., 1994, Do microplates in subduction zones leave a geological record? Tectonics, v. 13, p. 1472-1487.

Stock, J.M., Lewis, C.J., and Nagy, E.A., 1999, The Tuff of San Felipe: an extensive middle Miocene pyroclastic flow deposit in Baja California, Mexico: Journal of Volcanology and Geothermal Research, v. 93, p. 53-74.

Umhoefer, P.J., and Stone, K.A., 1996, Description of kinematics of the SE Loreto basin fault array, Baja California Sur, Mexico: a positive field test of oblique-rift models: Journal of Structural Geology, v. 18, p. 595-614.

Umhoefer, P.J., Mayer, L., Dorsey, R.J., 2002, Evolution of the margin of the Gulf of California near Loreto, Baja California peninsula, Mexico: Geological Society of America Bulletin, v. 114, p. 849-868.

Umhoefer, P.J., Dorsey, R.J., Willsey, S., Mayer, L., and Renne, P., 2001, Stratigraphy and geochronology of the Comondu Group near Loreto, Baja California Sur, Mexico: Sedimentary Geology, v. 44, p. 125-147.

Umhoefer, J.P., Dorsey, R.J. and Renne, P., 1994, Tectonics of the Pliocene Loreto basin, Baja California Sur, Mexico, and evolution of the Gulf of California: Geology, v. 22, p. 649-652.

Van der Pluijm, B., and Marshak, S., 1997, Earth Structure: An Introduction to Structural Geology and Tectonics: McGraw Hill, Inc., p. 389-403.

Vlad, A.M., 2001, Structure of the Escondido and Arroyo Blanco faults, Loreto rift segment, Baja California Sur, Mexico: M. S. thesis, Northern Arizona University, p. 1-205.

Wark, D.A., Kempter, K.A., and McDowell, F.W., 1990, Evolution of waning subduction-related magmatism, northern Sierra Madre Occidental, Mexico: Geological Society of America Bulletin, v. 102, p. 1555-1564.

Wehmiller, J. F., and Miller, G. H., 2000, Aminostratigraphy Dating Methods *in* Noller, J. S., Sowers, J. M., and Lettis, W. R., eds, Quaternary Geology, Quaternary Geochronology: Methods and applications, p. 187-222.

Willsey, S.P., Umhoefer, P.J., and Hilley, G.E., 2002, Early evolution of an extensional monocline by a propogating normal fault: 3-D analysis from combined field study and numerical modeling: Journal of Structural Geology, v. 24, p. 651-669.